PIV-BASED INVESTIGATION OF HAEMODYNAMIC FACTORS IN DISEASED CAROTID ARTERY BIFURCATION

AHMAD FAHMI HUWAIDI BIN MOHAMAD NOOR

اونيۏرسيتي مليسيا ڤهڠ السلطان عبدالله
UNIVERSITI MALAYSIA PAHANG
AL-SULTAN ABDULLAH

MASTER OF SCIENCE

UNIVERSITI MALAYSIA PAHANG
AL-SULTAN ABDULLAH

UNIVERSITI MALAYSIA PAHANG AL-SULTAN ABDULLAH

DECLARATION OF THESIS AND COPYRIGHT

Author's Full Name	:	AHMAD FAHMI HUWAIDI BIN MOHAMAD NOOR
Date of Birth	:	09-09-1997
Title	:	PIV-BASED INVESTIGATION OF HAEMODYNAMIC FACTORS IN DISEASED CAROTID ARTERY BIFURCATION
Academic Session	:	SEMESTER II 2023/2024

I declare that this thesis is classified as:

☐	CONFIDENTIAL	(Contains confidential information under the Official Secret Act 1997)*
☐	RESTRICTED	(Contains restricted information as specified by the organization where research was done)*
☒	OPEN ACCESS	I agree that my thesis to be published as online open access (Full Text)

I acknowledge that Universiti Malaysia Pahang Al-Sultan Abdullah reserves the following rights:

1. The Thesis is the Property of Universiti Malaysia Pahang Al-Sultan Abdullah
2. The Library of Universiti Malaysia Pahang Al-Sultan Abdullah has the right to make copies of the thesis for the purpose of research only.
3. The Library has the right to make copies of the thesis for academic exchange.

UMPSA
اونيۏرسيتي مليسيا ڤهڠ السلطان عبدالله
UNIVERSITI MALAYSIA PAHANG
AL-SULTAN ABDULLAH

Certified by:

(Student's Signature)

(Supervisor's Signature)

Date: 08 April 2024

Name of Supervisor: TS Dr. Nasrul Hadi bin Johari
Date: 08 April 2024

NOTE : * If the thesis is CONFIDENTIAL or RESTRICTED, please attach a thesis declaration letter.

اونيۏرسيتي مليسيا ڤهڠ السلطان عبدالله
UNIVERSITI MALAYSIA PAHANG
AL-SULTAN ABDULLAH

SUPERVISOR'S DECLARATION

I/~~We~~* hereby declare that I/~~We*~~ have checked this thesis/project* and in my/~~our*~~ opinion, this thesis/~~project~~* is adequate in terms of scope and quality for the award of the degree of Master of Science.

____
(Supervisor's Signature)

Full Name : TS Dr Nasrul Hadi bin Johari

Position : DR. NASRUL HADI BIN JOHARI
PENSYARAH
FAKULTI TEKNOLOGI KEJURUTERAAN
MEKANIKAL DAN AUTOMOTIF
UNIVERSITI MALAYSIA PAHANG
26600 PEKAN, PAHANG DARUL MAKMUR
TEL : 09-424 6267 FAX : 09-424 6222

Date : 08 April 2024

UMPSA
اونيۏرسيتي مليسيا ڤهڠ السلطان عبدالله
UNIVERSITI MALAYSIA PAHANG
AL-SULTAN ABDULLAH

STUDENT'S DECLARATION

I hereby declare that the work in this thesis is based on my original work except for quotations and citations which have been duly acknowledged. I also declare that it has not been previously or concurrently submitted for Master of Science at University Malaysia Pahang Al-Sultan Abdullah or any other institutions.

____

(Student's Signature)

Full Name : AHMAD FAHMI HUWAIDI BIN MOHAMAD NOOR

ID Number : MMH20002

Date : 08 April 2024

اونيۏرسيتي مليسيا ڤهڠ السلطان عبدالله
UNIVERSITI MALAYSIA PAHANG
AL-SULTAN ABDULLAH

PIV-BASED INVESTIGATION OF HAEMODYNAMIC FACTORS IN DISEASED CAROTID ARTERY BIFURCATION

AHMAD FAHMI HUWAIDI BIN MOHAMAD NOOR

Thesis submitted in fulfillment of the requirements
for the award of the degree of
Master of Science

Faculty of Mechanical and Automotive Engineering Technology

UNIVERSITI MALAYSIA PAHANG AL-SULTAN ABDULLAH

APRIL 2024

ACKNOWLEDGEMENTS

Bismillahhirahmannirrahim, in the name of Allah, the Gracious and the Merciful, Alhamdulillah I would like to praise the highest thank to Him, the Lord of worlds, for granting me the opportunity to complete my Master of Science studies.

First and foremost, I would like to express my sincerest gratitude to my supervisor, Ts Dr Nasrul Hadi bin Johari who guiding and advising me to throughout this study. I glad my supervisor have been sacrificed everything to help me especially give new knowledge during experiment and simulation. His dedication towards improve my research skill will be forever be inspiration for me in my future work.

I would like to express my gratitude towards to University Malaysia Pahang Al Sultan Abdullah (UMPSA) and Institute Postgraduate Student (IPS) for their assistance and encouragement throughout this journey.

Lastly, I am deeply grateful to my family and friends for their unwavering encouragement and understanding throughout this journey. Special thanks to my mother Rohima, my father Noor, and my close relatives for their continuous support. Their unwavering support provided me with the strength and motivation to overcome challenges and persevere until the completion of this thesis.

UMPSA
اونيۏرسيتي مليسيا ڤهڠ السلطان عبدالله
UNIVERSITI MALAYSIA PAHANG
AL-SULTAN ABDULLAH

ABSTRAK

Strok iskemia, keadaan yang dicirikan oleh pembentukan plak dalam arteri karotid yang membawa kepada stenosis arteri karotid, menimbulkan masalah asas yang ketara. Penyakit ini dipengaruhi oleh parameter hemodinamik dalam aliran darah, seperti profil halaju, tegasan ricih dinding, dan tekanan. Akibatnya, kajian ini bertujuan untuk menyiasat ciri aliran dalam bifurkasi arteri karotid menggunakan velocimetry imej zarah (PIV) dan model pengiraan. Ia juga bertujuan untuk menilai bagaimana lokasi stenosis mempengaruhi parameter hemodinamik. Bahagian pertama tesis melibatkan penyiasatan ciri aliran dalam geometri selepas stent hantu bifurkasi arteri karotid menggunakan 2D PIV dan 3D stereo-PIV (SPIV). Analisis kemudiannya dibandingkan dengan dinamik bendalir pengiraan (CFD), memfokuskan pada kawasan minat tertentu seperti kawasan masuk, bifurkasi dan stent. Selain itu, model ideal dengan stenosis di lokasi yang berbeza telah dicipta dan dianalisis berdasarkan profil halaju, tegasan ricih dinding dan tekanan di kawasan stenosis. Penemuan kajian menunjukkan perbezaan kecil kira-kira 16.66% dalam halaju aliran purata antara teknik 2D PIV dan 3D SPIV. Walaupun SPIV mempamerkan ketepatan yang lebih tinggi dalam menangkap lebih banyak vektor berbanding PIV, perbezaan yang diperhatikan kekal agak kecil dan berada dalam julat yang boleh diterima. Akibatnya, PIV masih boleh digunakan dengan berkesan untuk menjalankan perbandingan yang meluas dengan CFD dalam konteks kajian ini. Pengesahan kawasan pasca stent menggunakan vektor halaju daripada PIV dan CFD menunjukkan arah aliran yang sama, manakala kawasan salur masuk mempamerkan percanggahan yang lebih besar disebabkan oleh pengesanan halaju tinggi dalam CFD. CFD meramalkan halaju maksimum yang lebih tinggi sedikit sebanyak 0.98 m/s, kira-kira 10% lebih tinggi daripada yang dicatatkan dalam PIV. Kehadiran halaju rendah di sekeliling bifurkasi dan kelengkungan menggalakkan aliran peredaran semula, menyumbang kepada perkembangan aterosklerosis. Tambahan pula, kajian menunjukkan bahawa stenosis jenis I (stenosis hulu) lebih berkemungkinan mengakibatkan pendarahan intraplak (IPH), yang boleh memberi kesan buruk kepada pesakit. Hasil kajian ini yang boleh menyumbang kepada pemahaman yang lebih baik tentang kesihatan vaskular dan membimbing amalan klinikal dalam pengurusan penyakit arteri karotid.

UMPSA
UNIVERSITI MALAYSIA PAHANG
AL-SULTAN ABDULLAH

ABSTRACT

Ischemic stroke, often precipitated by the development of plaque within the carotid arteries leading to carotid artery stenosis, represents a significant health concern. This condition is heavily influenced by hemodynamic parameters such as velocity profiles, wall shear stress, and pressure within the blood flow. Addressing this, the current study endeavors to elucidate the flow characteristics at carotid artery bifurcations by employing particle image velocimetry (PIV) and computational models, and to ascertain the impact of stenosis placement on these hemodynamic parameters. The initial phase of this research involves the examination of flow patterns in a post-stent carotid artery bifurcation phantom using both 2D PIV and 3D stereo-PIV (SPIV). These findings are subsequently juxtaposed with those derived from computational fluid dynamics (CFD) analyses, concentrating on areas of interest that include the inlet, bifurcation, and stented segments. Additionally, this study constructs and examines idealized models of varying stenosis locations, evaluating them based on the velocity profiles, wall shear stress, and pressure at the sites of stenosis. Results reveal a reduced flow velocity in the bifurcation area, with consistent trends between PIV and SPIV methodologies. A notable yet acceptable variance of about 16.66% in average flow velocity was discerned between the 2D and 3D PIV approaches. Despite SPIV's enhanced precision in vector capture, this minor disparity validates the use of PIV for comprehensive CFD comparison within the purview of this research. Comparative analysis of velocity vectors in the post-stent area demonstrates analogous trends between PIV and CFD, while the inlet region displays more significant differences, notably the higher velocities detected by CFD. Here, CFD anticipates a maximum velocity of 0.98 m/s, approximately 10% higher than that measured by PIV. The observed low-velocity zones around bifurcations and curvatures are conducive to recirculatory flow, fostering atherosclerotic progression. Moreover, the research identifies that Type I stenosis upstream stenosis is more prone to result in intraplaque hemorrhage (IPH), potentially exacerbating patient outcomes. The insights from this study enhance our comprehension of vascular mechanics and hold the potential to refine clinical approaches to managing carotid artery disease.

UMPSA
اونيۏرسيتي مليسيا ڤهڠ السلطان عبدالله
UNIVERSITI MALAYSIA PAHANG
AL-SULTAN ABDULLAH

TABLE OF CONTENT

UMPSA
اونيۏرسيتي مليسيا ڤهڠ السلطان عبدالله
UNIVERSITI MALAYSIA PAHANG
AL-SULTAN ABDULLAH

UMPSA
اونيۏرسيتي مليسيا ڤهڠ السلطان عبدالله
UNIVERSITI MALAYSIA PAHANG
AL-SULTAN ABDULLAH

UMPSA
اونيۏرسيتي مليسيا ڤهڠ السلطان عبدالله
UNIVERSITI MALAYSIA PAHANG
AL-SULTAN ABDULLAH

LIST OF TABLES

UMPSA
اونيۏرسيتي مليسيا ڤهڠ السلطان عبدالله
UNIVERSITI MALAYSIA PAHANG
AL-SULTAN ABDULLAH

LIST OF FIGURES

UNIVERSITI MALAYSIA PAHANG AL-SULTAN ABDULLAH

UMPSA
اونيۏرسيتي مليسيا ڤهڠ السلطان عبدالله
UNIVERSITI MALAYSIA PAHANG
AL-SULTAN ABDULLAH

UMPSA
اونيۏرسيتي مليسيا ڤهڠ السلطان عبدالله
UNIVERSITI MALAYSIA PAHANG
AL-SULTAN ABDULLAH

LIST OF ABBREVIATIONS

CVD	Cardiovascular disease
CAS	Carotid artery stenting
CEA	Carotid artery endarterectomy
CCA	Common carotid artery
CFD	Computational fluid dynamics
FSI	Fluid structure interaction
WHO	World Health Organisation
PIV	Particle image velocimetry
ICA	Internal carotid artery
ECA	External carotid artery
WSS	Wall shear stress
IPH	Intraplaque haemorrhage
DICOM	Digital Imaging and Communication in Medicine
NASCET	North American Symptomatic Carotid Endarterectomy Trial
ACAS	Asymptomatic Carotid Atherosclerosis Study
ACST	Asymptomatic Carotid Surgery Trial
LDL	Low-density lipoprotein
PLA	Polylactic acid
PVA	Polyvinyl alcohol
PDMS	Polydimethylsiloxane

UMPSA
اونيۏرسيتي مليسيا ڤهڠ السلطان عبدالله
UNIVERSITI MALAYSIA PAHANG
AL-SULTAN ABDULLAH

LIST OF APPENDICES

اونيۏرسيتي مليسيا ڤهڠ السلطان عبدالله
UNIVERSITI MALAYSIA PAHANG
AL-SULTAN ABDULLAH

CHAPTER 1

INTRODUCTION

1.1 Introduction

In 2016, a staggering 15.2 million individuals succumbed to cardiovascular disease (CVD), accounting for nearly half of global deaths that year, as reported by the World Health Organization (WHO)(Velasquez-Valencia et al., 2018). This trend continued, with WHO estimating 17.9 million CVD-related deaths in 2019, where 85% of fatalities resulted from heart attacks and strokes. Atherosclerosis, characterized by the formation of arterial plaque or carotid stenosis, emerges as a significant contributor, constricting blood flow within arterial walls. The gravity of atherosclerosis intensifies when it impacts pivotal arteries like the carotid or coronary vessels, elevating the risk of stroke and heart attack. Figure 1.1 illustrates the top 10 global causes of deaths in 2019, emphasizing the prominence of CVD in the global health landscape.

As per the Department of Statistics Malaysia (DOSM), as depicted in Figure 1.2, ischemic heart disease continues to stand out as a primary cause of death even in the post-COVID-19 era of 2022. Other notable contributors to mortality include pneumonia (11.1%), cerebrovascular disease (8.3%), transport accidents (2.9%), and malignant neoplasm of the trachea, bronchus, and lung (2.5%).

Patients grappling with CVD often necessitate invasive treatments, involving surgeries aimed at restoring and enhancing blood flow. Procedures such as endarterectomy, angioplasty, stent placement, and arterial bypass graft surgery are considered, taking into account factors such as the patient's age, anatomical considerations, surgical risk, and clinical experience (Johari et al. 2020). Notably, stent implantation emerges as a less invasive technique for addressing narrowed arteries and restoring blood flow to the brain (Paisal et al., 2019). In contrast, endarterectomy involves an open surgical procedure designed to address narrowed or obstructed blood vessels supplying blood to the heart.

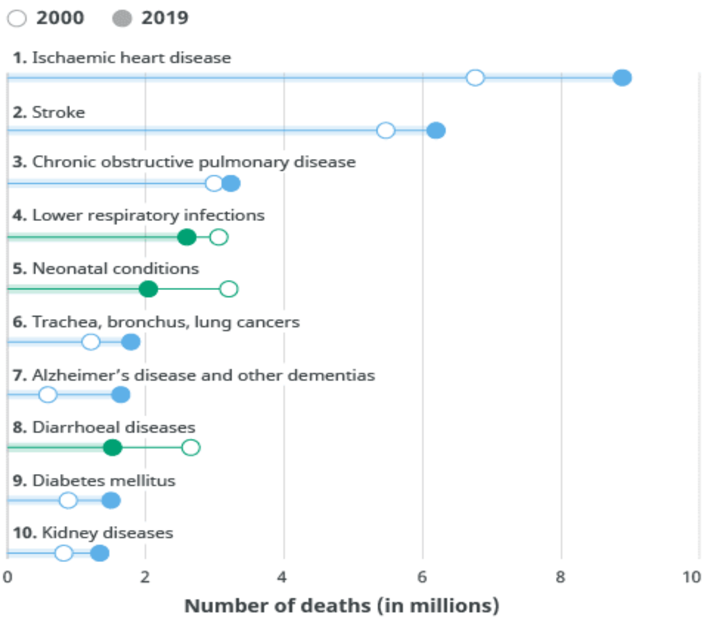

Figure 1.1 Top 10 global deaths in the world based on World Health Organisation (WHO)

Source: https://www.who.int/news-room/fact-sheets/detail/the-top-10-causes-of-death

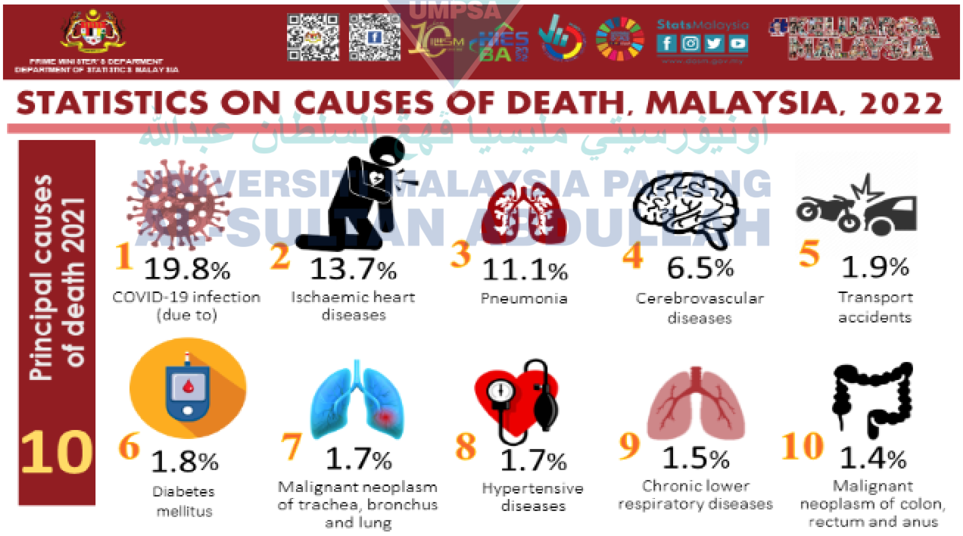

Figure 1.2 The statistics on causes of death in Malaysia 2022

Source: https://www.dosm.gov.my/portal-main/release-content/statistics-on-causes-of-death-malaysia-2022

UMPSA
اونيۏرسيتي مليسيا ڤهڠ السلطان عبدالله
UNIVERSITI MALAYSIA PAHANG AL-SULTAN ABDULLAH

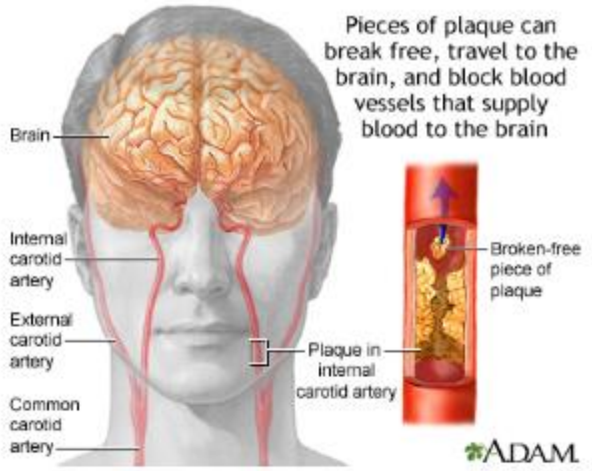

Figure 1.3 Carotid artery stenosis

Source: https://ufhealth.org/conditions-and-treatments/angioplasty-and-stent-placement-carotid-artery

Hemodynamic analysis has been extensively investigated through in-vitro techniques utilizing physical representations for measuring blood flow in the arterial system. Numerous in-vitro studies have been conducted for both qualitative and quantitative flow visualization. The hemorheologic and hemodynamic features are closely linked to geometric factors of vessels, such as artery size and shape (Hong et al., 2017), (Dolan et al., 2013). Previous research indicates that the initiation of atherosclerosis often stems from disturbed flow and low wall shear stress (WSS) (Sun et al., 2009) , (Hong et al., 2017), (Zarins et al., 1983). Conversely, other studies suggest that high wall shear stress gradient (WSSG) and a high oscillatory shear index (OSI) are associated with CVD (Chen et al., 2020), (Arzani & Shadden, 2016),(Hoving et al., 2020).

The bifurcation and curvature arterial such as carotid artery (Figure 1.3), are recognized as sites where atherosclerosis or plaque formation occurs (Tayefi et al., 2011). Due to increased bifurcation angles, WSS values decrease. The branching of the carotid artery introduces significant secondary flow motion with flow separation and reversal, particularly in the external carotid artery. WSS is measured along the inner and outer vessel walls, typically being higher in the internal carotid artery and lower in the external

UMPSA
UNIVERSITI MALAYSIA PAHANG
AL-SULTAN ABDULLAH

carotid artery (Buchmann & Jermy et al., 2009a). These parameters are intricately linked to the likelihood of cardiovascular diseases, making the measurement and analysis crucial for a deeper understanding of conditions like atherosclerosis. This is where Particle Image Velocimetry (PIV) imaging techniques and computational modelling become invaluable.

PIV is a commonly selected technique for understanding key parameters in medical and physiological phenomena such as arterial hemodynamics and respiratory mechanics (Yazdi et al., 2018). PIV measurements provide insights into the internal and external flow characteristics of 3D flow phantom models, offering parametric data like velocity and WSS at different locations and time points. PIV equipment includes a high-speed camera, laser, geometry specimen, blood mimicking fluid (BMF), dynamic studio, seeding particles, and a flow system circuit that includes a pump (Noor & Johari, 2022), (Y. Li et al., 2020).

Computational modelling has also been widely employed to assess blood flow behaviour in stenotic arteries, offering insights into cardiovascular disease conditions, progression, and therapeutic optimization (Carvalho et al., 2021), (Lopes et al., 2020). Simulations, aided by medical imaging techniques for geometry and realistic boundary conditions, are performed using computational fluid dynamics (CFD) or fluid-structure interaction (FSI). CFD focuses on hemodynamic parameters in geometries with rigid walls, while FSI considers both fluid and solid wall domains, particularly when the wall is compliant. The hemodynamics in the artery are investigated using CFD research, emphasizing the temporal and geographical distribution of blood pressure acting on the arterial wall (Buckler et al., 2022),(Carvalho et al., 2021).

To fully utilize capability on CFD for modelling blood flow within stents deployed in patient-specific aneurysm models, validation against physical measurements, validated with PIV is essential (Y. Li et al., 2020). The validation process, involving computational modelling and PIV, allows researchers to assess the trustworthiness and legitimacy of the computational model. This validation is crucial to ensure accurate comparisons between physical measurements obtained from both analyses. The integration of PIV with CFD in the study of stenosed carotid arteries stands as a valuable

UMPSA
UNIVERSITI MALAYSIA PAHANG
AL-SULTAN ABDULLAH

approach serving multiple purposes: ensuring accuracy, validating models, gaining insights into intricate flow physics, and enhancing the credibility of research findings.

1.2 Problem statement

The primary challenge in visualizing blood flow in diseased carotid artery bifurcation lies in mitigating the stenosis issue, particularly for clinical treatments. Current clinical diagnostic techniques for assessing the degree of stenosis in carotid arteries include X-ray angiography, magnetic resonance imaging (MRI), computed tomography angiography (CTA), and duplex ultrasound. However, these techniques face limitations, particularly in temporal and spatial resolution. To address these shortcomings, researchers have recently turned to PIV as a potential solution. PIV offers full-field measurement of instantaneous velocities with high spatial and temporal resolution, reaching down to the micron range and providing high-speed frame rates in the order of kilohertz (Kefayati et al., 2013).

This experimental approach, utilizing PIV, is vital for the validation and refinement of CFD simulations. Previous studies have delved into the risk factors of atherosclerosis, such as the size, eccentricity, and precise location of stenosis, by employing either experimental or computational methodologies. Nonetheless, a significant gap persists in the literature due to the lack of validation between computational predictions and experimental observations, which hinders a complete understanding of post-stenotic flow behavior (Buckler et al., 2022),(Carvalho et al., 2021). For instance, (C. Li et al., 2019) studied CFD through carotid artery stenosis without validating the computational results with experimental data.

Moreover, while various studies have delved into the size of stenosis through repeated research, the specific location of stenosis within the carotid artery has received comparatively less attention. Understanding the influence of different locations of stenosis on patient risk, as highlighted by (Lu et al., 2019), is crucial. The hemodynamics may also play a role in determining the location of plaque within the carotid artery (Woo et al., 2020). Therefore, insights into the location of stenosis are highly relevant for medical treatment and for comprehending flow patterns to reduce the incidence of cardiovascular diseases globally.

1.3 Research Objective

Based on the problem statement, the objectives of this research are:

1. To investigate flow profile in post stent geometry of carotid artery bifurcation phantom using PIV and SPIV.
2. To investigate computational model of post stent carotid artery bifurcation for evaluation of flow features in comparison with PIV measurement data.
3. To evaluate the influence of different location of high degree stenosis in the internal carotid artery on the hemodynamic parameters.

1.4 Research Scope

This research focus on:

1. The flow pattern measured in PIV was focused on the pre- and post-stenotic carotid area as it was expected to see an adverse haemodynamics.
2. Blood-mimicking fluid will be used in the PIV experiment to see the flow feature in different size, eccentricity and location of the stenosis.
3. Computational modelling study was based on computational fluid dynamics (CFD) using ANSYS FLUENT 19.0.

اونيورسيتي مليسيا ڤهڠ السلطان عبدالله
UNIVERSITI MALAYSIA PAHANG
AL-SULTAN ABDULLAH

1.5 Thesis Overview

Chapter 1 introduces the causes of cardiovascular disease and the statistics reported by the WHO, carotid stenosis, and treatment of CVD. Others studied haemodynamic factors of cardiovascular disease, particle image velocimetry in experiments, and simulation for visualising the blood flow are also diccussed in this chapter. Finally, this chapter describes the research objective, problem statement, scope of the study, and overview of each chapter.

Chapter 2 is a literature review that provides an outline of the clinical and engineering background of carotid artery stenosis. The clinical background covers the carotid vasculature, pathophysiology, risk factors of atherosclerosis, evaluation of patients and finally treatment options for atherosclerosis. The role of haemodynamic forces in regulating the progression of atherosclerosis in the carotid artery bifurcation is also discussed. In the engineering context, the background of fluid mechanics and computational methodologies for modelling blood flow and arterial wall mechanics are described, with a specific focus on laminar to turbulent transition modelling strategies. Lastly, a review of the literature regarding the evaluation of post-stenotic flow is based on experimental and computational modelling is offered.

The method used to reconstruct the 3D rigid phantom of a specific geometry carotid artery is evaluated in Chapter 3. The in vitro studies to study steady flow patterns used PIV and stereo-particle image velocimetry (SPIV). Moreover, PIV setups such as blood-mimicking fluid, pumps, 3D phantoms, circuit flow, lasers, and high-speed cameras, are also discussed in this chapter. Computational fluid dynamics (CFD) used in ANSYS Fluent will be analysed using post stent geometry of carotid artery. Both experimental and simulation results will be compared and analysed for post-stenotic flow features. Next, the study on different locations of stenosis that influence the risk for patients by simulation in CFD using idealised carotid artery geometry is described as well.

اونيۏرسيتي مليسيا ڤهڠ السلطان عبدالله
UNIVERSITI MALAYSIA PAHANG
AL-SULTAN ABDULLAH

The fourth chapter investigates the flow behavior analysis for both experiment and simulation on the post stent geometry of the carotid artery with steady flow. The validation will analyse the flow conditions in the experiment and simulation with the same boundary conditions. The analysis of the comparative result focuses on the velocity profile, velocity vector, scalar map of velocity and velocity on cross sectional line of interest area region. The influence flow through the different locations of stenosis also explain in this chapter. The results will be discuss based on the velocity profile, WSS and pressure.

Chapter 5 summarises the key findings and gives the conclusion of the research. Next, the chapter discusses on the limitation of the study and gives recommendations for the future research.

CHAPTER 2

LITERATURE REVIEW

2.1 Introduction

The literature review comprises two main components. The initial segment provides a clinical background on the carotid artery, elucidates medical treatments for carotid stenosis, and delineates the role of hemodynamic factors in the development of this disease. The second portion delves into fluid mechanics, detailing experimental procedures, and elucidating computational methodologies, specifically, computational fluid dynamics (CFD) and particle image velocimetry (PIV).

2.2 Carotid Artery Bifurcation

2.2.1 Circulatory System and Carotid Artery

The circulatory system which can also be called as a haemodynamic system is an organ system that permits blood to circulate blood and transport nutrients. The circulatory system can be divided into two major systems, the systemic circulation and pulmonary circulation (Figure 2.1). The systemic circulation transport oxygen-rich blood from the left ventricle of the heart to the body and returns oxygen-depleted blood back to the heart. Oxygen-depleted blood is subsequently transported by the pulmonary circulation from the right ventricle of the heart to the lungs, where gas exchange occurs, and oxygen-rich blood is then returned to the heart via the left atrium.

The left ventricle of the heart subsequently pumps the oxygenated blood through the aorta, the biggest and most important artery in the human body. Blood from the aorta's branches is delivered to all major organs, including the head, neck, arms, and kidney, through smaller arteries. One of the main blood vessels that nourishes the brain and a frequent location of vascular illness is the carotid arteries (Onaizah et al., 2017). The carotid arteries, which are found at the right and left necks and are among the arteries that

UMPSA
اونيۏرسيتي مليسيا ڤهڠ السلطان عبدالله
UNIVERSITI MALAYSIA PAHANG
AL-SULTAN ABDULLAH

branch from the aortic arc, are in charge of feeding the brain, faces, and neck with oxygenated blood.

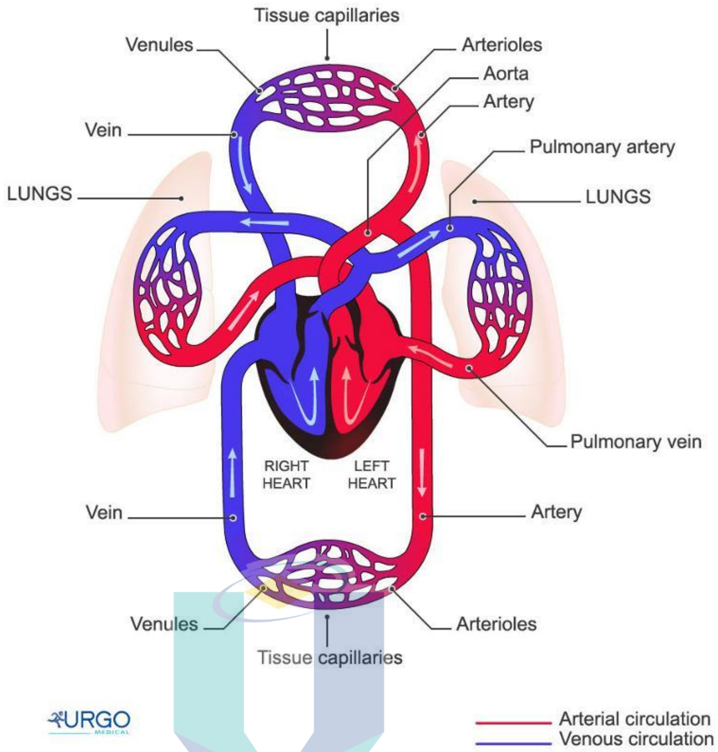

Figure 2.1 Cardiovascular system in human

Source: https://sphweb.bumc.bu.edu/otlt/mph-modules/ph/ph709_heart/ph709_heart2.html

UMPSA
اونيۏرسيتي مليسيا ڤهڠ السلطان عبدالله
UNIVERSITI MALAYSIA PAHANG
AL-SULTAN ABDULLAH

The common carotid artery further divides into the internal carotid arteries (ICA) and external carotid arteries (ECA) as shown in Figure 2.2. The carotid bulb, which is a small enlargement of the ICA immediately distal to the bifurcation point, serves as the brain's direct blood supply. The face muscle and external skull structure are supplied with blood through the ECA, which has a reduced luminal diameter.

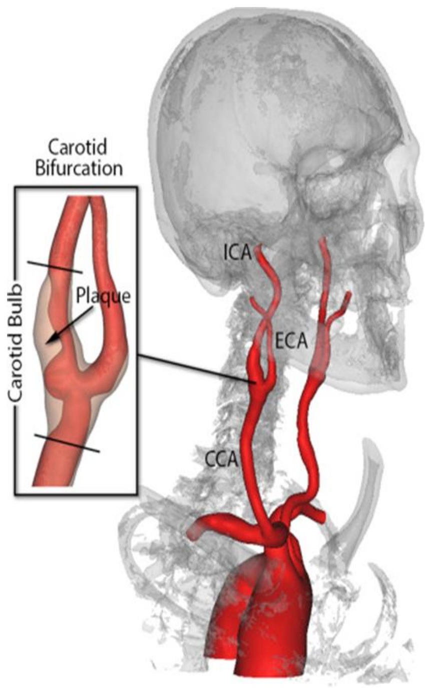

Figure 2.2 A set of carotid arteries in the neck. CCA, ICA, and ECA represent the common, internal, and external carotid artery, respectively (Moradicheghamahi et al., 2020)

The carotid arteries are composed of three layers of tissue, namely tunica intima, tunica media and tunica adventitia which include all arteries [(Yazdi et al., 2018),(S. Li et al., 2023)]. The vessel wall receives strength from these three layers, enabling it to endure high blood pressure. The inner layer, known as the intima, is endothelium, a smooth tissue. The media is a layer of muscle that enables arteries to withstand the intense heartbeat pressure. The adventitia, which is the last layer, is a connective tissue that anchors arteries to the adjacent tissues.

2.2.2 Carotid Artery Stenosis

Carotid artery stenosis is a narrowing of the lumen of the carotid artery and may block blood supply to the brain. The lipid and fatty acid deposits that result in the formation of atherosclerotic plaque, which narrows the artery wall. It could result in thromboembolism, one of the main causes of ischemic stroke, if untreated (Figure 2.3). Stroke has consistently recorded the second highest mortality rate globally for the last 15 years (WHO, 2016) and is a leading cause of long-term disability.

The risk of stroke is directly correlated with the severity of carotid stenosis, according to the NASCET research (North American Symptomatic Carotid Endarterectomy Trial). According to the study, internal carotid artery stenosis was linked to strokes at varied rates (70-79%, 80-89%, and 90-99%). ACAS (Asymptomatic Carotid Atherosclerosis Study) and ACST (Asymptomatic Carotid Surgery Trial), two additional important studies, also showed that stroke risks were increased in asymptomatic patients with at least 60% stenosis. A second randomised trial, the European Carotid Surgery Trial, looked at 3,024 symptomatic patients with above 80% stenosis and found that there was a 26.5% chance of having a major stroke or dying after three years without surgery. The areas of artery bifurcation and curvature are more likely to be the first places atherosclerosis or stenosis develops and are frequently disturbed by WSS and flow disturbance (Sousa et al., 2016).

One of the main risk factors for atherosclerosis is the high plasma content of low-density lipoprotein (LDL), which is transported in the blood. Atherosclerosis is also known as hardening of the arteries, where plaque build-up results in an inflammatory disease (Tarbell et al., 2003). Due to the deposition of LDL molecules, the inner artery wall (intima) stiffens, which promotes further LDL accumulation and the development of plaque. If the plaque breaks, releasing its contents into the bloodstream, the cerebral artery may become blocked. Blood flow to the area supplied by that artery may be reduced by a stenosis if the degree of restriction is severe enough. There are three key stages of the on development of atherosclerosis in Figure 2.3 (Libby & Plutzky et al., 2000). In the early stage, fatty streaks in the intima that include lipid deposits both within and outside of cells begin to emerge. There are no symptoms at this moment, and the fatty stripe may even become smaller with time. However, the altered layer of lipids creates a pro-inflammatory environment that allows leukocyte migration and foam cell growth since this step involves lipid entry and modification as a result of probable endothelial dysfunction.

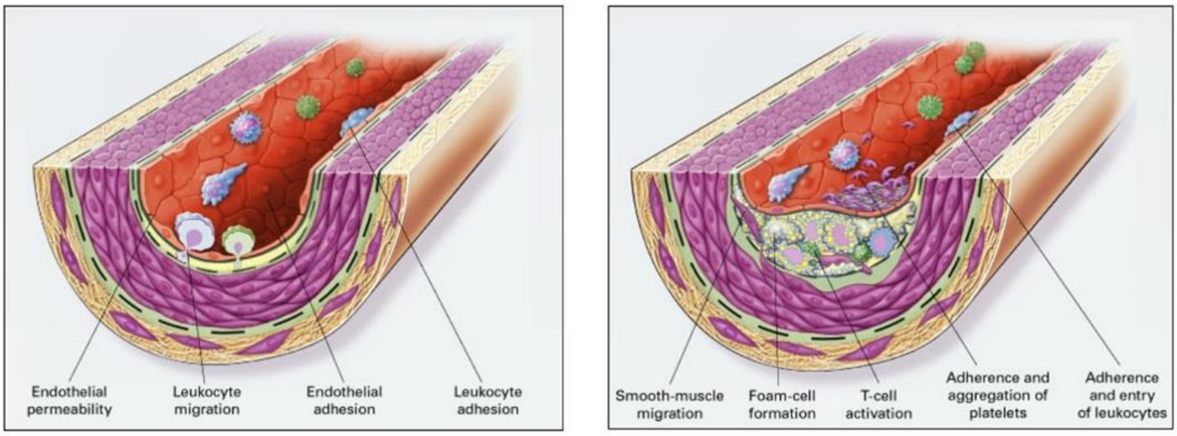

Figure 2.3 The formation of atherosclerosis. formation of fatty streaks (right) (Libby & Plutzky et al., 2000)

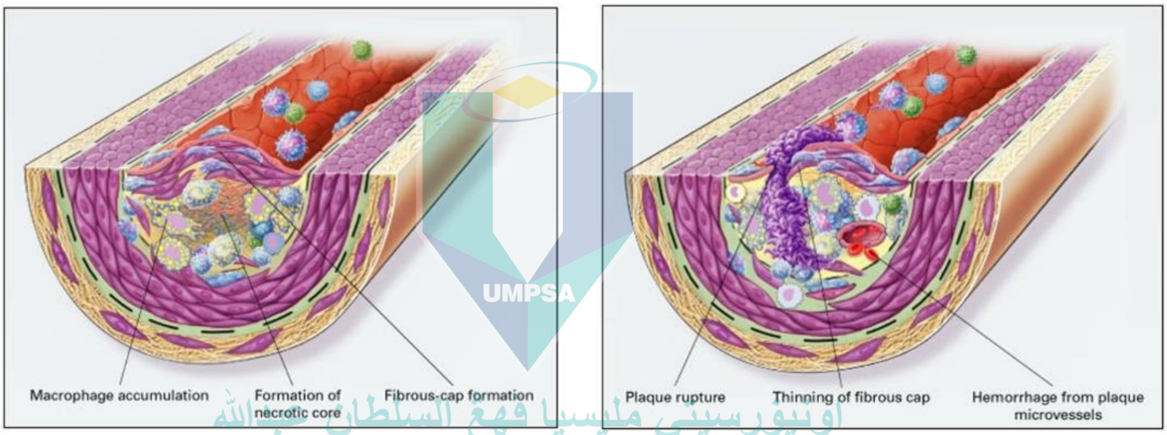

UMPSA
UNIVERSITI MALAYSIA PAHANG
AL-SULTAN ABDULLAH

Figure 2.4 Fibrous cap formation and necrotic core (left) and plaque rupture (right) (Libby & Plutzky et al., 2000)

The second stage of the plaque's development occurs in the inner layer of the vessel wall. The bulk of the plaque is composed of the proteoglycan-collagen matrix, smooth muscle cells, and very few to no invading inflammatory cells. Because endothelial function is compromised, circulating LDL can also reach the intima. Following its attachment to the proteoglycan, LDL builds up in the intima layer, which is an important phase because LDL may undergo chemical alterations while residing in the inner layer of the vessel wall. A fibrous crown and a necrotic core that is lipid-rich are developing at this stage (Figure 2.4). The plaque contains dead foam cells, macrophages, smooth muscle cells and extracellular matrix.

Finally, in the last stage, continuous plaque growth may cause fibrous cap to rupture. A vulnerable plaque contains a large lipid-rich necrotic core covered by a thin fibrous cap (Stroud et al., 2000). Fragility of the fibrous cap may be caused by several factors, including inflammation, size of lipid core, fibrous cap thinning, plaque calcification and haemorrhage in the plaque.

2.3 Treatment for Carotid Artery Stenosis

Carotid artery stenosis can be treated by either open surgery called carotid endarterectomy (CEA) or by a non-invasive procedure called carotid artery stenting (CAS) as shown in Figure 2.5. Stent implantation is a less invasive technique for treating the narrowed artery and can restore blood to the brain (Ho et al., 2020) whilst endarterectomy is an open surgery procedure to open narrowed or blocked blood vessels that supply blood to the heart.

Carotid artery stenting (CAS) is a recognised alternative procedure to Carotid Endarterectomy (CEA) for the treatment of severe carotid stenosis (Johari & et al., 2020). In-stent restenosis has been reported as a long-term complication that can arise from CAS. After 30 days following stent implantation, re-blockage or restenosis of the artery frequently occurs, which results in complications with the geometrical stent strut arrangement. (Paisal et al., 2019). On the other hand, CEA is open surgery that removes plaque that accumulates inside the artery. During the surgery, a tiny cut or incision on patient neck and the wall of artery affected to remove plaque (Figure 2.5).

Because CAS is less invasive and preferred by patients with high risk of surgery or restenosis compared to CEA, the number of patients who have had CAS has been rising (Sardar et al., 2017). However, due to the need to know the long-term effectiveness and safety results employing CAS and CEA, the therapy for carotid stenosis is still debatable and contentious. Another significant disadvantage of CAS and CEA is restenosis, which can result in an ipsilateral stroke, stenosis greater than 70%, or complete occlusion (Brott et al., 2016).

UMPSA
UNIVERSITI MALAYSIA PAHANG
AL-SULTAN ABDULLAH

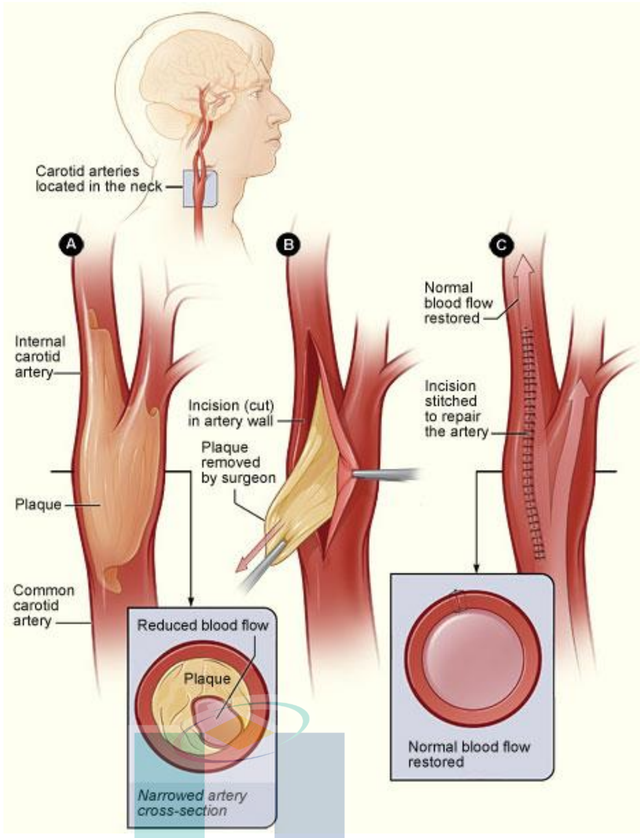

Figure 2.5 The procedure surgery carotid endarterectomy (CEA)

Source: https://surgery.ucsf.edu/conditions--procedures/carotid-endarterectomy.aspx

UMPSA
اونيۏرسيتي مليسيا ڤهڠ السلطان عبدالله
UNIVERSITI MALAYSIA PAHANG
AL-SULTAN ABDULLAH

2.4 Role of Haemodynamic Factor

Many studies have highlighted the role of haemodynamic forces on the vessel wall in the development of vascular pathologies such as atherosclerosis, aneurysm, post-stenotic dilation and arteriovenous malformations (Wood et al., 1999). Local geometric features of the artery are key factors in determining the biomechanical stresses that regulate the atherosclerotic lesion progression in the carotid artery bifurcation.

2.4.1 Wall Shear Stress and Related Parameters

There are several haemodynamic variables to evaluate performance of pulsatile flow in human body. Wall shear stress is a metric that is frequently studied in haemodynamic systems. Wall shear stress for typical arteries ranges from 10 to 70 dyne/cm^2. WSS values between -4 and 4 dyne/cm suggest a location that is prone to the development of atherosclerosis, whereas WSS values more than 70 dyne/cm^2 indicate a severe shear thrombosis of the artery wall (Paisal et al., 2019). Wall shear stress is a drag exerted by following blood arterial wall. Wall shear stress can be calculated using the following equation:

$$\tau = \mu \frac{du}{dr} \tag{2.1}$$

where τ is the shear stress, μ is the fluid or blood viscosity, u is the blood velocity, r is the radial position.

In addition to the disease states of stenosis (constriction) and aneurysm, geometrical characteristics of the channel, such as bifurcation, branching, bending, curvature, and tortuosity, may also cause local flow disruptions [(Fukuda et al., 2022) and (N.H.Johari et al, 2019)]. Numerous studies have demonstrated how geometric parameters affect WSS and pressure distribution at various circulatory system vessels. There might be areas of divided flow, recirculation, high and low shear stress, and reattachment. High WSS at the stenosis site might weaken the fibrous cap, causing it to break and release the plaque's contents into the bloodstream (Slagger et al., 2005). The results of this circumstance might lead to a stroke and are quite dangerous.

UMPSA
اونيۏرسيتي مليسيا ڤهڠ السلطان عبدالله
UNIVERSITI MALAYSIA PAHANG
AL-SULTAN ABDULLAH

2.4.2 Velocity Profile

The velocity profile of a fluid is the distribution of velocities across the cross-section of the flow. It is affected by many factors, including the viscosity of the fluid, the geometry of the flow, and the velocity of the flow itself. One of the most important factors affecting the velocity profile is the Reynolds number.

The Reynolds number is a dimensionless parameter that characterises the flow regime of a fluid. It is defined as the ratio of inertial forces to viscous forces and is given by:

$$Re = \frac{\rho VD}{\mu} \tag{2.2}$$

where ρ is the density of the fluid, V is the velocity of the fluid, D is the characteristic length of the flow, and μ is the dynamic viscosity of the fluid. Previous studies have investigated Reynolds number before and after endarterectomy of carotid artery stenosis (Guerciotti et al., 2016). After endarterectomy, the carotid artery becomes normal and the Reynolds numbers becomes low and laminar flow.

The Reynolds Number is important to predicting the flow behaviour either laminar flow, transitional flow and turbulent flow. At low Reynolds Number ($Re<2000$), flow moves in laminar flow. Next, transitional flow occurs in an intermediate range of Reynolds numbers ($2100 < Re < 4000$). The flow is unstable and alternates between laminar and turbulent. While turbulent flow occurred when $Re > 4000$. The turbulent flow is inertial forces take over the fluid movement becomes chaotic and hard to predict. Turbulent flow is marked by swirling patterns, eddies and a greater degree of mixing.

In conclusion, the interaction between velocity patterns and the stress on the walls offers information about the development of atherosclerosis. Knowing how blood flow factors impact the building up and advancement of plaques is crucial, for creating treatments and approaches to prevent or lessen the impact of cardiovascular disease caused by atherosclerosis.

2.5 Recent studies on Particle Image Velocimetry

UMPSA

Previous studies in computational modelling have used different medical imaging techniques in capturing the flow domains such as magnetic resonance imaging (MRI), computational tomography (CT) scan, optical coherence tomography (OCT) and intravascular ultrasound (IVUS). The acquired medical image were segmented based on thresholding and region growing technique using an available software such as MIMICS, CAD and Segment. Blood vessels are not homogeneous in diameter or wall thickness and have surface complexity and irregularity especially at bifurcation.

اونيۏرسيتي مليسيا ڤهڠ السلطان عبدالله
UNIVERSITI MALAYSIA PAHANG
AL-SULTAN ABDULLAH

Majority of previous studies have used idealised or simplified model for PIV experiments with the aims to compare different phantom geometry cases. A realistic patient-specific phantom requires special attention to the irregularities of the wall surface and its thickness (Johari et al., 2020). In carotid geometries, bifurcation and curvature are also essential considerations and are difficult to be created as a 3D phantom (Chen et al., 2020).

The only study with patient-specific phantom as shown in Table 2.1 reconstructed the geometry based on the MRI images using MIMICS software (N. H. Johari et al., 2019). Other studies used idealised phantom geometries due to the difficulties in the rapid prototyping (RP) of the mold and casting techniques that require advancement of the process. During the mold casting, the structure must be bubble-free, the wall must be transparent with a proper refractive index, suitable for PIV analysis. Conventional phantom-making process involve both mold and core fabrication and casting procedure. Four studies used lost-core casting technique without specific information on the core making process (N. H. Johari et al., 2019), (Medero et al., 2018), (Sharma et al., 2020), (DiCarlo et al., 2019) whilst three studies constructed the cores using steel or alloyed using computer numerical control (Yazdi et al., 2019), (P. H. Geoghegan et al., 2012), (Zhou et al., 2017) before the casting.

The advancement of technology in 3D printing has enabled manufacturing of low-cost 3D flow phantom to be used with a mold casting technique. Three studies have involved 3D printer in the printing the phantom core for the mold [(Yazdi et al., 2019), (P. H. Geoghegan et al., 2012), (Zhou et al., 2017)]. (Patrick H. Geoghegan et al., 2017) and (P. H. Geoghegan et al., 2012) are among the earliest researchers that utilised 3D printing in the core and mold making for the rigid and compliant phantoms. The core for the mold was usually printed usually using polylactic acid (PLA) materials. For the rapid prototyping (RP) of phantom materials, polydimethylsiloxane (PDMS), polyvinyl alcohol (PVA) and silicone (Sylgard-184) were mostly used. (DiCarlo et al., 2019) show the PIV-compatible carotid bifurcation phantoms were produced like a box in the square PDMS compartment using lost-core casting. The study varied the stenosis size in the internal carotid artery at 30%, 50% and 70% according to NASCET to see the post-stenotic flow conditions.

Table 2.1 Recent studies on carotid artery using PIV

Articles	Geometry	Image source	Software	RP technique	RP material	Wall characteristics	Analysis Method
(Zhou et al., 2017)	Idealised, stenotic			Alloyed mold	Polyvinyl alcohol (PVA) cryogel	Rigid	Echo PIV
(Medero et al., 2018)	Idealised, normal			Lost-core casting	Polydimethylsiloxane (PDMS) Silicone	Rigid	Stereo-PIV
(N. H. Johari et al., 2019)	Patient-specific, stenotic	MRI	MIMICS	Lost-core casting	PDMS Sylgard-184 silicone	Rigid	PIV
(Sharma et al., 2020)	Idealised, stenotic			Lost-core Casting	Acrylic	Rigid	PIV
(DiCarlo et al., 2019)	Idealised, stenotic	NASCET criteria (Barnett, 1991)		Lost-core casting	PDMS, Silicone	Rigid	Stereo-PIV
(Yazdi et al., 2019)	Idealised (Aortic arch)		SolidWorks	FDM 3D printed, CNC mold, Casting	ABS plastic, PVA, Sylgard-184 silicone	Compliant	Stereo-PIV
(Hong et al., 2017)	Idealised, stenotic			FDM 3D printed and PLA	PDMS	Rigid	PIV
(Patrick H Geoghegan et al., 2016)	Idealised, stenotic		SolidWorks	3D Printed, CNC mold	Sylgard-184 silicone	Compliant	Stereo PIV

UMPSA
UNIVERSITI MALAYSIA PAHANG
AL-SULTAN ABDULLAH

2.6 Computational Fluid Dynamic Simulation on Carotid Artery

The use of advanced Computational Fluid Dynamics techniques has the potential to shed more light in the further understandings of the causes of the disease and perhaps in its early diagnosis (Kumar et al., 2020). Moreover, CFD and FSI are currently widely applied in the study of blood flow parameters and their alterations under pathological conditions, which are important indicators for diagnosis of atherosclerosis (Lopes et al., 2020).

Computational fluid dynamics can be used to study and analyse the flow of blood in the human body (Kamada et al., 2022). This can be useful for understanding the flow patterns and hemodynamic in various parts of the body, as well as for predicting the effects of different factors on blood flow. Moreover, CFD simulations of blood flow are typically based on mathematical models that describe the motion of blood as it moves through the vascular system. These models often include factors such as blood viscosity, vessel geometry, and the presence of obstacles or stenoses. The results of CFD simulations can be used to visualise the flow patterns and to predict quantities such as blood velocity, pressure, and shear stress at different points in the vasculature. There are many potential applications of CFD in the study of blood flow, including the analysis of arterial stenoses [(Stroud et al., 2000),(Schirmer & Malek et al., 2007)], the design of stents [(Johari & et al., 2020),(Elshin Joel & Anburajan et al., 2013)] and other medical devices, and the prediction of the effects of different interventions on blood flow (Syed et al., 2023).

UMPSA
اونيۏرسيتي مليسيا ڤهڠ السلطان عبدالله
UNIVERSITI MALAYSIA PAHANG
AL-SULTAN ABDULLAH

Computational fluid dynamic is numerical method to obtain physical properties of mass and momentum such as velocity and pressure of fluid flow by solving conservation equations – the continuity and Navier-Stokes equation (Kamada et al., 2022). Furthermore, studies have provided valuable results for understanding the pathology of carotid artery Conditions such as flow separation or flow recirculation in areas with low or high shear stress have shown to play a role in the formation or development of atherosclerosis [(DiCarlo et al., 2019) , (N. H. Johari et al., 2019). & (Sousa et al., 2016)]. The areas susceptible to atherosclerosis at carotid bifurcation point are identified as the point from where CCA is bifurcated to ICA and ECA and the carotid sinus (Akagawa et al., 2016). In addition to parameters such as hypertension, hyperglycemia and hyperlipidemia, the carotid geometry can affect the pattern of blood flow and increase (Moradicheghamahi et al., 2020). Numerical simulations such as computational fluid dynamics (CFD) based on medical imaging have been employed to analyse blood flow in different arteries with and without luminal stenosis (Mendieta et al., 2020)

Recent studies on the carotid artery spanning from 2018 to 2022, encompassing both patient-specific and idealized geometries, are summarized in Table 2.2 . In terms of geometry type, the simulations predominantly focus on healthy cases and those involving stenosis. However, only one study (Yao et al., 2019) has explored stented geometries. Notably, in this case, although the geometries were derived from patients who had undergone stent placement, they did not include the indentations caused by the stent struts.

As for the flow types considered in these studies, blood flow simulations have primarily modeled laminar flow, with only one instance of pulsatile flow being investigated. Laminar flow is characterized by a fluid moving through a tube in such a manner that it exhibits a parabolic flow velocity distribution. This results in higher velocities at the tube's center, gradually decreasing towards the edges (Lopes et al., 2020). While (Fukuda et al., 2022) delved into the hemodynamic risk factors leading to the development of carotid artery stenosis by employing CFD to simulate pulsatile flow, offering a critical insight into the dynamic nature of blood flow and its implications for arterial health.

The hemodynamic parameters mostly investigated on velocity profiles, and wall shear stress (WSS) and indices, i.e. time-average wall shear stress (TAWSS), time-average wall shear stress gradient (TAWSSG), oscillatory shear index (OSI), relative residence time (RRT), as shown in Table 2.2. Validation of the results is a very important step in any kind of simulation and, unfortunately, it is frequently overlooked (Lopes et al., 2020). CFD is commonly used and powerful tool for researching the role of blood flow in disease processes (Campbell et al., 2017) but requires a rigorous validation with

UMPSA
اونيۏرسيتي مليسيا ڤهڠ السلطان عبدالله
UNIVERSITI MALAYSIA PAHANG
AL-SULTAN ABDULLAH

experimental data. Table 2.2 shows none of the selected articles investigate the validity of their CFD results with experimental measurements.

UMPSA
اونيۏرسيتي مليسيا ڤهڠ السلطان عبدالله
UNIVERSITI MALAYSIA PAHANG
AL-SULTAN ABDULLAH

Table 2.2 Recent studies on carotid artery bifurcation using CFD

Articles	Artery	Type Geometry	Viscosity model	Flow type	Parameters
(Fukuda et al., 2022)	Carotid	Stenosed	Newtonian	Pulsatile	WSS/TAWSS/ TAWSSG/OSI
(Ningappa et al., 2022)	Carotid	Healthy	Newtonian	Laminar	V, P, Vorticity, TAWSS, Helicity
(Hernández-López et al., 2021)	Carotid	Healthy	Newtonian	Laminar Transient	TAWSS, OSI
(Sia et al., 2019)	Carotid	Stenosed	Newtonian	Laminar	V, VS, WSS, OSI, P
(S. H. Lee et al., 2019)	Carotid	Healthy	Newtonian, Casson, Carreau, HCT-based equation	Laminar	V, WSS
(Azar et al., 2019)	Carotid	Healthy	Newtonian,	Laminar	V / WSS
(Yao et al., 2019)	Carotid	Post-Stent placement	Newtonian	Laminar	WSS, TAWSS, OSI, RRT
(Kumar et al., 2019)	Carotid	Stenosed	Newtonian, Carreau	Laminar	V, VS, VV, WSS
(C. Li et al., 2019)	Carotid	Healthy and Stenosed	Newtonian	Laminar	V, VS, VV, VO, WSS, TAWSS, P

UMPSA
اونيورسيتي مليسيا قهڠ السلطان عبدالله
UNIVERSITI MALAYSIA PAHANG
AL-SULTAN ABDULLAH

2.7 In Vitro Technique to Analyse Haemodynamic

2.7.1 Experimental Analysis of a Haemodynamic

In experimental analyses, there are many methods to analyse the blood flow such as particle image velocimetry (PIV) and laser doppler fusion. Particle image velocimetry is a laser based optical measurement technique to capture fluid velocity fluids. This technique uses a light source of high intensity to illuminate small tracer particle across plane of interest within phantom. The PIV setup consists of a laser source to highlight the plane for the highspeed camera to record, 3D phantom geometry, a set of pumps for the flow profile generator and a computer interface for the data processing (Yazdi et al., 2018).

Successful PIV analysis includes transparent and physiological relevant phantoms because the blood flow can be easily observed during experiment (Yousif et al., 2011). The assumption of flow symmetry is commonly used to obtain the velocity vector field in PIV measurements. This indicates that symmetry of the flow with regard to a certain plane or axis is expected. Viewing the 3D model from any angle can cause the optical distortion across image. Thus, need a proper calibration step is needed by placing Cartesian grid calibration on a target plane during the experiment.

UMPSA
اونيۏرسيتي مليسيا ڤهڠ السلطان عبدالله
UNIVERSITI MALAYSIA PAHANG
AL-SULTAN ABDULLAH

2.7.1.1 Particle Image Velocimetry (PIV) and Stereo-Particle Image velocity (SPIV)

Particle image velocimetry is a laser-based optical two dimensions (2D) measurement technique to capture fluid velocity fluids. On the other hand, SPIV employs on three-dimension (3D) measurement technique on fluid flow shown in Figure 2.6. This technique uses a light source of high intensity to illuminate small tracer particle across plane of interest within phantom. The PIV measurement may determine 3D flow phantom model's internal and external flow characteristics and provide parametric data such as velocity and wall shear stress data.

Moreover, PIV also could be useful for evaluating and validating numerical works that differ in their solutions according to the assumptions made (Yazdi et al., 2018). The

PIV setup consists of a laser source to highlight the plane for the highspeed camera to record, 3D phantom geometry, a set of pumps for the flow profile generator and a computer interface for the data processing (Yazdi et al., 2018). The difference of mean velocity data measured by the 2D PIV and SPIV techniques is nearly proportional to the mean out-of-plane velocity component (Yoon & Lee et al., 2002).

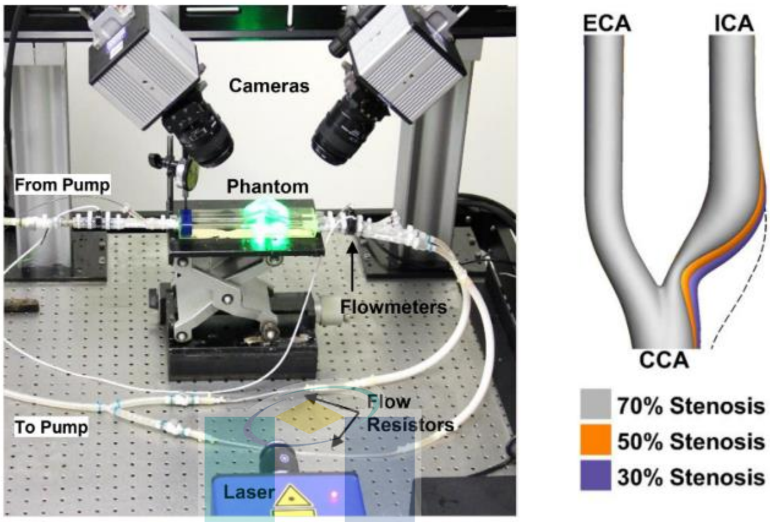

Figure 2.6 SPIV experimental setup that includes flow circuits and carotid bifurcation with different stenosis sizes (Akagawa et al., 2016)

UMPSA
اونيۏرسيتي مليسيا ڤهڠ السلطان عبدالله
UNIVERSITI MALAYSIA PAHANG
AL-SULTAN ABDULLAH

2.7.1.2 Micro-Particle Image Velocimetry

Micron resolution particle image velocimetry (Micro-PIV) is a tool for measuring the velocity profile across a plane in a microfluidic device illustrate in Figure 2.7. Because of the small dimensions of the flow field in micro channel flow, it is impossible to use the conventional PIV systems to obtain two orthogonal planes for optical access to the flow field. Instead, Micro-PIV systems use a volume illumination technique where the light source and the view field are introduced through the same optics. With this approach the focal plane is moved down through the flow field to map the entire volume. Micro-PIV and PIV is a whole-field, non-intrusive measurement technique where the fluid velocity is measured by recording the displacement of small tracer particles added to the fluid.

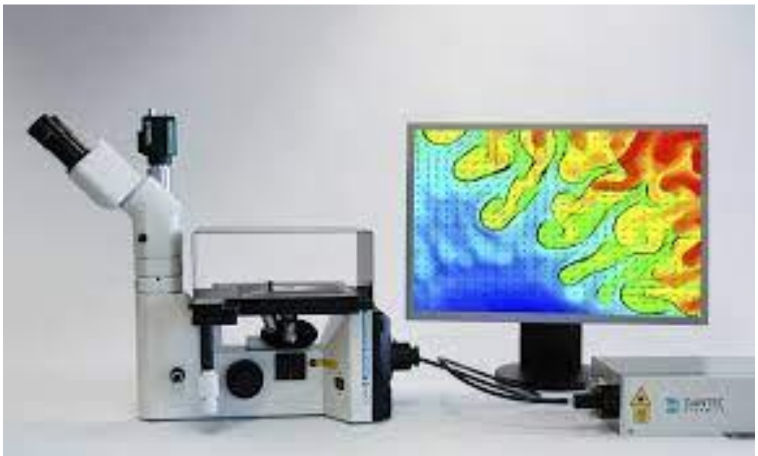

Figure 2.7 Micro-PIV used for analysing a micro-particle.
Source: https://images.app.goo.gl/84DSJN2LiVvVRXdK7

2.7.1.3 Tomography Particle Image Velocimetry (TPIV)

Tomographic Particle Image Velocimetry (Tomo-PIV) is an advanced technique for obtaining three-dimensional velocity measurements, as illustrated in Figure 2.8. This method expands upon the traditional PIV approach by enabling the measurement of velocity across a volumetric space within a fluid. Unlike conventional PIV, which provides two-dimensional planar data, Tomo-PIV captures comprehensive three-dimensional flow information. This is achieved through the simultaneous use of multiple high-speed cameras, typically four, arranged to observe the fluid volume from different angles. The images captured are then reconstructed to provide a detailed three-dimensional velocity field of the fluid. Tomo-PIV is particularly advantageous for studying vortical structures, turbulent flow, and intricate interactions within the fluid, providing insights into phenomena like flow separation, mixing processes, and the development of turbulence.

However, most tomographic measurements are conducted at a relatively low frequency or within a small volume of measurement. This limitation arises from the computational and logistical challenges associated with capturing and processing the vast amounts of data required for high-resolution, three-dimensional flow visualization. Despite these challenges, Tomo-PIV stands as a powerful tool for fluid dynamics research, offering unprecedented detail and accuracy in the study of three-dimensional

UMPSA
اونيورسيتي مليسيا ڤهڠ السلطان عبدالله
UNIVERSITI MALAYSIA PAHANG
AL-SULTAN ABDULLAH

flow patterns. The integration of Tomo-PIV into experimental fluid mechanics has paved the way for significant advancements in our understanding of complex flow phenomena.

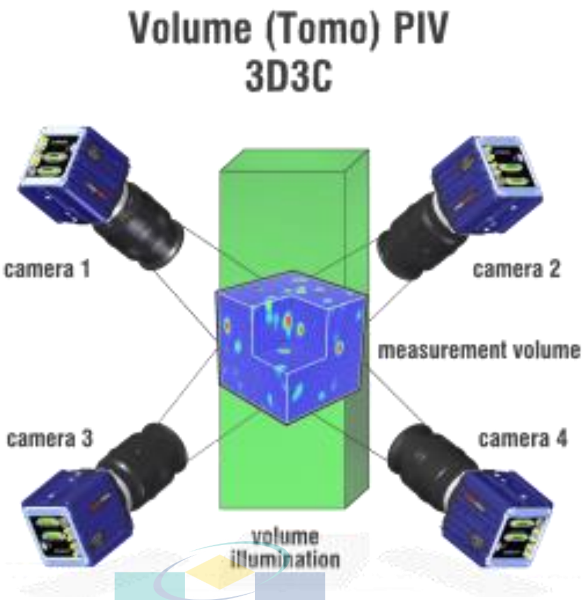

Figure 2.8 Tomographic Particle Image Velocimetry (TPIV)
Source: https://images.app.goo.gl/stw6bFCs5oeLoxLu8

2.8 The studies on different location of stenosis

Previous studies have investigated the effect of severity size of stenosis to the blood flow (DiCarlo et al., 2019), the influence of bifurcation angle (Hong et al., 2017), and turbulence model for stenosis cases. (DiCarlo et al., 2019) has analysed the effect of different stenosis sizes i.e. 30, 50 and 70% on the hemodynamic parameters. The study reported that only the 70% stenosis size affects the blood flow to become abnormal at the downstream of the stenosis. Hence, a proper turbulent model is required to visualize the flow vorticity and eddy viscosity at that area. (N. H. Johari et al., 2019) has compared the effectiveness of two promising turbulence models, i.e. Reynold-averaged Navier-Stokes (RANS) shear stress transport- transitional model (SST-Tran) and large eddy simulation (LES).

Both SST-Tran and LES models were compared with particle image velocimetry (PIV) measurement to evaluate the velocity profiles in a patient-specific carotid bifurcation model with 80% stenosis size. Both SST-Tran and LES predicted the

UMPSA
UNIVERSITI MALAYSIA PAHANG
AL-SULTAN ABDULLAH

experimental velocity profiles reasonably well, with LES being slightly superior especially at the post-stenotic area. However, SST-Tran also managed to capture important flow features as observed in the experiment although slightly differed distal to the stenosis. Other studies like in (Banks & Bressloff et al., 2007; Tan et al., 2011) also reported the influence of stenosis sizes in idealized straight carotid and patient-specific carotid geometry (N. H. Johari et al., 2019) that extend the flow separation and recirculation zone distal to stenosis.

Based on the previous carotid stenosis studies, the severity of stenosis size is reported to cause different levels of disturbed flows especially in the downstream of the stenosis. However, the study on the effect of location of the severe stenosis is still lacking. Hence, the present study aimed to investigate the influence of stenosis locations (Lu et al., 2019) that contribute to higher risk of flow disturbances. The decrease of velocity field and flow separation zone will result in low wall shear stress that could potentially initiate progression of atherosclerosis (Nagargoje & Gupta et al., 2020).

2.9 Summary

This research is centered on the carotid artery, conducting experimental and computational studies to explore and compare the relationship between hemodynamic parameters and arterial diseases. Geometric features and hemodynamic parameters, including flow patterns, wall shear stress, and pressure distribution, are widely acknowledged as crucial indicators of stenosis formation and in-stent restenosis. In both particle image velocimetry and stereo particle image velocimetry (SPIV), the construction of geometry has been extensively investigated, encompassing comparisons between patient-specific and idealized geometries.

Additionally, the boundary conditions of wall geometry are examined, distinguishing between compliant and rigid models. The specification of boundary conditions, particularly at the velocity inlet, is determined based on the Reynolds number, categorizing the flow as laminar, transitional, or turbulent.

Moreover, these studies hold significant importance in understanding flow patterns, particularly for mitigating cardiovascular diseases in worldwide. Addressing the

UMPSA
اونيۏرسيتي مليسيا ڤهڠ السلطان عبدالله
UNIVERSITI MALAYSIA PAHANG
AL-SULTAN ABDULLAH

problem statement, the influence of different stenosis locations on patient risk is highlighted. Varied stenosis locations can induce complex and chaotic flow disturbances, correlating with plaque rupture and thromboembolic events. In essence, both CFD and PIV studies offer clinically relevant insights into hemodynamic factors affecting the development of atherosclerosis.

UMPSA
اونيۏرسيتي مليسيا ڤهڠ السلطان عبدالله
UNIVERSITI MALAYSIA PAHANG
AL-SULTAN ABDULLAH

CHAPTER 3

METHODOLOGY

3.1 Introduction

This chapter outlines the methodology employed throughout the study, organized into several phases aligned with the specific objectives. The initial phase involves the establishment of the experimental setup for particle image velocimetry measurements. This encompasses the preparation of the geometry phantom, configuration of the high-speed camera, calibration of lasers, and setup of related equipment. Following this, a comparative analysis is conducted on PIV measurements obtained through standard 2D PIV and Stereo-PIV, aimed at validating their accuracy. Subsequently, the PIV measurements serve as a means to validate computational fluid dynamics simulations performed on the identical geometry. In the final phase, the study delves into a comparative discussion of hemodynamic parameters across different stenotic geometries. This comprehensive approach ensures a systematic and rigorous investigation, aligning with the specific goals outlined in the study.

اونيۏرسيتي مليسيا ڤهڠ السلطان عبدالله
UNIVERSITI MALAYSIA PAHANG
AL-SULTAN ABDULLAH

3.2 Flow Chart of the Research

Figure 3.1 illustrates the comprehensive methodology adopted in this research, with a primary focus on investigating and analyzing flow features in the carotid artery using both patient-specific and idealized geometries. The study incorporates the utilization of particle image velocimetry measurements and computational fluid dynamics analysis.

A rigid phantom wall, replicating patient-specific carotid geometry, was fabricated to facilitate experimentation. Specifically, was semi-transparent polylatic acid (PLA) 3D printed phantom was employed in this experiment and undergo surface finishing to get better transparent than others phantom. The outcomes of both computational and experimental studies on patient-specific carotid arteries were meticulously compared to analyze blood flow behavior. The subsequent phase of the study focused on assessing the impact of high-risk location stenosis in the carotid artery on blood flow within the patient's artery. This aligns with the third objective, which involves a comparative analysis of different stenosis locations.

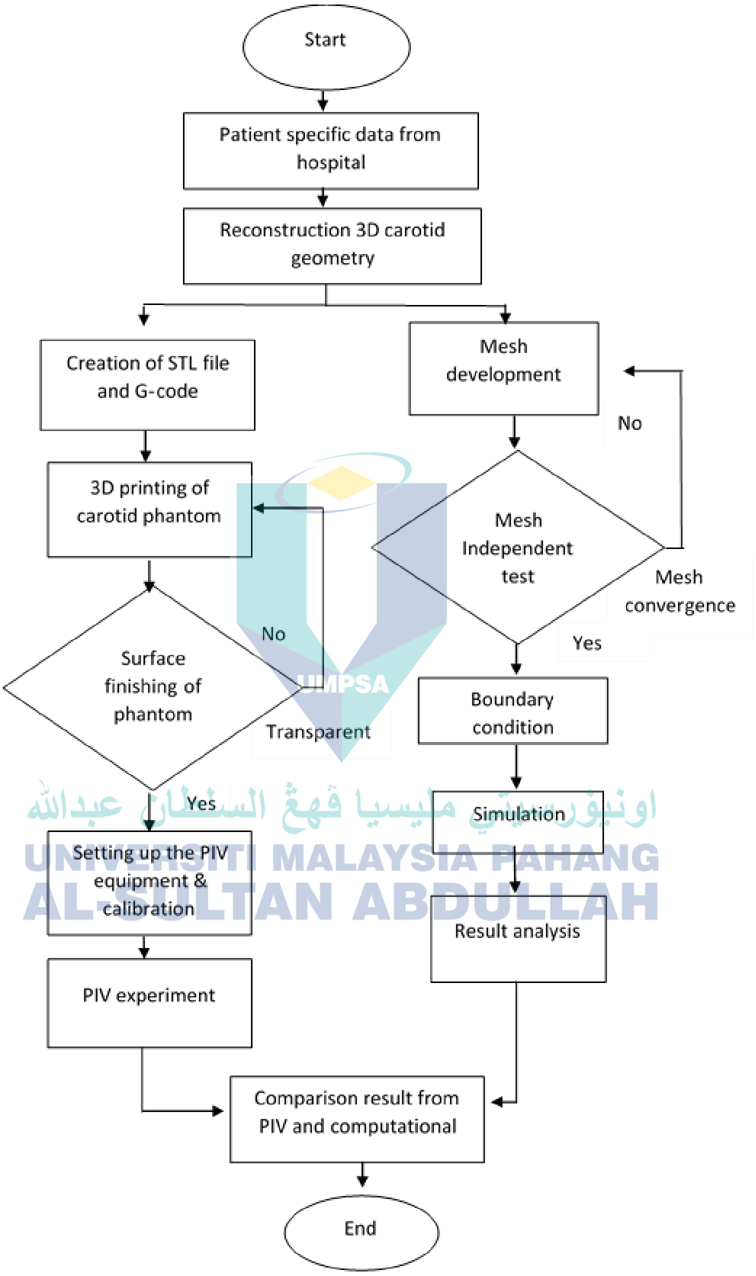

UMPSA
UNIVERSITI MALAYSIA PAHANG
AL-SULTAN ABDULLAH

Figure 3.1 Flow chart of overall methodology in this study

3.3 Geometry Construction

This study employed two carotid artery geometries based on the modified patient-specific and idealised carotid geometry for both PIV and CFD modelling. For the patient-specific carotid geometry, the model is based on the stented carotid of a 68-year-old male patient with asymptomatic chronic stenosis (90%). Comprehensive details regarding patient information can be found in (Johari et al., 2020). In parallel, the idealized model involves the reconstruction of three carotid artery bifurcations with different types of stenosis, referencing a recent clinical report by (Lu et al., 2019). These geometries feature a 70% stenosis size at the common carotid artery (CCA) to internal carotid artery (ICA), primarily situated in the carotid bulb but with variations in shape and location. Further details on the idealized geometry are available in 3.9, titled "Influence of Different Stenosis Locations."

3.3.1 Fabrication of Rigid Phantom for PIV experiment

To date, the most common method of flow phantom construction includes the core or mold making, casting using silicone and extraction (Yazdi et al., 2019). As the process is laborious and time-consuming, recent advances of 3D printing technology has enabled the flow phantoms to be constructed using transparent resin. The 3D printing techniques could print optically clear wall resolution, typically using PolyJet and Stereolithography (SLA) and PLA (Ho et al., 2020). This is an alternative low-cost option to study an internal flow in complex geometries. However, it requires special attention to meet the suitable refractive index as compared to conventional cast silicone.

In this PIV study, the CAD file created from the segmented post-stent geometry was scaled up to double of its original size. The scaled up geometry is required to enable the flow visualization using the high speed camera during PIV experiments. The same scaled-up geometry was used in all experiments and simulations to avoid flow comparison discrepencies. The phantom was 3D printed using SLA material. However,

UMPSA
اونيۏرسيتي مليسيا ڤهڠ السلطان عبدالله
UNIVERSITI MALAYSIA PAHANG
AL-SULTAN ABDULLAH

the transparent SLA was not fully transparent for this experiment. The reflective index was in between 1.3 – 1.6, as also reported by (Ho et al., 2020),.

Figure 3.2 shows different transparent phantoms A and B. The phantom A only undergo finishing outer surface of phantom, while phantom B underwent two finishing processes by cleaning its inside and outside using the splitting process on two parts which were internal carotid artery (ICA) and before bifurcation area. The geometry of carotid artery phantom was hollow with thickness of wall of around 2 mm. This study, both the geometry was not fully transparent of phantom. But, phantom B was used because it was more transparent than phantom A. Phantom A not used in the research because only finishing outside but phantom B undergo finishing both side inside and outside to get clear view of phantom.

اونيۏرسيتي مليسيا ڤهڠ السلطان عبدالله
UNIVERSITI MALAYSIA PAHANG
AL-SULTAN ABDULLAH

Figure 3.2	Carotid artery phantom.

## 3.4	Blood mimicking fluid (BMF)

A blood-mimicking fluids (BMF) is liquid substances that are designed to closely mimic the physical and chemical properties of human blood. In addition to research and development of medical equipment and procedures, these fluids are frequently utilised in medical simulations and training exercises. The viscosity and flow properties of blood are modelled in blood analogues.

Blood is a non-Newtonian fluid that is almost 3 to 4 times more viscous than water at high shear rates and considerably more so at low shear rates. Blood viscosity changes according to gender, age, health, and shear rate (Yazdi et al., 2018). In the PIV experiment, blood-imitating fluid is typically utilised to approximate the realistic characteristics of blood material. The fluid used in optical experiments to simulate blood has a refractive index, which is another crucial consideration. Optical refraction happens at each interaction of the model and liquid. By matching the refractive indices of the phantom and the fluid that simulates blood, this problem may be avoided.

The blood-mimicking fluid usually a mixture of glycerine (47.38%), water (36.94%) and sodium iodide (15.68%) (Shuib et al., 2011), (Noor & Johari et al., 2022) using a magnetic stirrer (Muda et al., 2019) by range of working temperature from 20 to 25°C (Yousif et al., 2011). The properties of this solution should replicate the human blood to get real flow feature especially in human body. The viscosity and density are mostly comparable with human blood as shown in Table 3.1. The range of refractive index blood-mimicking fluid is around 1.40-1.43 (Yousif et al., 2011),(P. H. Geoghegan et al., 2012),(Shuib et al., 2011). The refractive index blood-mimicking fluid use in this experiment was 1.334 using refractometer (anton paar/abbemat 300), which is slightly lower than in the previous studies. During this study, the BMF was used based on on the mixture of 60% of water and 40% glycerine (Webb et al., 2020) using magnetic stirrer at room temperature.

UMPSA
اونيۏرسيتي مليسيا ڤهڠ السلطان عبدالله
UNIVERSITI MALAYSIA PAHANG
AL-SULTAN ABDULLAH

Table 3.1 Properties of blood-mimicking fluid

Blood-mimicking fluid properties	**Composition**	**Glycerol, water and NaI salt**
	Density, ρ	≈ 1050 - 1100 kg/ m^3
	Refractive index	1.334
	Viscosity, μ	≈ 0.00400 – 0.00350 Pa.s

The BMF was added with polyamide seeding particles, 5µm (PSP) (Medero et al., 2018) as shown in Figure 3.3. The seeding particle was used to increase the visibility of flow in the phantom. It was mostly used for flow investigations in liquid and offered suitable tracers to generate sufficient light scattering (Huang et al., 2010), high visibility signals, particle density close to water density and excellent traceability to the flow. A safe handling of these particles is guaranteed because of their non-toxic, non-water polluting nature.

The seeding particles in the PIV experiment are illuminated with a light source i.e. laser, and images of the particles are captured using a high-speed camera (Yazdi et al., 2019). By analysing the movement of the seeding particles in successive images, it was possible to determine the velocity and flow patterns of the fluid at different points within the field of view.

UMPSA
UNIVERSITI MALAYSIA PAHANG
AL-SULTAN ABDULLAH

Figure 3.3 Polyamid seeding particles (PSP)

3.5 Equipment Preparation for PIV experiment

The equipments for the PIV experiment included a high speed camera with proper camera lens, steady flow pump, transparent connector tubes, transverse control for the camera positioning, dual laser machine and the geometry phantom. The carotid artery phantom was properlly attached to a holder throughout the experiments (Figure 3.4). The carotid artery was assembled and connected with transparent tubes at the inlet and outlets. A black cardboard was used to reduce the reflection during the experiment.

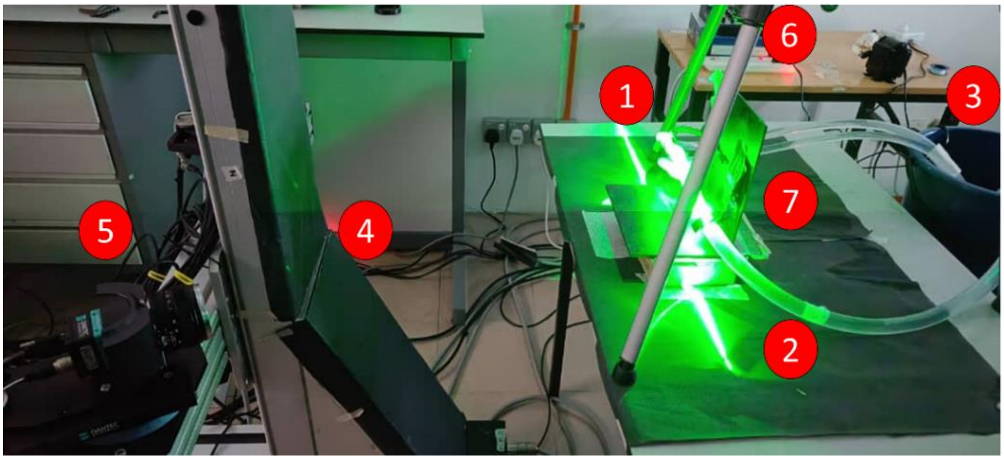

Figure 3.4 The equipment had been used during PIV. (1) The laser light, (2) connecting tubes, (3) flow pump and reservoir tank, (4) transverse platform, (5) high speed camera, (6) dual laser machine, and (7) the carotid phantom.

The equipment setup for the PIV experiment is depicted in Figure 3.4, showcasing the essential components required to conduct the experiment. These include a geometry phantom, a transparent tube facilitating fluid flow through the phantom, a simple centrifugal pump (EJET 6800 Pump), a transverse control connected to a high-speed camera with a lens, blood mimicking fluid, and a laser. In this particular experiment, the pump generated a steady flow of 0.82 m/s through the carotid artery geometry phantom. It's noteworthy that while the average blood velocity in the human carotid artery typically ranges between 0.3-0.4 m/s (W. Lee et al., 2014), and it was expected that the steady flow is no longer laminar.

The inlet velocity was deliberately doubled to ensure dynamic similarities with the geometry. The calculation of velocity is detailed as follows:

$$Q = AV \tag{3.1}$$

$$A = \frac{\pi d^2}{4} \tag{3.2}$$

$$Q_{in} = Q_{out} \qquad 3.3$$

$$Re = \frac{VD}{\mu} \qquad 3.4$$

where Q is the flow rate, A refers to area and V refers to velocity profile. D refer to the diameter of carotid artery phantom (inlet). Next, Re refer to Reynolds number while μ refer to viscosity in 3.4. The conservation of mass principle for fluid systems asserts that the mass flow rate into a control volume must equal the mass flow rate out of the control volume. In the PIV experiment, the BMF flow was estimated with a Reynolds number of approximately 4260.

The setup involved connecting a transparent tube to the phantom, pump, and tank, forming a complete system flow circuit. This tube, featuring both an inlet and an outlet, comprised three different diameters: 1.8 cm for the common carotid artery, 1.6 cm for the internal carotid artery, and 1.4 cm for the external carotid artery. The BMF flowed through the common carotid artery, internal carotid artery, and external carotid artery before returning to the tank.

UMPSA
اونيۏرسيتي مليسيا ڤهڠ السلطان عبدالله
UNIVERSITI MALAYSIA PAHANG
AL-SULTAN ABDULLAH

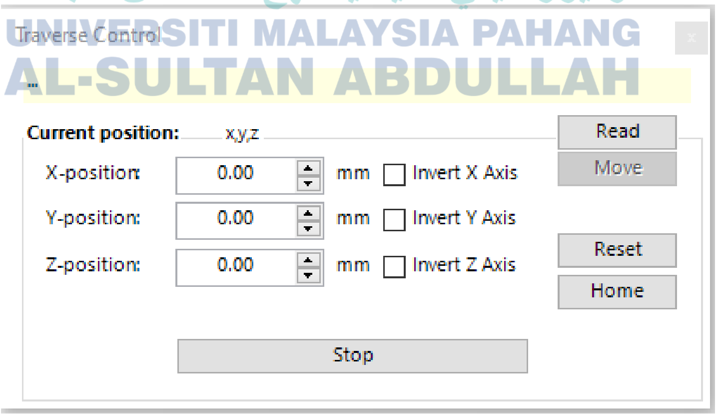

Figure 3.5 Transverse platform control monitor.

Figure 3.5 illustrates the Transverse System (Dantec Dynamics) that connected to the high-speed camera. This dynamic system is equipped with the capability to move along the x-, y-, and z-axes, allowing for specific height adjustments and positioning parallel to the region of interest on the phantom, facilitating image capture (refer to Figure 3.6). The transverse platform is additionally outfitted with a dual high-speed camera and adjustable lenses to ensure optimal positioning. The transverse system boasts a range of approximately 610 mm and a maximum speed movement of 25 mm/s.

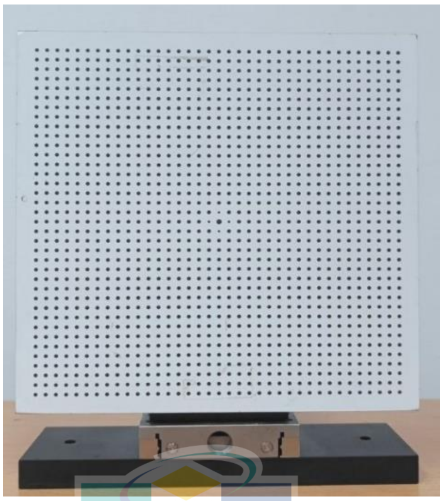

Figure 3.6 Calibration plane

Figure 3.6 shows the calibration plane for the image calibration purpose. To calibrate PIV images, it is important to ensure that the spatial and temporal calibration parameters, i.e., the pixel size and time interval, are accurately determined and applied during the image acquisition and processing stages.

UMPSA
اونيۏرسيتي مليسيا ڤهڠ السلطان عبدالله
UNIVERSITI MALAYSIA PAHANG
AL-SULTAN ABDULLAH

The camera used for the PIV experiment was a high-speed camera (FlowSense EO 2M, Dantec Dynamics, Denmark) with the resolution of 1600 × 1200 maximum pixels at 44 fps (Figure 3.7). The study also employed two types of camera lenses: Carl Zeiss lens and a micro lens (Nikon, AFS-S VR Micro-Nikkor lens) to increase the particle images visibility. The specification of lens used in this study shown in Table 3.2. The micro lens was used in 2D experiments to focus on a specific area of the phantom, whereas the Carl Zeiss lens was used in 3D. The micro lens was coated with an optical coating that absorbed or blocked light.

Table 3.2 The specification of the lens

Specification	Normal Lenses	Micro lenses
Type of lens	Carl Zeiss lens	G-type AF-S Micro-Nikkor lens
Focal length	50 mm	105mm
Maximum aperture	f/2	f/2.8

In this study, dual power laser system with the capacity of 135-15Hz was used. The system is a green continuous wave diode laser (Nd:YAG 800 mJ, Dantec Dynamics, Denmark) a class 4 laser category that could be harmful to individuals especially eyes and skins, depending on the power of laser density and the duration of exposure. Figure 3.8 shows that the dual laser system included the on/off laser button, internal and external laser. The dual laser system can be controlled by internal and external system during PIV experiment. The internal system can be controlled by system controller while the external system manually controlled on Dynamic studio.

Figure 3.7 High speed camera (FlowSense EO 2M). (1) the micro lens, and (2) the camera.

The specification of the dual power laser of PIV experiment includes of maximum output, pulse duration, wavelength and laser medium. The laser used in the experiment had a maximum output of 800 mJ and a pulse duration of 4ns. It operated at two wavelengths, i.e. 1064 nm and 532 nm, utilizing a Nd:YAG laser medium.

Next, the Dynamic studio (V8, Dantec Dynamics) software was used for PIV to analyse the character flow in the carotid artery phantom. The equipment connected to Dynamic Studio included transverse agent, FlowSenseEO, DualPower laser l35-15 and high-speed camera Figure 3.9. Figure 3.10 shows the Dynamic Studio on PC screen with its functionality.

(a) 

(b) 

(c) 

UMPSA
UNIVERSITI MALAYSIA PAHANG
AL-SULTAN ABDULLAH

Figure 3.8 Dual power laser Nd:YAG, (a) continuous green diode dispenser, (b) the dual laser system, and (c) the system controller

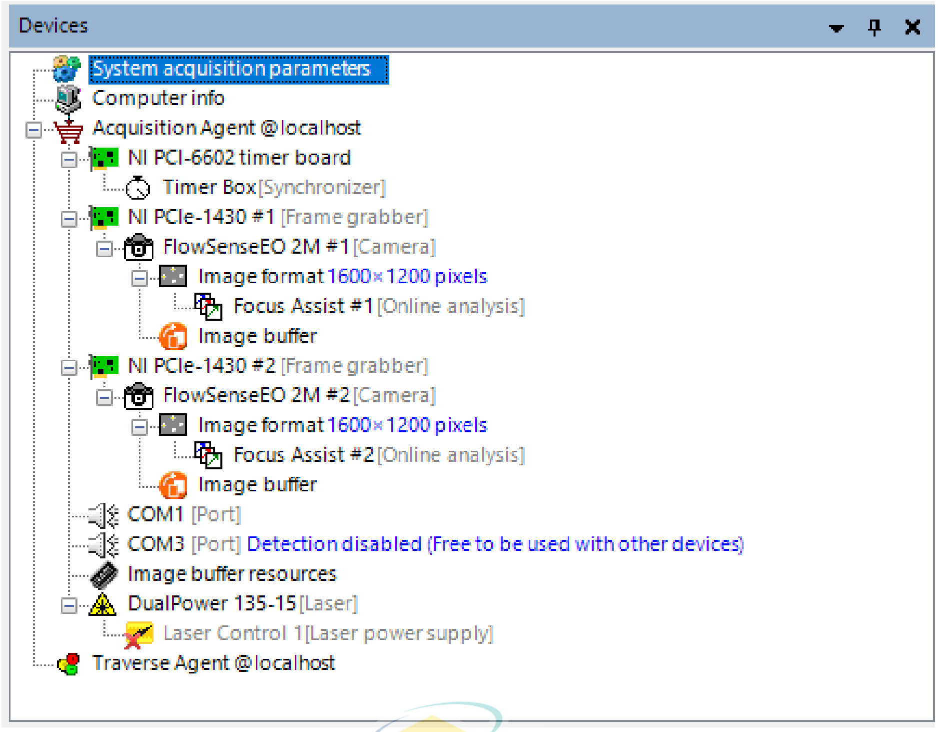

Figure 3.9 The device connected to the Dynamic Studio

Figure 3.10 The Dynamic Studio software screen

UMPSA
اونيۏرسيتي مليسيا ڤهڠ السلطان عبدالله
UNIVERSITI MALAYSIA PAHANG
AL-SULTAN ABDULLAH

3.5.1 Stereo-Particle Image Velocimetry (SPIV) and Particle Image Velocimetry

Particle Image Velocimetry is an optical measurement technique that utilizes laser-based technology to capture fluid velocities in experimental setups. This method employs a high-intensity light source to illuminate small tracer particles within a plane of interest in the phantom. The PIV and SPIV procedure illustrated in Figure 3.11 from the setup PIV to analysis of flow profile.

The PIV system is equipped with a dual high-speed camera (Flowsense EO camera 2MP, 1600 × 1200 pixels), a dual-power laser (135-15Hz), a 3D transverse system (inclusive of a transverse controller and an emergency stop button), a set of pumps for generating flow profiles, and a computer interface for data processing and the phantom (representing the post-stent geometry of the carotid artery bifurcation). To be ensure optimal performance, the laser is warmed up for approximately 20 minutes. Additionally, the distilled water level in the laser system is carefully monitored, as a low water level could impact the laser's functionality (refer to Figure 3.12). All hardware components and the PC system, running the Dynamic Studio software, are powered on.

Figure 3.12 shows the laser system should was pushed to become external so we can control by the software on pc. The internal system can be used for calibration purposes and to set the thickness of laser. The power of laser set around 5 to run the experiment. The thickness of the laser light sheet determined the effective size of the depth dimension over which tracer particles contributed the velocity measurement (Roloff et al., 2018). The environment was closed with a dark curtain to make sure the room was dark because the light would affect reflection on the phantom during the experiment. The speed of frequency of laser was 15 Hz (Shuib et al., 2011).

UMPSA
اونيۏرسيتي مليسيا ڤهڠ السلطان عبدالله
UNIVERSITI MALAYSIA PAHANG
AL-SULTAN ABDULLAH

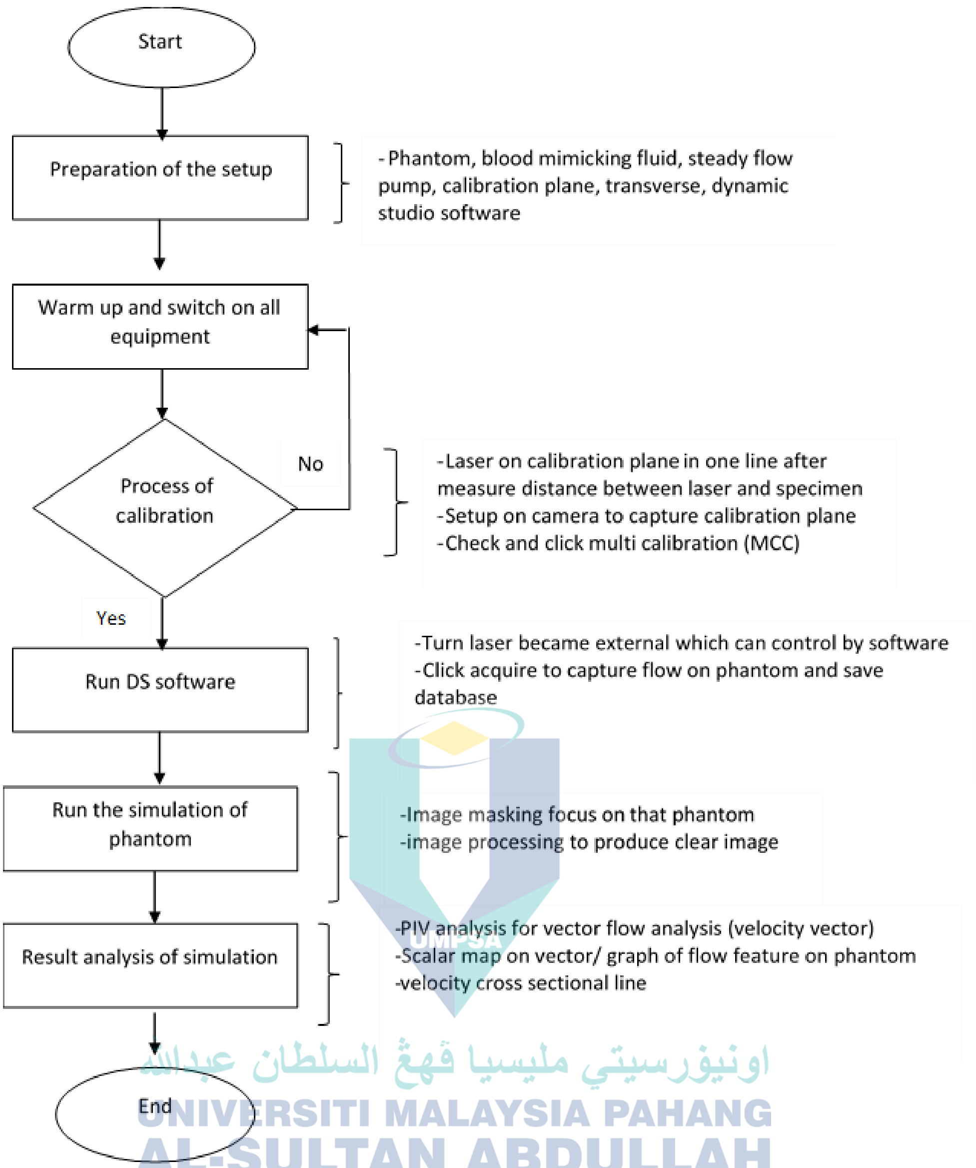

Figure 3.11 Procedure of PIV and SPIV experiment.

UMPSA
اونيۏرسيتي مليسيا ڤهڠ السلطان عبدالله
UNIVERSITI MALAYSIA PAHANG
AL-SULTAN ABDULLAH

Figure 3.12 Dual laser system

3.6 PIV Experiment Procedure

The experiment setup played a crucial role in obtaining clear views, ensuring effective seeding of particles throughout the phantom, and minimizing reflection effects on the images. The calibration plane was adjusted to align with the phantom setup, which was suspended horizontally on a plate connected to a transparent tube (as illustrated in Figure 3.4). The holder for the carotid artery phantom was linked to the transparent tube (inlet and outlet), placing the phantom perpendicular to both the camera and laser. The external button on the laser setup was configured for control through Dynamic Studio, and the software was initiated with the opening of a new project.

To ensure optimal image capture, a duo high-speed camera setup was employed with two lenses-Carl Zeiss and a micro lens (Micro-Nikkor lens). Suggestions for capturing better images included three critical components: manual control of laser power, adjusting the camera aperture, and positioning the laser through the phantom. Adjusting the aperture on the camera increased light intake, improving visibility. Proper laser positioning was crucial to minimizing reflections from the patient-specific carotid artery. The laser was centrally positioned within the geometry, and the pump circulated blood-mimicking fluid through the suspended carotid artery phantom, as depicted in the following figure.

In consideration of schematic diagrams for PIV and SPIV, differences in camera requirements were noted. PIV utilizes one camera, initiating a 2-Dimensional view, while SPIV provides a 3-Dimensional perspective. The system equipment required for the experiment included the phantom, blood-mimicking fluid, transverse control, laser, and camera, as illustrated in Figure 3.13 and Figure 3.14. The method had been used through PIV in room temperature like [(Buchmann & Jermy et al., 2009a) & (Shuib et al., 2011)] but another method can submerged in same working fluid such as BMF like [(Yazdi et al., 2019) & (Ho et al., 2020)].

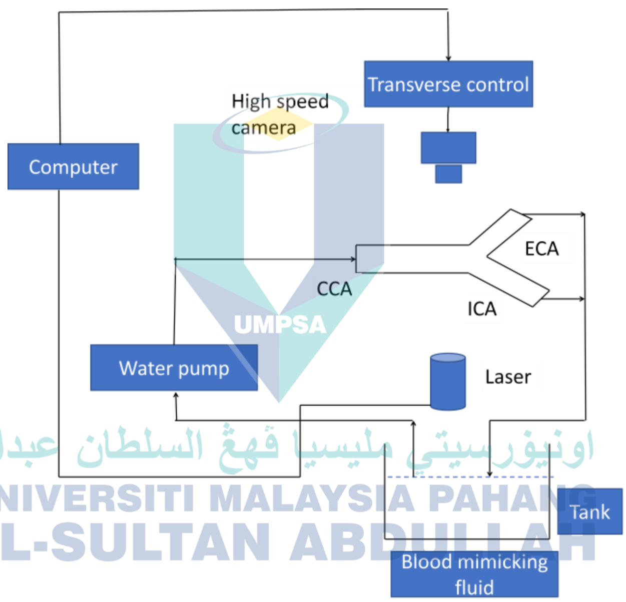

UMPSA
اونيۏرسيتي مليسيا ڤهڠ السلطان عبدالله
UNIVERSITI MALAYSIA PAHANG
AL-SULTAN ABDULLAH

Figure 3.13 PIV experiment systematic diagram.

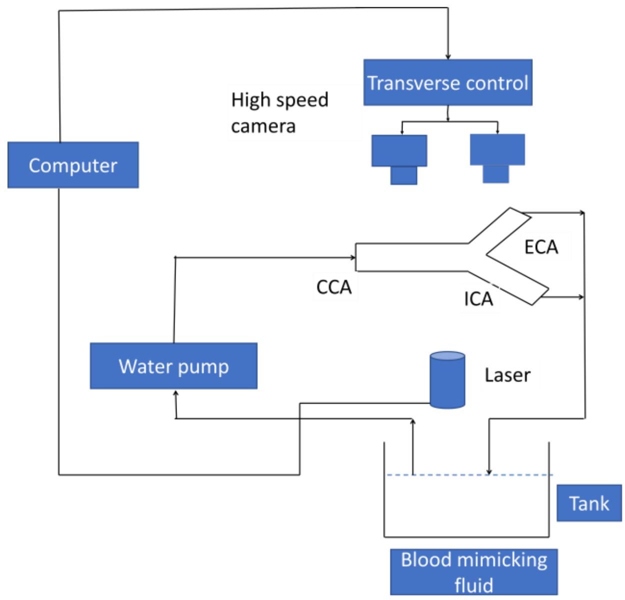

Figure 3.14 Stereo-PIV (SPIV) systematic diagram.

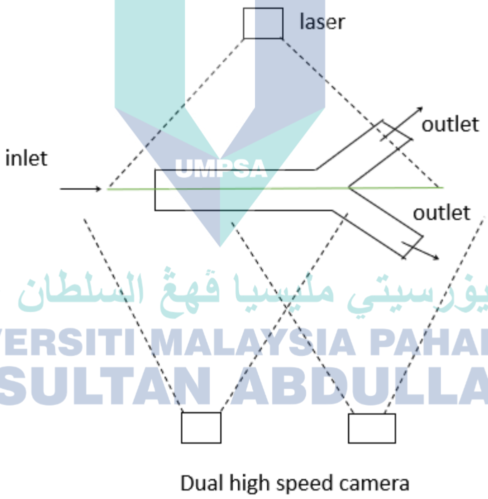

UMPSA
اونيۏرسيتي مليسيا ڤهڠ السلطان عبدالله
UNIVERSITI MALAYSIA PAHANG
AL-SULTAN ABDULLAH

Figure 3.15 The top view SPIV captured the carotid artery phantom.

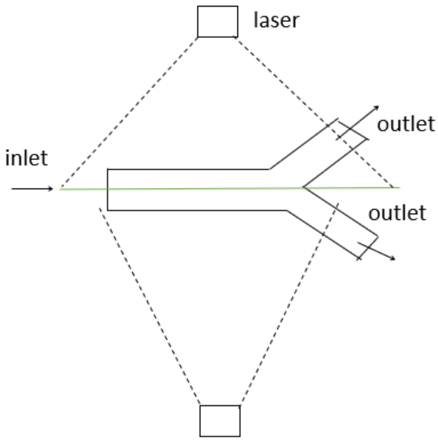

Figure 3.16 The top view PIV capture the carotid artery phantom.

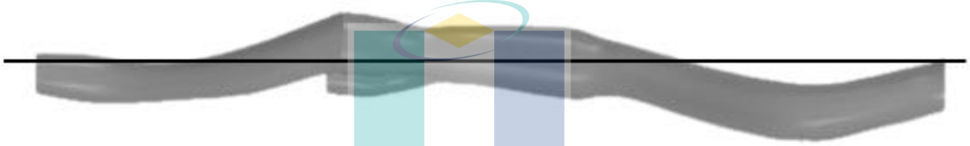

Figure 3.17 Top view of laser through the carotid artery.

UMPSA
اونيۏرسيتي مليسيا ڤهڠ السلطان عبدالله
UNIVERSITI MALAYSIA PAHANG
AL-SULTAN ABDULLAH

From a top view, as illustrated in Figure 3.15 and Figure 3.16, the PIV and SPIV experimental setup offers a comprehensive visualization of fluid flow dynamics through the carotid artery bifurcation. These figures capture velocity patterns, revealing flow separation and turbulence within this vascular geometry. Figure 3.17 and Figure 3.18 provide a top view of the laser through the phantom. In patient-specific cases, addressing the challenge of the complex and curved vascular geometry is crucial. To obtain optimal results, precise balancing of the laser's focal line in the middle of the region of interest is required to minimize reflections on the phantom.

The higher points in the graph (see Figure 3.19, Figure 3.20 and Figure 3.21) indicate successful capture of seeding particles through the phantom. However, due to the phantom not being fully transparent, reflections in the external carotid artery (ECA) area are not clearly defined by the camera. The method was repeated to analyze other areas, such as the bifurcation area, post-stenotic area, inlet area, and the full geometry.

For SPIV, the process was captured only for the full image geometry of the carotid artery due to technical limitations, as the micro lens was not suitable for 3D. The micro lens required more light from the back of the camera during the experiment.

To ensure optimal image capture, the software's preview feature was utilized to observe seeding particle flow passing through the phantom, and particle density was checked to confirm that the camera could capture the flow vector. The color gradient was unchanged during image capture to avoid blurry images. The double-frame mode was activated, and 100 images were captured. During the experiment, a dark room condition was necessary to minimize reflections and produce higher-quality results. Subsequently, the images were acquired with lasering, and the database was saved in the Dynamic Studio software.

UNIVERSITI MALAYSIA PAHANG
AL-SULTAN ABDULLAH

Figure 3.18 Laser light passing through the middle of carotid artery phantom.

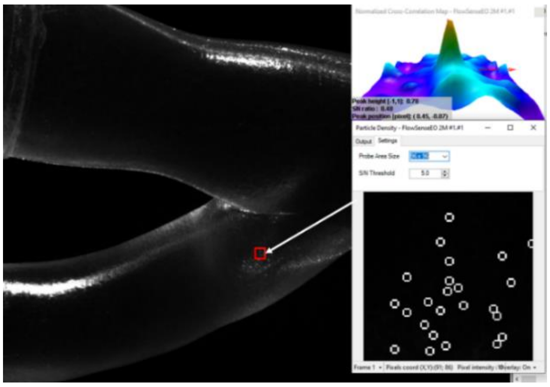

Figure 3.19 The preview of the seeding particle through phantom

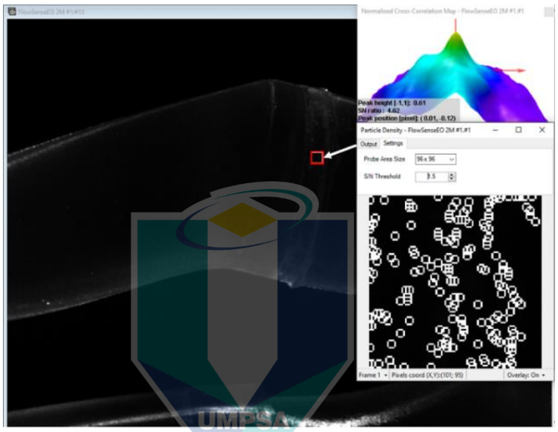

Figure 3.20 The preview of seeding particle around the split method fabrication on phantom

اونيۏرسيتي مليسيا ڤهڠ السلطان عبدالله
UNIVERSITI MALAYSIA PAHANG
AL-SULTAN ABDULLAH

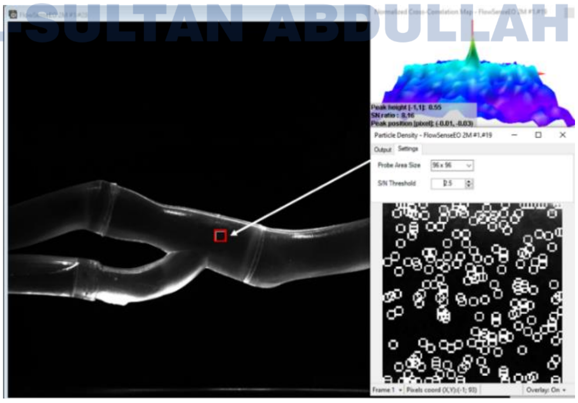

Figure 3.21 The preview full image of carotid artery phantom

3.7 PIV Post Processing Procedure

Following the image capture, a series of post-processing steps were performed, involving the editing and analysis of a sequence of 100 images. These operations encompassed establishing minimum and maximum image values, as well as generating a mean image that combine the sequence into a cohesive composite image. This approach markedly enhanced the clarity and overall quality of the final image. Additionally, adjustments to the brightness gradient were applied to further refine the clarity of the phantom.

After the capture phase, the geometry of the carotid artery was masked to isolate specific regions of interest, as illustrated in Figure 3.22. The masking method was employed to exclude areas not relevant to the investigation, resulting in the removal of the green coloration and leaving only the investigated geometry of the carotid artery.

Various methods were available for analysis in the software, including adaptive PIV, adaptive correlation, cross-correlation, auto-correlation, and others. Adaptive PIV was chosen for analysis, focusing on vector images, scalar maps of the velocity vector, and velocity along a cross-sectional line. Meanwhile, SPIV analysis required the integration of two PIV analyses from the duo high-speed camera results, combining both analyses.

UMPSA
اونيۏرسيتي مليسيا ڤهڠ السلطان عبدالله
UNIVERSITI MALAYSIA PAHANG
AL-SULTAN ABDULLAH

Successful PIV or SPIV analysis necessitated the use of transparent and physiologically relevant phantoms to facilitate the observation of blood flow during the experiment. Therefore, a proper calibration step was essential, accomplished by placing a Cartesian grid calibration on the target plane during the experiment.

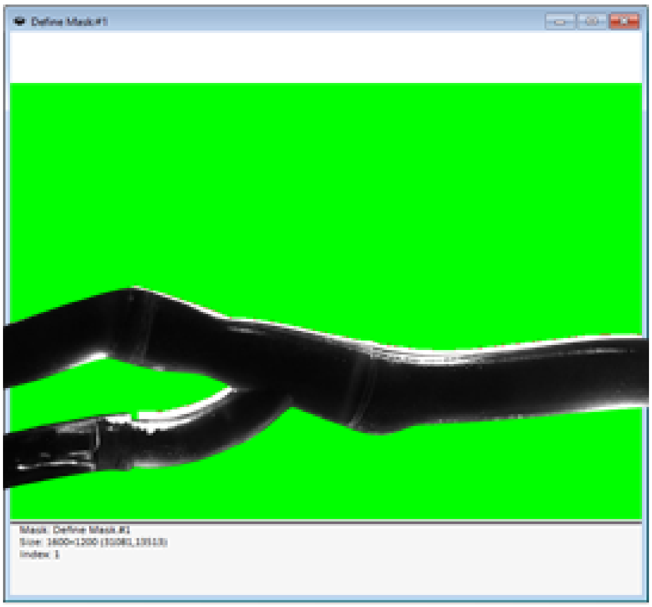

Figure 3.22 The masking process of carotid artery bifurcation model.

3.8 Region of interest for Carotid artery

Figure 3.23 illustrates the points and data collected and analyzed during PIV and SPIV experiments on the patient-specific carotid artery. The experimental data were scrutinized at different points along the artery to discern distinct flow characteristics using Dynamic Studio software with steady flow conditions.

Point A: Represents the blood flow entering from the common carotid artery (CCA) through the inlet.

Point B: Indicates the position in the bifurcation area, which is the stented area of the CCA-ICA.

Point C: Illustrates the blood flow passing through the downstream of stented area.

The analysis focused on the specific geometry of the carotid artery, emphasizing velocity vectors and velocities along cross-sectional lines. This study involved a comparison and validation of flow behavior in 2D PIV and 3D PIV. The regions of interest were investigated for velocity profiles along cross-sectional lines in bifurcation

UMPSA
اونيۏرسيتي مليسيا ڤهڠ السلطان عبدالله
UNIVERSITI MALAYSIA PAHANG
AL-SULTAN ABDULLAH

and curved areas. Data from the regions of interest were derived from previous research on stenosis development.

The analysis encompassed both the full image and regions of interest along cross-sectional lines, resulting in velocity profiles displayed in Figure 3.22,Figure 3.23,Figure 3.24 and Figure 3.25. The choice of vertical lines was deliberate, as these lines represented regions of interest for atherosclerosis development around the bifurcation, curve, and sinus bulb. These cross-sectional lines were strategically positioned based on the intricacies of flow dynamics, particularly around the curve area, sinus bulb, and bifurcation area, which are prone to atherosclerosis development (Chen et al., 2020)..

The specific location lines chosen were inspired by studies such as (Zhao et al., 2000), who employed two lines to delineate the curve area in the internal carotid artery (ICA) concerning Wall Shear Stress (WSS) for comparative purposes using CFD. Additionally,(Medero et al., 2018) used different cross-sectional lines with Particle Image Velocimetry (PIV) to investigate flow profiles at the ICA, comparing the results with MRI.

UMPSA
اونيۏرسيتي مليسيا ڤهڠ السلطان عبدالله
UNIVERSITI MALAYSIA PAHANG
AL-SULTAN ABDULLAH

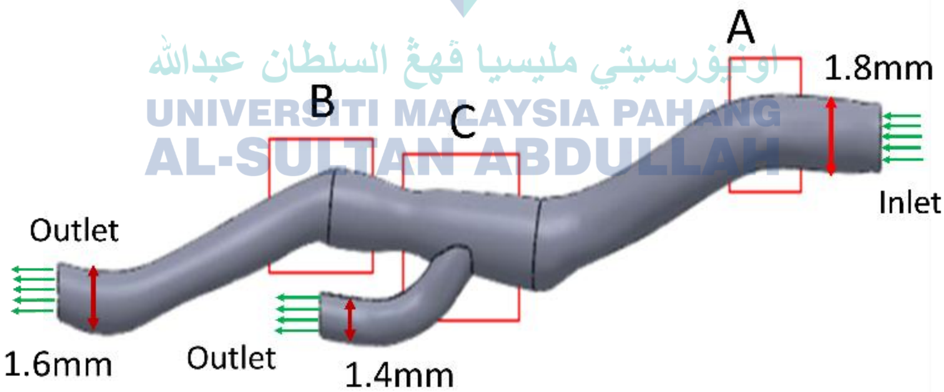

Figure 3.23 Several interest point / regions of carotid artery

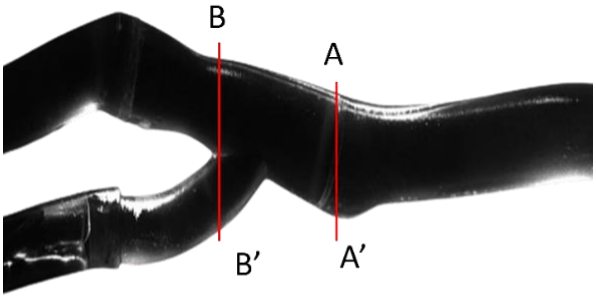

Figure 3.24 Full image captured of carotid artery geometry.

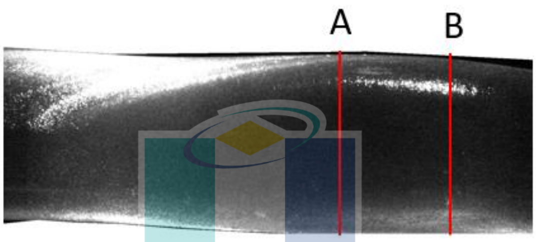

Figure 3.25 The cross-sectional line in CCA region.

اونيۏرسيتي مليسيا ڤهڠ السلطان عبدالله
UNIVERSITI MALAYSIA PAHANG
AL-SULTAN ABDULLAH

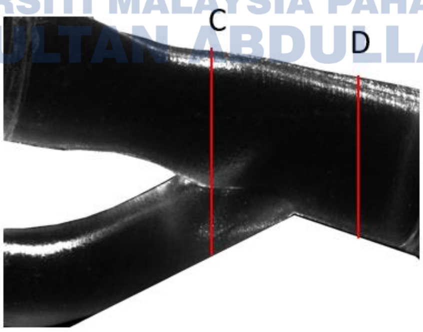

Figure 3.26 The cross-sectional line in bifurcation region of phantom

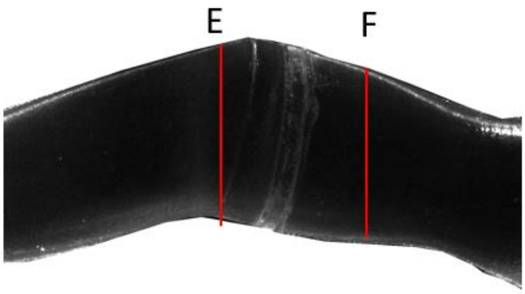

Figure 3.27 Cross line in the downstream of stented area of the phantom.

3.9 Computational Modelling of Blood Flow in Carotid Artery

The flowchart on computational modelling had been shown in Figure 3.28. There three steps of run the computational modelling such as pre-processing, solver and post-processing. The pre-processing is initial stage where input data is prepared which data geometry carotid artery of patient specific. Next, the solver performs numerical calculations to solve equations for fluid flow. Lastly, post-processing was analysed and visualized on simulation results.

The specific geometry of carotid artery from software MIMICS was used to build the carotid bifurcation geometry and exported to ANSYS FLUENT for the Computational fluid dynamics. The specific geometry was initially reported in (Johari et.al, 2019). The geometry was chosen a 68-years-old male patient with post-stenting after inflammation of asymptomatic chronic stenosis (90%). The STL file was converted to parasolid file and exported to the ANSYS 19.0. The geometry was scaled up by double size from normal size. All simulations were conducted using Intel ® Core (TM) i5-4500 CPU@3.30GHz, 8.00GB and 64-bit Operating system.

UMPSA
UNIVERSITI MALAYSIA PAHANG
AL-SULTAN ABDULLAH

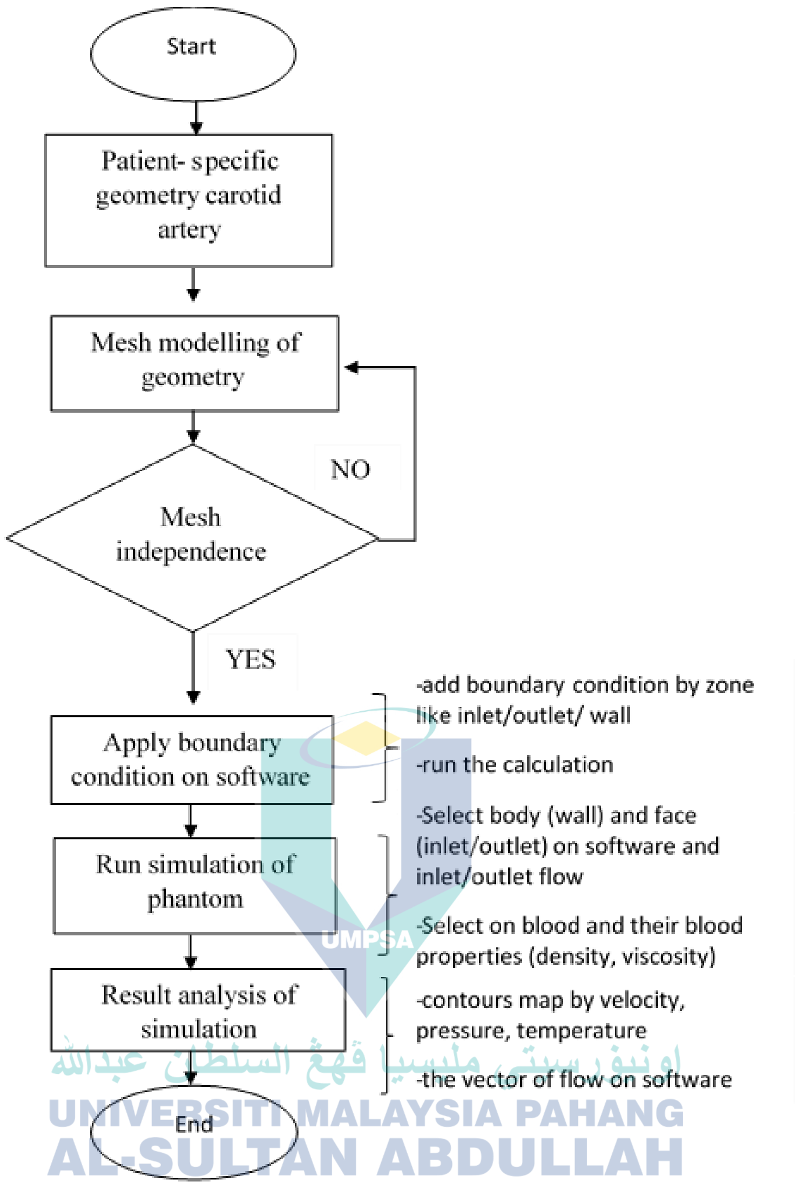

اونيۏرسيتي مليسيا ڤهڠ السلطان عبدالله
UNIVERSITI MALAYSIA PAHANG
AL-SULTAN ABDULLAH

Figure 3.28 The procedure of computational modelling using ANSYS FLUENT.

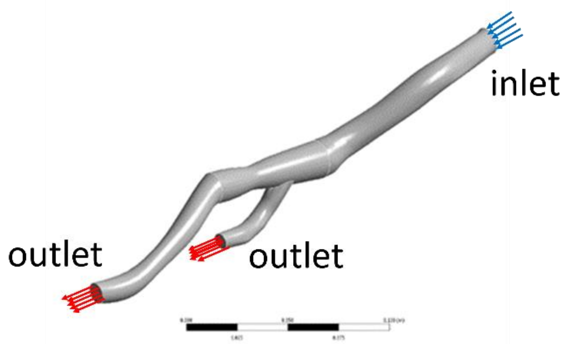

Figure 3.29 The post-stented carotid artery geometry.

All geometries employed unstructured tetrahedral parts (Kumar et al., 2019) & (Usmani & Muralidhar et al., 2016) with size of elements at the stenosis. By contrasting post-stenotic velocity profiles obtained with various mesh sizes, grid independence for simulations employing the SST-Tran turbulence models in post stent geometries. On other hand, SST-Tran model able to capture important flow features (N. H. Johari et al., 2019). A mesh with about 2 million elements was determined to be appropriate in this scenario after the element size was changed and a mesh independence test was carried out. The importance of mesh independence in obtain the accurate and reliable results. Hence, the size element was 0.45 mm had been investigated based on mesh quality compare with another size elements. All geometries utilized unstructured tetrahedral meshing, as suggested by [(Kumar et al., 2019) & (Usmani & Muralidhar et al., 2016)], with a specific focus on controlling element size at the stenosis. To ensure the reliability and accuracy of simulations using the SST-Tran turbulence models in post-stent geometries, a grid independence study was conducted by comparing post-stenotic velocity profiles across different mesh sizes.

Contrasting post-stenotic velocity profiles across various mesh sizes was crucial to establishing grid independence. Through this process, a mesh with approximately 2 million elements was identified as suitable for this scenario. This determination followed adjustments to the element size and the execution of a mesh independence test. The significance of achieving mesh independence lies in obtaining results that are both accurate and reliable. To specify, a mesh size of 0.45 mm was thoroughly investigated, considering mesh quality in comparison with other element sizes. This investigation aimed to highlight the critical significance of achieving mesh independence, also known as mesh convergence in ensuring the accuracy and reliability of the simulation results.

UMPSA
اونيۏرسيتي مليسيا ڤهڠ السلطان عبدالله
UNIVERSITI MALAYSIA PAHANG
AL-SULTAN ABDULLAH

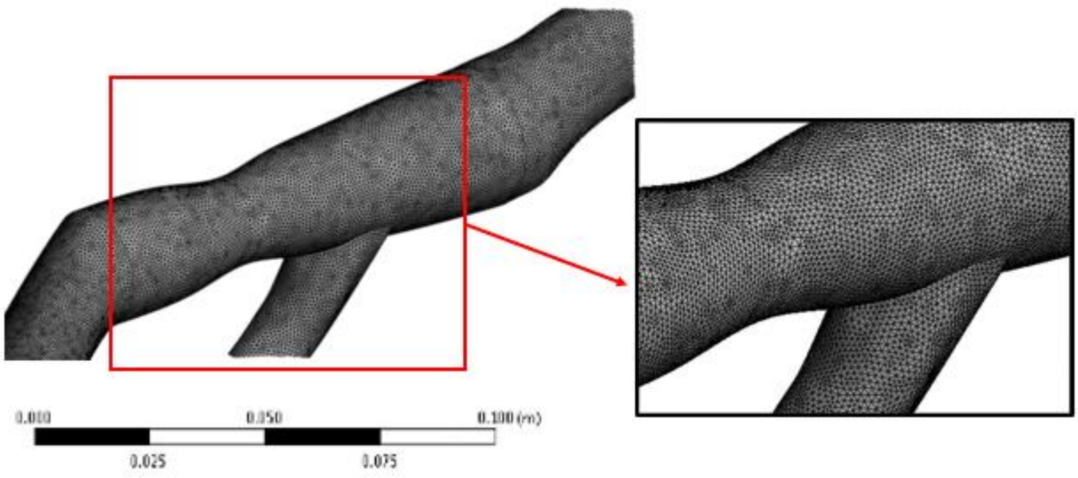

Figure 3.30 Mesh model for ANSYS Fluent simulation.

Assuming a blood density of 1060 kg/m³ and a viscosity of 0.0035 Pa·s, as reported (Noor & Johari et al., 2023), the blood flow conditions were considered constant, steady, and adhering to incompressible Newtonian flow, mirroring the conditions of the experimental steady flow pump. A velocity of approximately 0.82 m/s was imposed at the common carotid artery (CCA) inlet, aligning with the inlet conditions of the PIV experiment. The CCA inlet featured a fully evolved flow profile with a Reynolds number (Re) of 4260. At the outlets of the external carotid artery (ECA) and internal carotid artery (ICA), a relative gauge pressure of 0 Pa was applied. The walls were modeled as rigid, assuming a no-slip condition. All simulations were executed using ANSYS Fluent, a finite volume-based CFD code. The simulation parameters involved running calculations with 250 iterations, and the solver would automatically halt upon meeting either the completion of 250 iterations or the achievement of specified convergence criteria.

In the post-processing phase, the simulation analysis delved into flow characteristics, examining velocity vectors, contour maps of velocity, pressure distributions, and velocity profiles along cross-sectional lines. Placing the cross-sectional line in the middle of the carotid artery geometry posed challenges in patient-specific cases due to the intricate geometry, as depicted in Figure 3.17.

3.10 Influence the Different Location of Stenosis in Carotid Artery

The third objective aimed to elucidate the impact of stenosis location on patients through a comprehensive computational fluid dynamics (CFD) analysis. Three distinct stenosis locations and a geometry representing a healthy carotid artery were scrutinized. The internal carotid artery (ICA), external carotid artery (ECA), and common carotid artery (CCA) exhibited diameters of 4.6 mm, 5.6 mm, and 8 mm, respectively. Stenosis severity was consistently set at 70%, a threshold associated with a heightened risk and confirmed presence of separated flow adjacent to the jet in the post-stenotic zone, as reported by (N. H. Johari et al., 2019).

The chosen geometries for investigation featured a 70% stenosis size from the CCA to the ICA, predominantly situated in the carotid bulb but with variations in shape and location. Figure 3.31 illustrate the classification into types I, II, and III was based on atherosclerotic plaques observed in carotid arteries through magnetic resonance imaging (MRI). In type I, the arc-length of the plaque extended upstream, type II exhibited equal plaque distribution upstream and downstream, and type III showed plaque extension downstream. Due to a lack of statistical dimensions for patients' carotid geometries in (Lu et al., 2019), an idealized carotid bifurcation geometry served as the basis for the fluid domain (refer to Figure 3.32). Subsequently, atherosclerotic plaque shapes corresponding to types I-III were reconstructed and integrated into the idealized geometry. Additionally,

UMPSA
UNIVERSITI MALAYSIA PAHANG
AL-SULTAN ABDULLAH

a healthy carotid bifurcation geometry was reconstructed as part of the idealized representation.

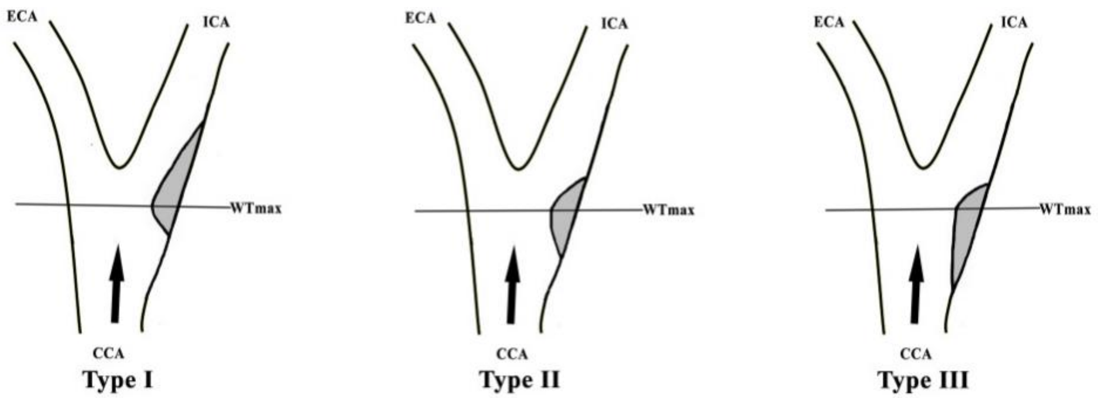

Figure 3.31 The different types of atherosclerosis plaque shape at the area of CCA-ICA. WT-max is the maximum wall thickness measured (Lu et al., 2019)

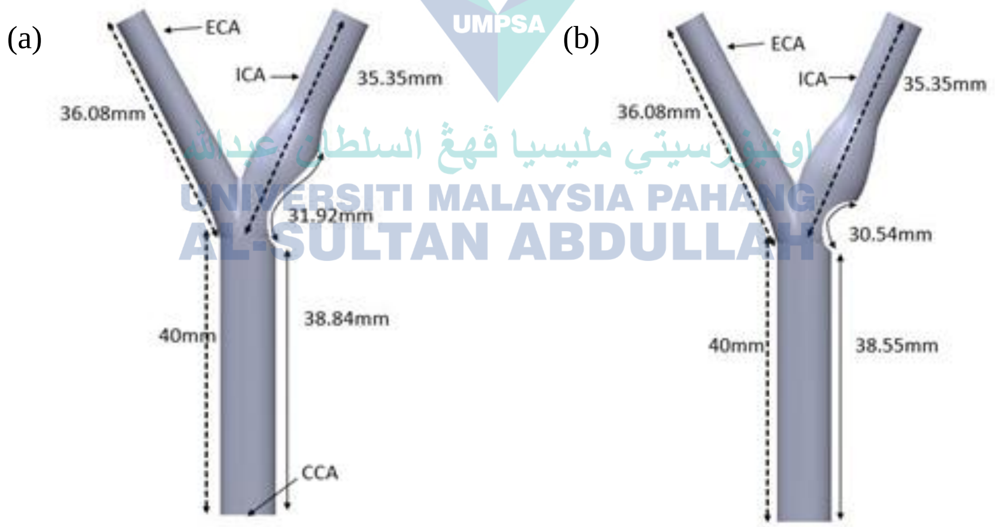

UMPSA
اونيۏرسيتي مليسيا ڤهڠ السلطان عبدالله
UNIVERSITI MALAYSIA PAHANG
AL-SULTAN ABDULLAH

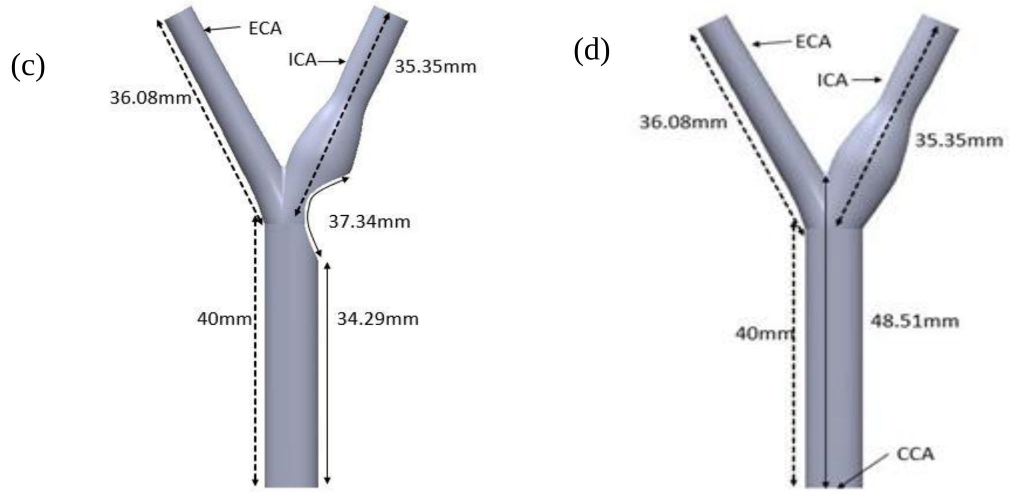

Figure 3.32 a) Model Type I (upstream stenosis), (b) Type II (equal upstream and downstream), (c) Type III (downstream stenosis) and (d) healthy carotid artery.

The stenosed carotid geometries were exported to ANSYS for mesh generation. Unstructured tetrahedral elements were adopted for all geometries around the area of stenosis. Simulations using the SST-Tran turbulence model in stenotic geometries were conducted to evaluate grid independence. To assess how the mesh affected the outcomes, the post-stenotic velocity profiles obtained with varied mesh sizes were compared.

Mesh independence research was carried out to determine that the results were not influenced by the mesh size. The size of elements of meshing was changed ranges globally from 0.3 mm to 0.15 mm. It is shown that all the results of total element generated in range of 800K to 2M number of elements respectively. The mesh quality such as orthogonal quality, skewness and aspect ratio were applied to determine suitable type of mesh to be use throughout the study. The fine mesh with size of element of 0.2mm globally was determined adequately precise for the computations study. (Moradicheghamahi et al., 2020) studied on mesh independence in computational studies through patient specific carotid artery. Their research emphasized achieving mesh independence, finding that the third mesh element are satisfied finding mesh from fourth mesh element. The mesh refinement is reached mean that the geometry was already converged and not necessary additional mesh to obtain accurate results.

UMPSA
اونيۏرسيتي مليسيا ڤهڠ السلطان عبدالله
UNIVERSITI MALAYSIA PAHANG
AL-SULTAN ABDULLAH

The SST-Tran model combines $k - \varepsilon$ and $k - \omega$ models where the $k - \varepsilon$ is dedicated to resolve flow in the inner region of boundary layer whilst the $k - \omega$ is for the outer region and free shear flows. The model has additional of a transitional model comprising two additional formulated transport equations for intermittency and the transition onset criterion in terms of the momentum thickness Reynolds number (Menter et al., 2006). The correlation between the $k - \varepsilon$ and $k - \omega$ together with the transition model has been successfully employed in cardiovascular flow applications with promising results (N. H. Johari et al., 2019), (Johari & et al., 2020), (Tan et al., 2011). For the healthy model laminar model was adopted in the simulation.

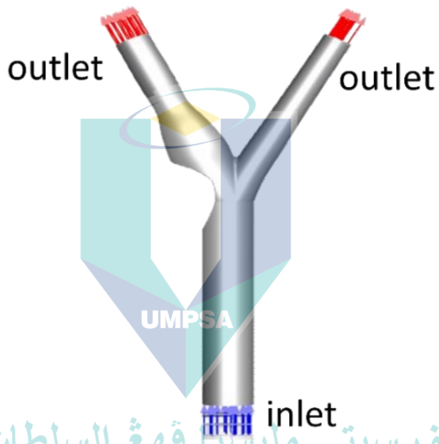

اونيۏرسيتي مليسيا ڤهڠ السلطان عبدالله
UNIVERSITI MALAYSIA PAHANG
AL-SULTAN ABDULLAH

Figure 3.33 The setup for idealised geometry of stenosis carotid artery

The blood flow was assumed to be steady and incompressible Newtonian flow with blood density of 1060 kg/m^3 and viscosity of 0.0035 Pa.s. Based on Figure 3.33 shown the boundary condition setup for inlet and outlet of carotid artery in CFD. The inlet velocity around 0.8 m/s was applied in CCA. The fully developed flow profile was specified at the CCA inlet with typical Reynolds number of Re =1940. At the ECA and ICA outlets, a relative 0 Pa of gauge pressure was applied. The walls were assumed to be rigid with no-slip conditions. All simulations to solve the governing equations were completed using a finite volume based CFD code ANSYS Fluent. The analysis of CFD simulation for different location stenosis and healthy of carotid artery has focused on velocity profiles, wall shear stress, pressure distributions around the stenosis area.

CHAPTER 4

RESULTS AND DISCUSSION

4.1 Introduction

This chapter undertakes a comprehensive exploration of the study's outcomes, aligning them with the predefined research objectives. The focal analysis focuses on the validation of outcomes derived from particle image velocimetry (PIV) experiments and their association with computational fluid dynamics (CFD) simulations. The primary analysis encompasses velocity profiles within specified regions of interest within the carotid artery. The focal point of investigation is the concordance between PIV experimental results and CFD simulations, seeking to discern similarities, disparities, and the overall reliability of the methodologies employed. Furthermore, this chapter delves into an examination of risk factors associated with the occurrence of stenosis, particularly at specific locations within the idealized geometry of the carotid artery. These locations are identified as high-risk areas for the initiation and progression of stenosis in patient scenarios. By elucidating these factors, the study contributes to a deeper comprehension of the intricate relationship between hemodynamic and the development of arterial stenosis.

UMPSA
اونيۏرسيتي مليسيا ڤهڠ السلطان عبدالله
UNIVERSITI MALAYSIA PAHANG
AL-SULTAN ABDULLAH

4.2 Flow Profiles in Carotid Phantom using PIV and SPIV Measurements

Following the post-processing phase, the Dynamic Studio software was employed to apply the geometry for PIV instructions. It's pivotal to observe the distinctions between the 2D and 3D procedural setups, equipment utilization, and subsequent analyses. Notably, calibration processes and high-speed cameras played integral roles in both procedures. The data for analysis were extracted from velocity vector statistics. Steady flow from a pump facilitated the passage of blood-mimicking fluid through the carotid artery, extending from the common carotid artery (CCA) to both the internal carotid artery (ICA) and external carotid artery (ECA).

Table 4.1 reveals the intricacies of flow profiles in a post-stent carotid artery, gleaned through both PIV and SPIV techniques. It is paramount to acknowledge that the interpretation of the data may exhibit subtle differences due to the disparity in dimensionality between the two techniques. A visible variance in colour gradients is discernible around the inlet and bifurcation zone.

In PIV, where velocity vectors are predominantly represented in two dimensions, a relatively uniform distribution is observed, characterized by analogous yellow and green colours. Conversely, SPIV capturing velocity vectors in three dimensions, exhibits a higher degree of accuracy. This is particularly evident in the colour gradient at the CCA inlet, where red hues signify elevated velocity vectors. This divergence underscores the enhanced precision offered by SPIV, contributing to a more nuanced understanding of flow dynamics, especially in regions of high complexity such as the carotid bifurcation.

Table 4.1 Velocity vectors in 2D (PIV) and 3D (SPIV)

2D (PIV)		3D (SPIV)
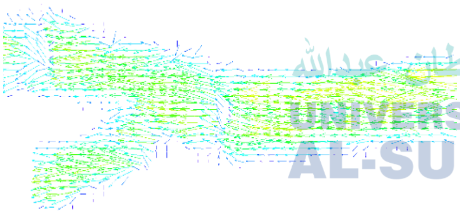		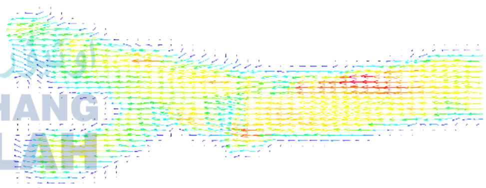

UMPSA
UNIVERSITI MALAYSIA PAHANG
AL-SULTAN ABDULLAH

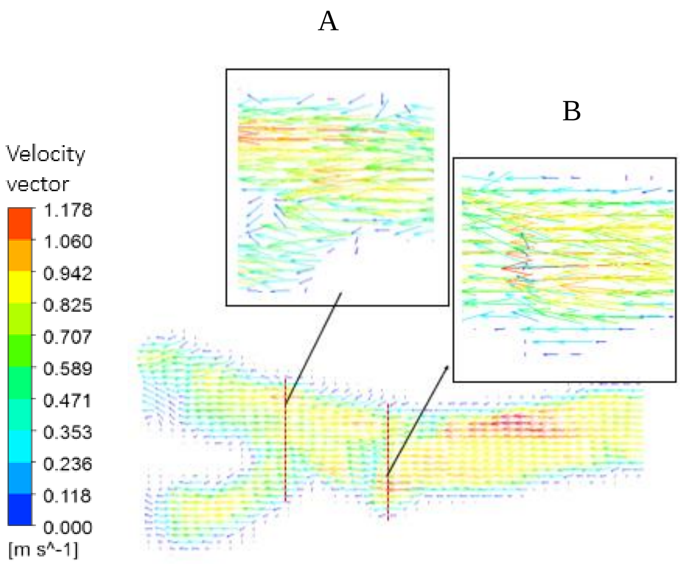

Figure 4.1 Velocity vectors at (a) bifurcation and (b) curve area.

Figure 4.1 illustrates the identified region of interest in the research, which focuses on the velocity profile within a post stent carotid artery. The arrows in the figure indicate the direction of flow, while the colour represents the velocity. Due to the irregular shape or geometry of the artery, there can be regions where the velocity is higher, particularly in the common carotid artery (CCA) region. It is observed that the velocity tends to increase in the CCA as blood accelerates.

UMPSA
اونيۏرسيتي مليسيا ڤهڠ السلطان عبدالله
UNIVERSITI MALAYSIA PAHANG
AL-SULTAN ABDULLAH

The analysis reveals a low velocity region in the bifurcation area, primarily due to the flow distribution between the internal carotid artery and external carotid artery. This finding is consistent with previous studies conducted by (Ningappa et al., 2022), (Johari et al. 2020), (Sharma et al., 2020) and (Nagargoje & Gupta et al., 2020), which also reported low velocities in the bulb of a post stent carotid bifurcation. The observed low velocities are attributed to a localized enlargement of the lumen region, leading to flow separation and recirculation phenomena.

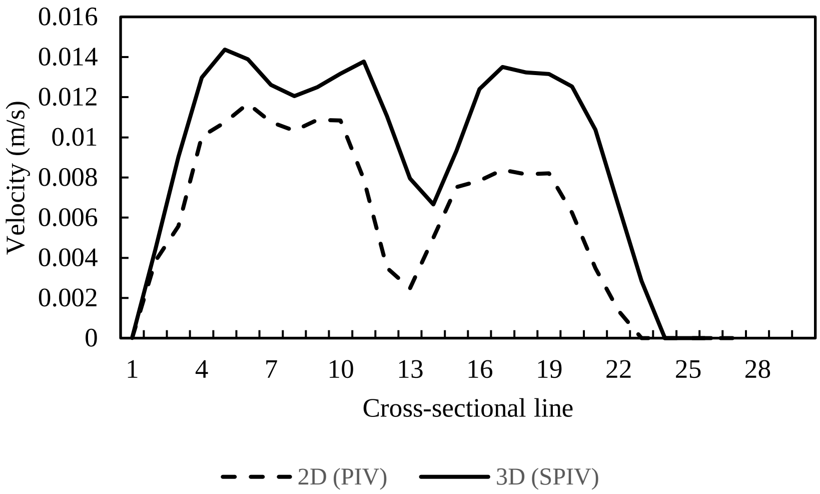

Figure 4.2 The velocity for cross sectional line on curve area in A

Figure 4.2 and Figure 4.3 present the velocity graphs along a cross-sectional line on the carotid artery geometry depicted in Figure 4.1. The y-axis displays velocity readings across the x-axis, representing a point in the cross-sectional line within the interest of region. The percentage difference in velocity profiles between PIV and SPIV using formula 4.1 is found to be only around 16.66%, indicating a relatively small disparity between the two techniques. This observation aligns with the study conducted by (Roloff et al., 2018), which reported smaller differences in averaged velocity between SPIV and PIV, typically below 5%. These findings suggest that exploring additional dimensions can lead to more accurate results. The value taken from maximum value velocity for both methods to get the error difference between PIV and SPIV at point 4.

$$\%\ Error\ Difference = \frac{V_{SPIV} - V_{PIV}}{V_{PIV}}\ x\ 100\% \tag{4.1}$$

A fluctuating flow profile is detected in the curved area due to a slight increase in the velocity of the blood-mimicking fluid (BMF) flowing downward along the curved geometry and the normal flow from the common carotid artery (CCA) to the bifurcation area. The line graph indicates a significant decline in velocity magnitude between points 11 and 13, attributed to the disturbance caused by the interaction of the BMF flow and the wall, resulting in low velocities around the bifurcation area. Beyond point 15, the flow pattern demonstrates a stable trend as the flow can pass through the bifurcation without further disruptions. The zero-velocity observed along the carotid artery wall is due to the no-slip condition, which states that the velocity of a fluid at the surface of a solid object is zero.

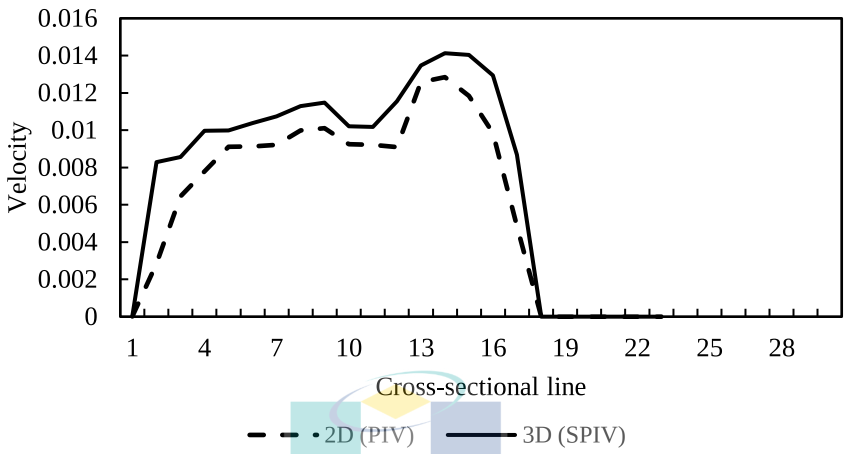

Figure 4.3 The velocity on cross sectional line on bifurcation area B

The line graph indicates that the velocity from points 1 to 11 are slightly lower compared to points 13 to 17, which can be attributed to the presence of a low-velocity region in the curved section of the carotid artery. This low-velocity region is associated with increased recirculation of flow. The occurrence of recirculation flow in this region can initiate the progression of atherosclerosis. In contrast, points 13 to 17 exhibit higher velocities since the flow remains undisturbed along the cross-sectional line.

The results obtained from PIV and SPIV techniques show a relatively small difference in the velocity vector patterns. However, SPIV has the advantage of potentially providing velocity pattern data with higher spatial resolution due to its ability to capture flow in three dimensions. This improved spatial resolution enables a more accurate depiction of flow characteristics and allows for a more comprehensive visualization of the velocity field.

UMPSA
اونيۏرسيتي مليسيا ڤهڠ السلطان عبدالله
UNIVERSITI MALAYSIA PAHANG
AL-SULTAN ABDULLAH

4.3 Comparison of PIV Measurement and CFD

This study also dedicated to analysing distinct regions of interest within patient-specific carotid artery geometries using both PIV measurement and CFD. The investigation examines the flow profile in the inlet area, bifurcation area, and post-stent area. The analysis of the flow profile encompasses an assessment of several velocity parameters, including velocity vectors, velocity scalar maps, and velocity measurements along cross-sectional lines Figure 4.4.

The geometries of the carotid artery in this study were characterized by their non-symmetrical and complex shapes. In the PIV measurement process, a laser was directed through the middle of the carotid artery geometry to illuminate the fluid containing seeding particles, which were then captured by a high-speed camera. Conversely, in CFD simulations, a cross-sectional plane was created in the middle section of the carotid artery geometry to analyse the flow results (Figure 4.4). For PIV, vector statistics are derived from a mean image obtained from a series of 100 captured images.

UMPSA
UNIVERSITI MALAYSIA PAHANG
AL-SULTAN ABDULLAH

Figure 4.4 Cross-sectional line of carotid artery

Table 4.2 presents the results detailing the flow patterns acquired PIV and CFD simulations in the carotid artery bifurcation. Overall, velocity vector values in all areas exhibit comparability between PIV and CFD. However, an evident dissimilarity emerges, notably the presence of more higher velocity areas in CFD compared to PIV. This variance can be ascribed to various limitations inherent in each method, encompassing aspects such as experimental setup, numerical modelling, and measurement techniques.

The precision of PIV data may be influenced by factors like spatial and temporal resolution, camera capabilities, and the accuracy of the calibration method employed. The limitation on the cross-sectional line through the patient-specific model could lead to inaccuracies in velocity measurements, failing to capture the complete range of velocities in the flow field. In a study by (Roloff et al., 2018), the average velocity magnitude difference between PIV and CFD was found to be less than 5%. Comparable investigations have been conducted to assess flow patterns in intracranial aneurysms, employing diverse techniques such as PIV, CFD, and MRI (Roloff et al., 2018).

The uncovered disparities in velocity patterns between PIV and CFD methodologies highlight a nuanced interplay of strengths and limitations. This highlights the importance of developing a comprehensive understanding of the details inherent in interpreting flow dynamics within the carotid artery bifurcation. To delve deeper into the comparison of flow dynamics, it is imperative to scrutinize the specific regions of interest in the carotid geometry. Such a focused exploration aims to discern any distinctive similarities or disparities between PIV and CFD results. This approach ensures a more comprehension of the intricacies involved in elucidating the complex flow behaviours within the sophisticated vascular geometry of the carotid artery bifurcation.

Table 4.2 Comparison of PIV and CFD on full geometry

PIV	CFD
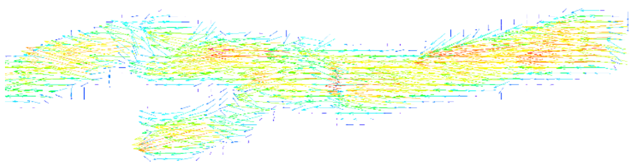	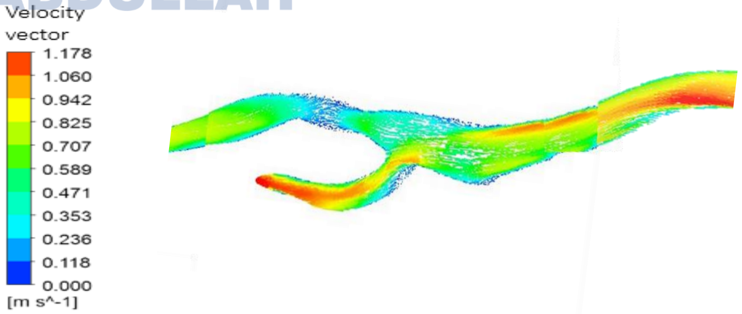

UMPSA
اونيۏرسيتي مليسيا ڤهڠ السلطان عبدالله
UNIVERSITI MALAYSIA PAHANG
AL-SULTAN ABDULLAH

4.3.1 Flow Profiles in Region of Interest

Table 4.3 meticulously outlines the comparison of velocity vectors in distinct areas of the carotid artery between PIV and CFD. The recorded velocity values range from a minimum of 0 m/s to a maximum of 1.178 m/s, with both methodologies utilizing an inlet velocity of 0.82 m/s at the common carotid artery inlet.

As mentioned earlier, velocity vector in all areas exhibit comparability between PIV and CFD. Nevertheless, subtle disparities emerge in terms of distribution, where alignment between CFD and PIV is not entirely uniform. Notably, a pronounced difference manifests in the inlet position (Table 4.3,Area A). CFD demonstrates higher velocity skewed toward the bottom wall, while PIV portrays higher velocity skewed to both the top and bottom walls. This discrepancy is anticipated, given the non-uniform and slightly chaotic blood flow attributed to the bending and curved shape in area CCA towards the bifurcation.

Within the stented region (Area B), both PIV and CFD illustrate a marginal increase in velocity at the entrance of the External Carotid Artery (ECA) due to flow splitting in the bifurcation. Pre-bifurcation, low velocities are evident, and upon contact with the artery wall, CFD reveals recirculation flow atop the Internal Carotid Artery (ICA) wall. (Johari et al. 2020) reported the existence of low-momentum fluid near the wall, giving rise to symmetrical counter-rotating vortices known as Dean vortices in the outer ICA. Intriguingly, these intricate flow patterns elude detection in the PIV measurements. (Buchmann & Jermy et al., 2009b) similarly observed non-uniform velocity profiles in the bifurcation area based on MRI data. Nevertheless, the flow patterns predicted by CFD in Area C are more consistent with PIV. A noticeable higher velocity is recorded, skewed towards the bottom wall immediately after the curved and bent shape of the stented ICA.

UMPSA
اونيۏرسيتي مليسيا ڤهڠ السلطان عبدالله
UNIVERSITI MALAYSIA PAHANG
AL-SULTAN ABDULLAH

Table 4.3 Velocity vector on different area using PIV and CFD

Area	PIV		CFD
A) 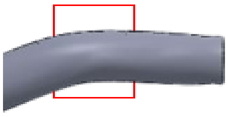	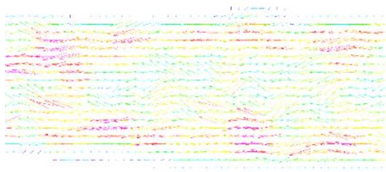	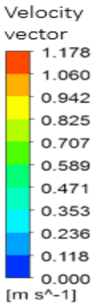	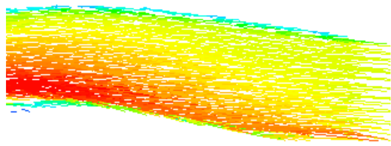
B) 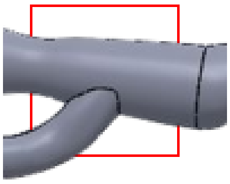	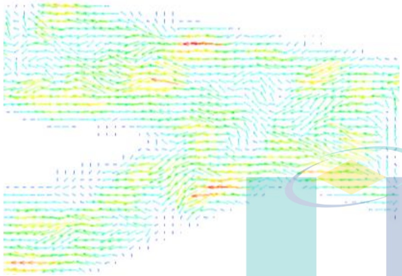	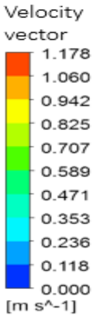	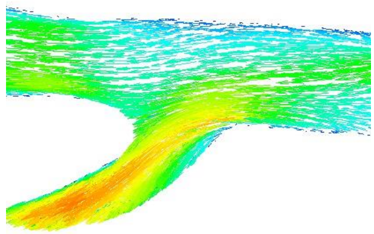
C) 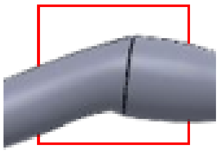		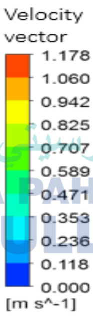	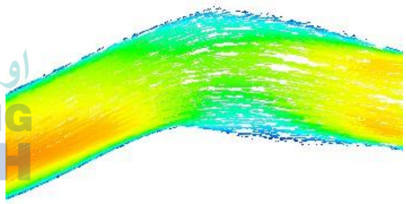

4.3.2 Velocity Contours Comparison

Table 4.4 illustrates the velocity contours measured in the patient-specific carotid artery, revealing the impact of branching and vessel curvature on the radial pressure gradient and the formation of secondary flows. The curvature, radius, and flow velocity collectively contribute to the generation of secondary vortex pairs in this dynamic system (Buchmann & Jermy et al., 2009a).

UMPSA
اونيۏرسيتي مليسيا ڤهڠ السلطان عبدالله
UNIVERSITI MALAYSIA PAHANG
AL-SULTAN ABDULLAH

Given the higher curvature of the internal carotid artery (ICA) compared to the external carotid artery (ECA) in bifurcation models, flow separation predominantly occurs along the outer wall of the ICA, directing increased flow toward its inner wall, consistent with clinical observations (Ningappa et al., 2022). While the colour contour map in the PIV measurement may not distinctly indicate flow separation in the bifurcation regions, the concentration of higher velocity flow in the 'waist' shape post-bifurcation highlights the influence of the radial pressure gradient resulting from sudden diameter reduction. In the CFD analysis, the ICA section reveals higher velocity near the inner wall, reaching approximately 1.178 m/s.

These findings align with research by (Nagargoje & Gupta et al., 2020) who explored the impact of sinus size and position in the carotid artery on hemodynamic parameters. Their CFD study observed low-recirculating velocity near the sinus bulb compared to other regions, suggesting that the sinus bulb areas may be susceptible to atherosclerotic changes (C. Li et al., 2019).

UMPSA
اونيۏرسيتي مليسيا ڤهڠ السلطان عبدالله
UNIVERSITI MALAYSIA PAHANG
AL-SULTAN ABDULLAH

Table 4.4 Velocity contour map of interest region between PIV and CFD.

Area	PIV	RANGE	CFD
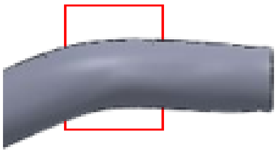	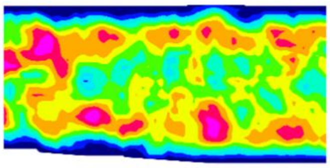	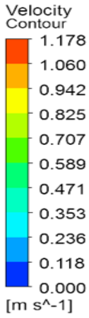	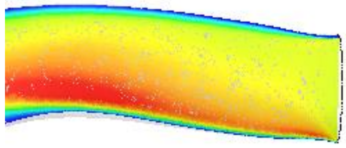
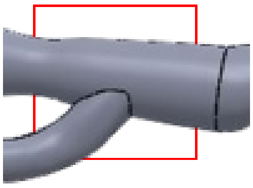	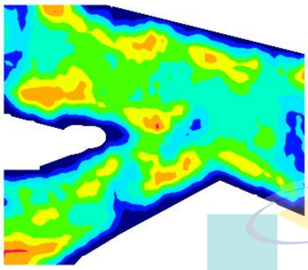	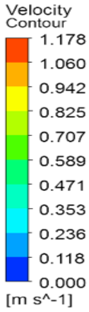	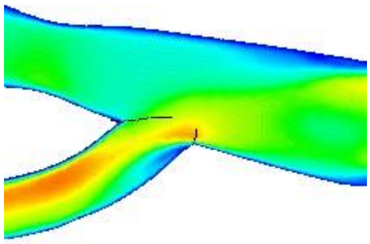
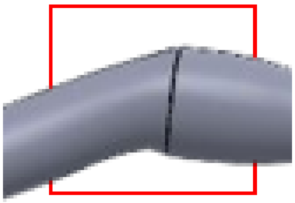	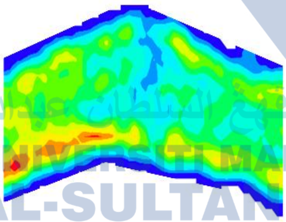	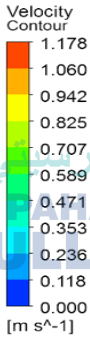	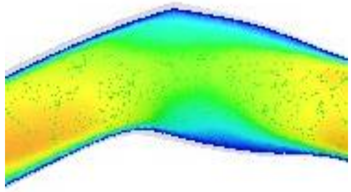

UMPSA
اونيۏرسيتي مليسيا ڤهڠ السلطان عبدالله
UNIVERSITI MALAYSIA PAHANG
AL-SULTAN ABDULLAH

4.3.3 Velocity on Cross Sectional Line Comparison

Table 4.5 and Table 4.6 present a cross-sectional analysis of interest regions in the carotid artery using two cross-sectional lines for each geometry in both PIV and CFD. The graph's display length corresponds to the cross-sectional line in both PIV and CFD, and velocity values are extracted from both methods.

In the common carotid artery area, the axial velocity recorded by PIV does not synchronize with CFD in both lines A and B. PIV fails to capture the velocity towards the bottom of the wall, resulting in very low velocity. However, both PIV and CFD record the highest velocity at similar locations, not far from the top wall of the artery. CFD predicts a slightly higher maximum velocity of 0.98 m/s, about 10% higher than recorded in PIV. Both PIV and CFD show an 'm-shaped' axial velocity at the middle of the cross-sectional line, indicating that the flow struggles to settle for full uniformity.

In the bifurcation area, low velocity is clearly recorded close to the top wall on the line A, consistently increasing towards the bifurcation and the top wall of the external carotid artery (ECA). The velocity then immediately decreases at the bottom of the ECA wall. Both PIV and CFD record almost similar maximum velocity values in this area, approximately 0.65 m/s. On the line B, both PIV and CFD predicted similar highest velocity value even though the location is slightly different. The flow seems to skew to the bottom wall where the flow is starting to split into ECA and ICA. This finding supports (Tada & Tarbell et al., 2005) study, which concluded that low velocity occurs around the bifurcation in a compliant carotid artery. The presence of recirculation flow and low velocity zones in this region may promote the accumulation of inflammatory compounds, such as low-density lipoprotein (LDL) particles, on the artery wall, potentially leading to the formation of atherosclerotic plaques. Meanwhile, downstream of the stented region, both CFD and PIV results accurately replicate the velocity magnitudes with slight variations, demonstrating the flow pattern's shape near the center and indicating the influence of the flow divider.

As reported by (N. H. Johari et al., 2019) in their investigation comparing LES, SST-Trans, and PIV on the stenosed carotid artery bifurcation, a small dent in the axial velocity profile near the center was observed. At all points, the PIV measurements showed slightly lower velocities compared to CFD predictions.

Table 4.5 Velocity profiles on cross-sectional line A, comparing CFD and PIV.

Interest region	Velocity Profiles
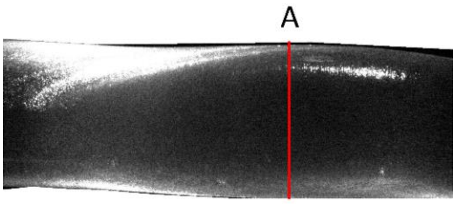	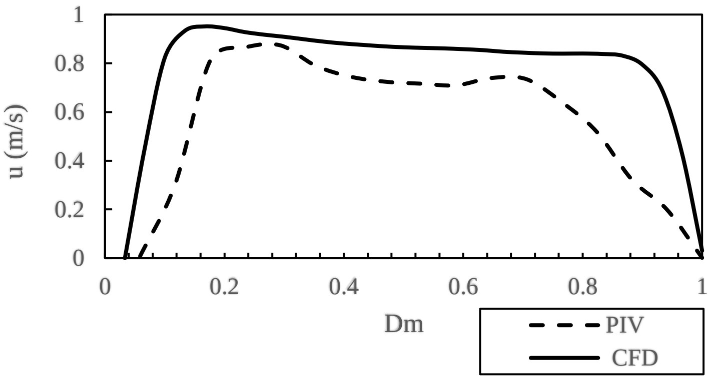
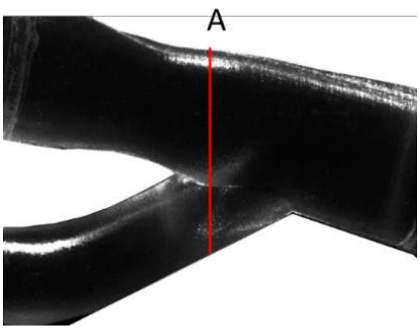	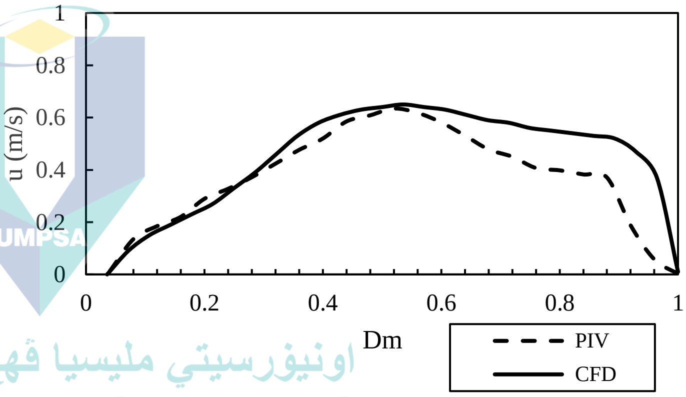
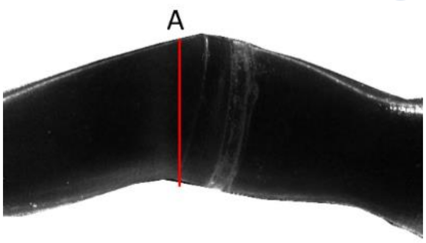	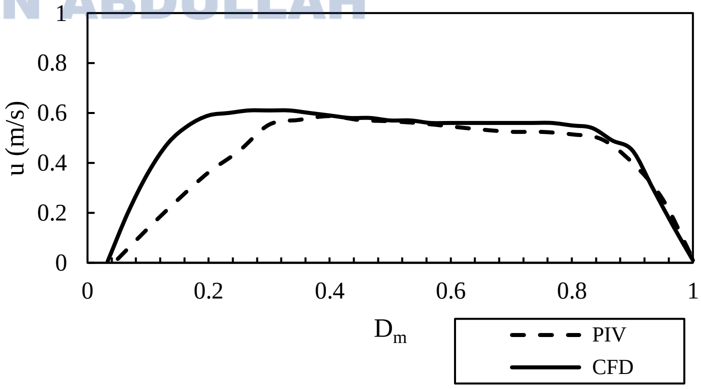

اونيۏرسيتي مليسيا ڤهڠ السلطان عبدالله
UNIVERSITI MALAYSIA PAHANG
AL-SULTAN ABDULLAH

Table 4.6 Velocity profiles on cross-sectional line B, comparing CFD and PIV.

<table>
<tr><th>Interest region</th><th>Velocity Profiles</th></tr>
<tr><td>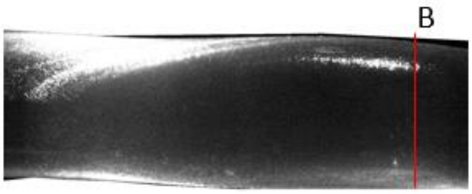
</td><td>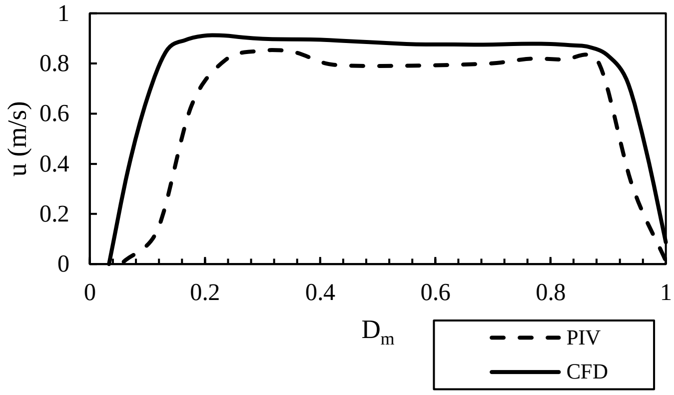
</td></tr>
<tr><td>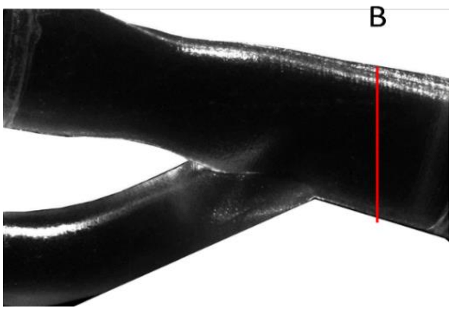
</td><td>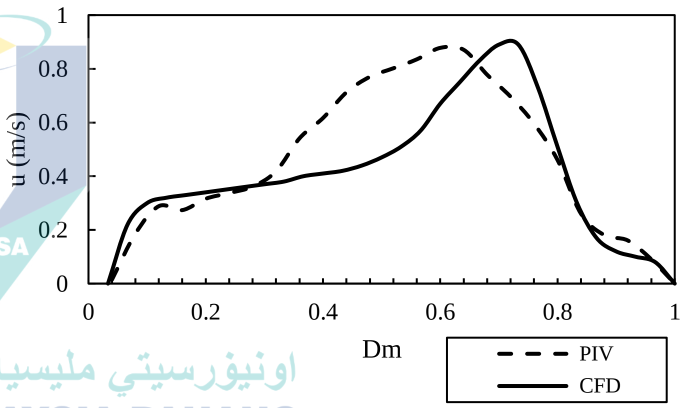
</td></tr>
<tr><td>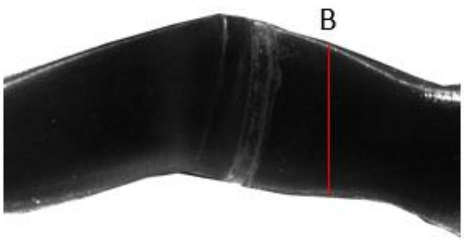
</td><td>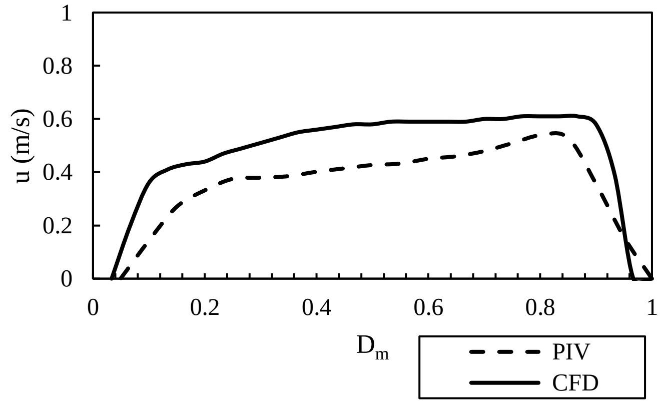
</td></tr>
</table>

اونيۏرسيتي مليسيا ڤهڠ السلطان عبدالله
UMPSA
UNIVERSITI MALAYSIA PAHANG
AL-SULTAN ABDULLAH

4.4 Hemodynamic Parameters Through Different Location of Stenosis.

4.4.1 Velocity Streamlines.

Figure 4.5 presents the velocity streamlines patterns in three different models of stenotic carotid arteries with varying locations of stenosis patches, as well as a healthy carotid model. In the healthy model, low velocity profiles are observed in the carotid bulb due to localized expansion of the lumen area, resulting in flow recirculation. However, the presence of stenosis significantly alters the flow pattern, particularly downstream of the stenosis. The velocity is higher at the stenosis throat, followed by flow separation immediately after the stenosis, and the formation of a strong helical flow structure distal to the stenosis (also shown in Figure 4.6). Similar observations have been reported in previous studies by (N. H. Johari et al., 2019), (Banks & Bressloff et al., 2007), (Tan et al., 2011), (Lancellotti et al., 2017), and (Z. Y. Li et al., 2015).

In general, the flow patterns in Type I-III geometries exhibit some similarities but differ in the proximal and distal regions of the artery. Type I geometry displays a complex helical post-stenotic flow pattern, with low velocity streamlines before reattaching to the axial flow stream. This indicates an area prone to stenosis growth and extension (Z. Y. Li et al., 2015). The prediction also demonstrated that carotid plaques located above the bifurcation (upstream) exhibited a higher likelihood of experiencing intraplaque haemorrhage (IPH). On the other hand, the velocity streamlines in Type II and III geometries are comparable, featuring a large area of low velocity flow recirculation distal to the stenosis.

UMPSA
اونيبورسيتي مليسيا قهڠ السلطان عبدالله
UNIVERSITI MALAYSIA PAHANG
AL-SULTAN ABDULLAH

To further analyse the velocity profiles, Figure 4.7 depicts the velocity vectors in all carotid models. It is evident that a 70% stenosis significantly alters the flow, leading to distinct recirculation zones compared to the healthy model. However, a detailed comparison between Type I-III geometries is not readily apparent, possibly due to the similar sizes of the stenoses. Nonetheless, Type I geometry exhibits a higher density of velocity vectors immediately after the stenosis and closer to the outer wall. Low velocities are indicated by the blue coloration observed along the artery wall, sinus bulb, and bifurcation area. Conversely, high velocities are observed in the internal carotid artery (ICA) and around the stenosis region shown in

Figure 4.7. As the flow exits the throat of the stenosis, flow separation takes place due to the decrease in velocity and increase in pressure in the expansion region (Shuib et al., 2011).

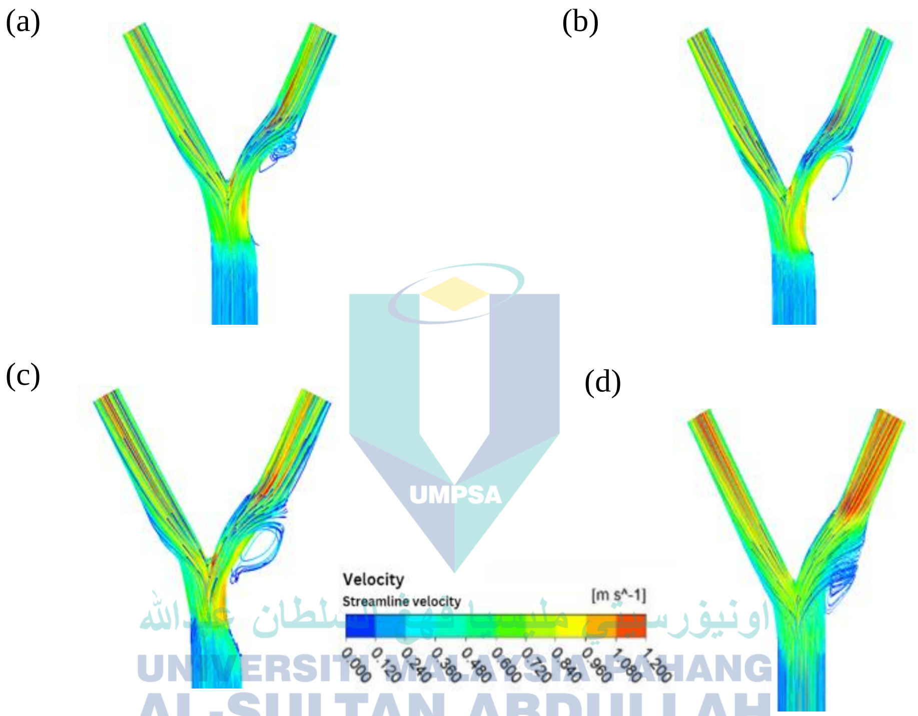

UNIVERSITI MALAYSIA PAHANG
AL-SULTAN ABDULLAH

Figure 4.5 Velocity streamline at mid-plane in (a) Type I, (b) Type II, (c) Type III and (d) Heathy models.

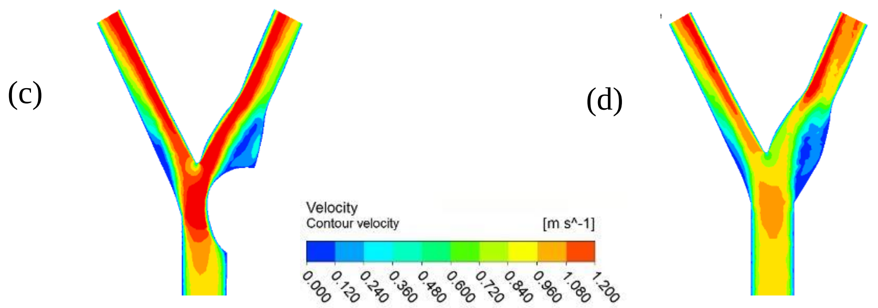

Figure 4.6 Velocity contours map at mid-plane in (a) Type I, (b) Type II, (c) Type III and (d) Heathy models.

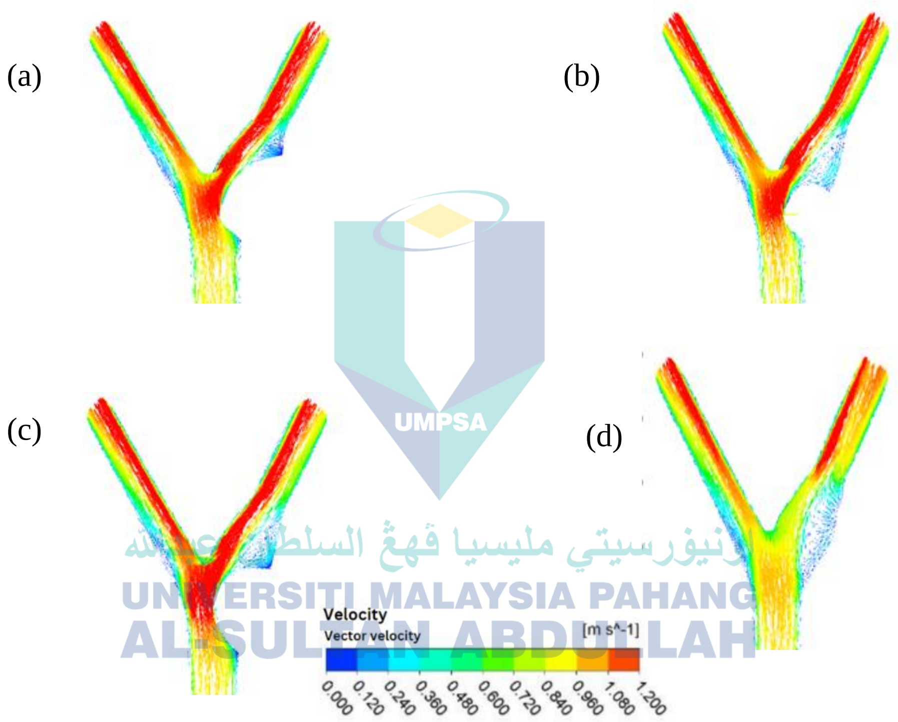

UMPSA
UNIVERSITI MALAYSIA PAHANG
AL-SULTAN ABDULLAH

Figure 4.7 Velocity vectors in (a) Type I, (b) Type II, (c) Type III and (d) Heathy models.

4.4.2 Velocity Profile Development

Figure 4.8 provides an overview of the steady flow patterns observed using CFD analysis in the four carotid models, namely the healthy, Type I, Type II, and Type III geometries. The analysis includes volumetric and central plane flow patterns, with velocity profiles obtained from cross-sectional lines along the carotid artery, including the inlet common carotid artery (CCA), the bifurcation area, and the stenosis region.

To ensure consistency, the greatest velocity value at the centreline of the CCA inlet was used to normalize all the velocities (Dong et al., 2013). The laminar model employed in the numerical simulation accurately captures flow separation and the formation of recirculation zones resulting from the sudden expansion of the cross-sectional area at the internal carotid artery (ICA) sinus region. The graph illustrates that the presence of stenosis significantly alters the flow pattern, leading to high velocity regions. As demonstrated by (Johari et.al, 2019), the flow pattern exhibits a high-velocity jet emanating from the stenosis throat, followed by flow separation shortly after the stenosis, and the emergence of a strong helical flow structure downstream of the stenosis. Notably, the flow pattern is greatly influenced by the presence of a 90% stenosis in the pre-stent model.

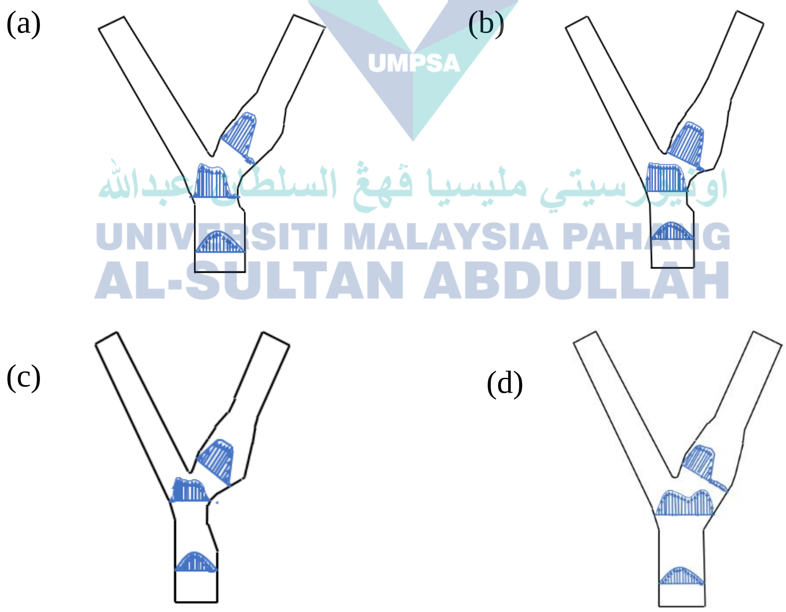

Figure 4.8 Velocity pattern in (a) Type I, (b) Type II, (c) Type III and (d) Heathy models.

UMPSA
UNIVERSITI MALAYSIA PAHANG
AL-SULTAN ABDULLAH

4.4.3 Wall Shear Stress

Wall shear stress (WSS) is a critical hemodynamic factor that plays a significant role in the development of atherosclerosis. Figure 4.9 illustrates the maximum WSS contour set at 10 Pa to ensure consistent comparisons between different models and to focus on WSS within the carotid bulb and the internal carotid artery (ICA).

Within the carotid bulb, high WSS values (represented by the red colour) are observed along the outer curvature, where the blood flow accelerates and sharply turns toward the external carotid artery. On the other hand, the inner curvature of the bulb, where the blood flow slows and divides into the internal and external carotid arteries, exhibits the lowest WSS values. The maximum and minimum value of WSS are 10 Pa and 0 Pa.

Compared to the healthy model, the stenotic carotid models display greater spatial variation in WSS. The presence of 70% stenosis leads to high WSS at the throat of the stenosis and in the distal region along the inner wall impacted by high-velocity flow. Similar observations were previously reported by [(N. H. Johari et al., 2019), (Z. Y. Li et al., 2015). While areas of stenosis in the carotid artery exhibit regions of low wall shear stress causing flow separation, recirculation zones and disturbed flow patterns of the stenosis area [(Malek & Alper et al., 1999) and (Slagger et al., 2005)]. Low WSS is associated with endothelial dysfunction, increased permeability, inflammation, and the accumulation of lipids and immune cells within the arterial wall, promoting the progression of atherosclerosis and plaque destabilization (Trigui et al., 2021).

In a study conducted by (Yang et al., 2023), the investigation focused on various degrees of stenosis in the carotid artery under steady flow conditions using plane wave vector Doppler. The areas with stenosis exhibited the highest WSS values. As the degree of stenosis increased, the separation zones in the post-stenotic region, characterized by recirculation flow, became larger.

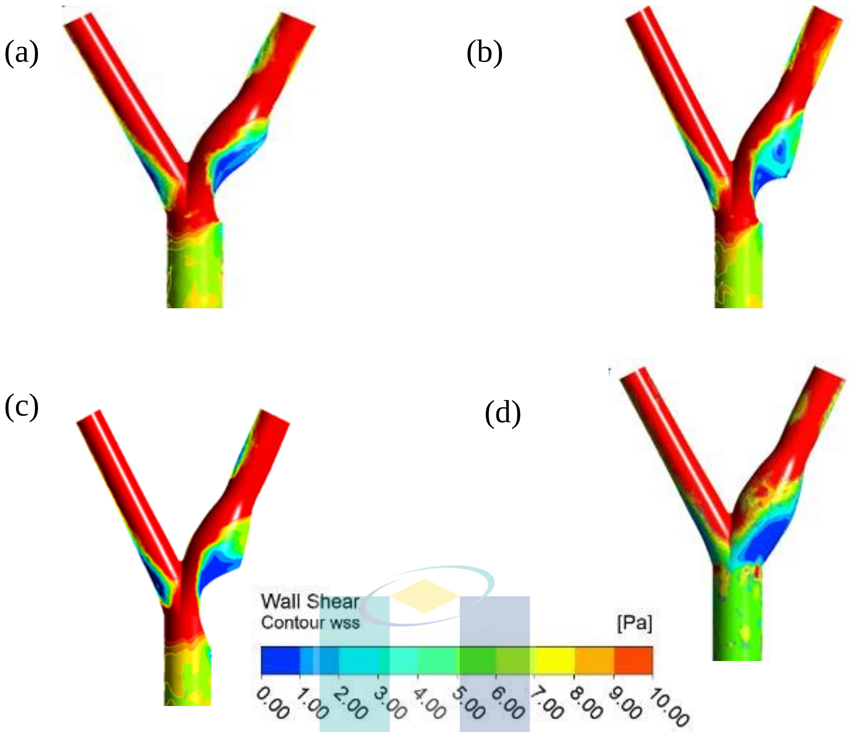

Figure 4.9 Wall shear stress (WSS) in (a) Type I, (b) Type II, (c) Type III and (d) Heathy models

UMPSA
اونيۏرسيتي مليسيا ڤهڠ السلطان عبدالله
UNIVERSITI MALAYSIA PAHANG
AL-SULTAN ABDULLAH

4.4.4 Pressure Distribution

The normal pressure range at the carotid artery bifurcation in adults is typically between 60 and 80 mmHg for diastolic pressure and 100 to 120 mmHg for systolic pressure, as reported by (Liu et al., 2021). However, it's important to note that blood pressure can be influenced by various factors such as age, gender, level of physical activity, and underlying medical conditions, leading to variations in individual cases.

In the presence of stenosis, particularly in Type I, Type II, and Type III geometries, lower pressure regions can be observed (Figure 4.10). As can be seen, the pressure had been dropped in stenotic area. It shown and analysed by other research like (Filardi et al., 2013). Generally, and particularly upstream of the stenosis, the pressure within a stenotic artery may be higher compared to a non-stenotic artery. This is because the stenosis restricts blood flow, leading to increased turbulence and a decrease in pressure across the constricted area (Kumar et al., 2022). The severity and location of the stenosis, the flow rate, and the compliance of the artery wall are among the variables that determine the extent of pressure elevation.

These alterations in pressure and flow can have clinical implications, including the development of downstream ischemia, the formation of blood clots, or the occurrence of aneurysms. In addition to increased pressure, stenosis can also cause changes in blood flow velocity and direction, further influencing the pressure distribution within the affected arterial segment. Blood pressure at the carotid artery bifurcation tends to be higher compared to other regions of the artery due to the presence of the bifurcation and the resulting changes in blood flow patterns. The bifurcation can induce variations in blood flow velocity and direction, leading to the generation of turbulence and an increased risk of plaque formation and other vascular diseases.

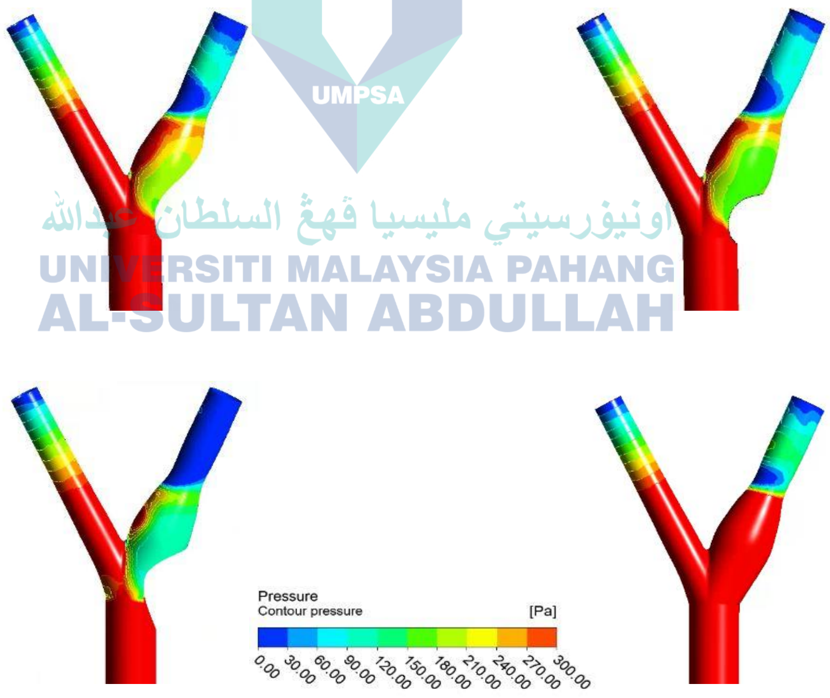

Figure 4.10 Pressure distribution in (a) Type I, (b) Type II, (c) Type III and (d) Heathy models

CHAPTER 5

CONCLUSION

5.1 Conclusion

Cardiovascular diseases (CVD) are the leading cause of mortality worldwide, resulting in 17.9 million deaths annually according to the World Health Organization (WHO). In Malaysia, there has been a recent 5% increase in CVD cases every year, as reported by the National Heart Institute. Atherosclerosis, a significant contributor to CVD, leads to the thickening and hardening of vessel walls due to plaque formation.

The flow characteristics of the carotid artery bifurcation were investigated through fabrication and examination using Particle Image Velocimetry (PIV) and Stereo Particle Image Velocimetry (SPIV). The results obtained from cross-sectional lines around the bifurcation and curved areas were used to verify the flow characteristics. The analysis reveals a low velocity region in the bifurcation area, primarily due to the flow distribution between the internal carotid artery and external carotid artery. SPIV, with its capability to capture three-dimensional data, provided higher spatial resolution and more accurate results compared to PIV. The difference in velocity between PIV and SPIV data was found to be approximately 16.66%.

UMPSA
اونيۏرسيتي مليسيا ڤهڠ السلطان عبدالله
UNIVERSITI MALAYSIA PAHANG
AL-SULTAN ABDULLAH

The study aimed to compare and validate the PIV results with CFD simulations of patient-specific carotid artery models under healthy conditions. Various regions of interest, including velocity vectors, scalar maps of velocity, and cross-sectional lines, were analysed. The velocity vectors in the post-stent area exhibited similar flow behavior between PIV and CFD. However, noticeable differences were observed, particularly in the inlet region, where high velocities were present in the Common Carotid Artery (CCA). CFD predicts a slightly higher maximum velocity of 0.98 m/s, about 10% higher than recorded in PIV. These differences can be attributed to the limitations and deficiencies in the experimental setup, boundary conditions of the blood-mimicking fluid, and other factors.

Moreover, the study investigated the flow characteristics in idealized geometries representing various stenosis locations, as well as in a healthy geometry without stenosis. Stenosis levels of 70% were introduced at three different positions: upstream, middle, and downstream of the carotid bifurcation. The results demonstrated that carotid plaques located above the bifurcation (upstream) exhibited a higher likelihood of experiencing intraplaque hemorrhage (IPH). This characteristic, IPH, is associated with vulnerable plaques and plays a crucial role in risk stratification for patients with carotid atherosclerosis, indicating a heightened susceptibility to future events. Thus, Type I stenosis, situated at the upstream region of the carotid artery, represents the most critical high-risk location.

This study has made significant contributions to the fields of medicine and engineering, particularly in improving the understanding of atherosclerosis progression through the results obtained from PIV and CFD. The investigations have provided valuable insights into the underlying pathophysiology of this condition by identifying areas of low shear stress and flow recirculation in the carotid artery bifurcation, which are associated with atherosclerotic plaques. Additionally, the studies have enhanced our knowledge of fluid dynamics in blood flow within the carotid artery bifurcation, aiding in the design of medical devices such as stents and grafts used in treatments.

UMPSA
اونيۏرسيتي مليسيا ڤهڠ السلطان عبدالله
UNIVERSITI MALAYSIA PAHANG
AL-SULTAN ABDULLAH

5.2 Recommendation

Based on the findings of this research, there are several recommendations that can be made to enhance and improve future studies, particularly in relation to PIV measurements and model geometry.

Firstly, it is suggested to shift from using rigid geometries to compliant geometry phantoms. Compliant geometries offer a more complex and flexible representation of human arteries, closely replicating their behavior. However, during the casting process of the compliant geometry, issues were encountered when attempting 3D printing of the carotid artery using Polyvinyl alcohol (PVA) as the material. The soft nature of PVA made it fragile and unable to support vertical printing without additional support structures. As a result, the 3D printed models ruptured. To address this, it is recommended to incorporate support structures during the 3D printing of carotid artery geometries in future endeavours.

Furthermore, future research in PIV should strive to use fully transparent phantoms. In the present study, the fabrication of the carotid artery geometry resulted in only semi-transparent phantoms. This limited transparency can adversely affect the quality of captured images and velocity vectors during experimental studies. To overcome this limitation, it is advisable to employ fully transparent materials for phantom fabrication. Additionally, the use of a spotlight to support the micro lens during SPIV experiments is recommended. The lack of sufficient lighting can make it challenging to capture high-quality images, especially during the calibration process and image capture.

Lastly, it is proposed to investigate turbulent flow by utilizing a different pump in PIV experiments and CFD simulations. Turbulent flow more accurately simulates the realistic and complex flow behavior observed in the cardiovascular system, particularly under complicated geometries and physiological conditions. By incorporating turbulent flow, more precise and realistic predictions of hemodynamic variables such as wall shear stress and pressure can be obtained, providing valuable insights for clinical applications.

UMPSA
اونيۏرسيتي مليسيا ڤهڠ السلطان عبدالله
UNIVERSITI MALAYSIA PAHANG
AL-SULTAN ABDULLAH

By implementing these recommendations, future research can advance the understanding of carotid artery flow dynamics and contribute to improvements in experimental techniques and model simulations, ultimately benefiting the field of cardiovascular research and medical device development.

REFERENCES

Akagawa, O., Fukazu, K., Nagaoka, R., & Saijo, Y. (2016). Two-dimensional blood flow vector and wall shear stress of carotid artery obtained with dual-angle Doppler method. *IEEE International Ultrasonics Symposium, IUS*, *2016-Novem*, 0–3. https://doi.org/10.1109/ULTSYM.2016.7728523

Arzani, A., & Shadden, S. C. (2016). Characterizations and Correlations of Wall Shear Stress in Aneurysmal Flow. *Journal of Biomechanical Engineering*, *138*(1). https://doi.org/10.1115/1.4032056

Azar, D., Torres, W. M., Davis, L. A., Shaw, T., Eberth, J. F., Kolachalama, V. B., Lessner, S. M., & Shazly, T. (2019). Geometric determinants of local hemodynamics in severe carotid artery stenosis. *Computers in Biology and Medicine*, *114*(September), 103436. https://doi.org/10.1016/j.compbiomed.2019.103436

Banks, J., & Bressloff, N. W. (2007). Turbulence modeling in three-dimensional stenosed arterial bifurcations. In *Journal of Biomechanical Engineering* (Vol. 129, Issue 1, pp. 40–50). https://doi.org/10.1115/1.2401182

Barnett. (1991). Benefial effect of carotid endarterectomy in symptomatic patients with high-grade carotid stenosis. *The New England Journal of Medicine*, *325*(7), 445–453.

Brott, T. G., Howard, G., Roubin, G. S., Meschia, J. F., Mackey, A., Brooks, W., Moore, W. S., Hill, M. D., Mantese, V. A., Clark, W. M., Timaran, C. H., Heck, D., Leimgruber, P. P., Sheffet, A. J., Howard, V. J., Chaturvedi, S., Lal, B. K., Voeks, J. H., & Hobson, R. W. (2016). Long-Term Results of Stenting versus Endarterectomy for Carotid-Artery Stenosis. *New England Journal of Medicine*, *374*(11), 1021–1031. https://doi.org/10.1056/nejmoa1505215

Buchmann, N. A., & Jermy, M. C. (2009a). *Experimental investigation of carotid artery haemodynamics in an anatomically realistic model Chuong V . Nguyen*. *1*(2), 172–192.

Buchmann, N. A., & Jermy, M. C. (2009b). In-vitro blood flow and wall shear stress measurements in idealised and patient specific models of the carotid artery bifurcation. *Proceedings of the ASME Summer Bioengineering Conference, SBC2008*, *PART B*, 723–724. https://doi.org/10.1115/sbc2008-193263

Buckler, A. J., Wanrooij, M. Van, Andersson, M., Karl, E., Perisic, L., Hedin, U., & Gasser, T. C. (2022). *Journal of the Mechanical Behavior of Biomedical Materials Patient-specific biomechanical analysis of atherosclerotic plaques enabled by histologically validated tissue characterization from computed tomography angiography : A case study*. *134*(August). https://doi.org/10.1016/j.jmbbm.2022.105403

Bulusu, K. V., & Plesniak, M. W. (2016). Experimental investigation of secondary flow structures downstream of a model type IV stent failure in a 180° curved artery test section. *Journal of Visualized Experiments*, *2016*(113), 1–18.

UNIVERSITI MALAYSIA PAHANG AL-SULTAN ABDULLAH

https://doi.org/10.3791/51288

Campbell, I. C., Ries, J., Coulter, W. H., Quyyumi, A. A., Taylor, W. R., Coulter, W. H., Oshinski, J. N., & Coulter, W. H. (2017). *Effect of Inlet Velocity Profiles on Patient-Specific Computational Fluid Dynamics Simulations of the Carotid Bifurcation*. *134*(May 2012), 1–8. https://doi.org/10.1115/1.4006681

Carvalho, V., Maia, I., Souza, A., Ribeiro, J., Costa, P., Puga, H., Teixeira, S., & Lima, R. A. (2021). In vitro Biomodels in Stenotic Arteries to Perform Blood Analogues Flow Visualizations and Measurements: A Review. *The Open Biomedical Engineering Journal*, *14*(1), 87–102. https://doi.org/10.2174/1874120702014010087

Chen, Y., Yang, X., Iskander, A. J., & Wang, P. (2020). On the flow characteristics in different carotid arteries. *Physics of Fluids*, *32*(10). https://doi.org/10.1063/5.0022092

DiCarlo, A. L., Holdsworth, D. W., & Poepping, T. L. (2019). Study of the effect of stenosis severity and non-Newtonian viscosity on multidirectional wall shear stress and flow disturbances in the carotid artery using particle image velocimetry. *Medical Engineering and Physics*, *65*, 8–23. https://doi.org/10.1016/j.medengphy.2018.12.023

Dolan, J. M., Kolega, J., & Meng, H. (2013). High wall shear stress and spatial gradients in vascular pathology: A review. *Annals of Biomedical Engineering*, *41*(7), 1411–1427. https://doi.org/10.1007/s10439-012-0695-0

Dong, J., Inthavong, K., & Tu, J. (2013). Image-based computational hemodynamics evaluation of atherosclerotic carotid bifurcation models. *Computers in Biology and Medicine*, *43*(10), 1353–1362. https://doi.org/10.1016/j.compbiomed.2013.06.013

Elshin Joel, M., & Anburajan, M. (2013). *3D Modeling of Stenotic Internal Carotid Artery Treated with Stent: A CFD Analysis of Blood*. *Iccnce*, 148–151. https://doi.org/10.2991/iccnce.2013.36

Filardi, V. (2013). Carotid artery stenosis near a bifurcation investigated by fluid dynamic analyses. *Neuroradiology Journal*, *26*(4), 439–453. https://doi.org/10.1177/197140091302600409

Fukuda, S., Shimogonya, Y., Yonemoto, N., Fukuda, M., Watanabe, A., Fujiwara, K., Enomoto, R., Hasegawa, K., Yasoda, A., & Tsukahara, T. (2022). Hemodynamic risk factors for the development of carotid stenosis in patients with unilateral carotid stenosis. In *World Neurosurgery*. Elsevier Inc. https://doi.org/10.1016/j.wneu.2022.01.019

Gates, P. E., Gurung, A., Mazzaro, L., Aizawa, K., Elyas, S., Strain, W. D., Shore, A. C., & Shandas, R. (2018). Measurement of wall shear stress exerted by flowing blood in the human carotid artery: Ultrasound Doppler velocimetry and echo particle image velocimetry. *Ultrasound in Medicine and Biology*, *44*(7), 1392–1401. https://doi.org/10.1016/j.ultrasmedbio.2018.02.013.Measurement

Geoghegan, P. H., Buchmann, N. A., Spence, C. J. T., Moore, S., & Jermy, M. (2012).

UMPSA
UNIVERSITI MALAYSIA PAHANG
AL-SULTAN ABDULLAH

Fabrication of rigid and flexible refractive-index-matched flow phantoms for flow visualisation and optical flow measurements. *Experiments in Fluids*, *52*(5), 1331–1347. https://doi.org/10.1007/s00348-011-1258-0

Geoghegan, Patrick H., Jermy, M. C., & Nobes, D. S. (2017). A PIV comparison of the flow field and wall shear stress in rigid and compliant models of healthy carotid arteries. *Journal of Mechanics in Medicine and Biology*, *17*(3). https://doi.org/10.1142/S0219519417500415

Geoghegan, Patrick H, Docherty, P. D., Sellier, M., & Jermy, M. C. (2016). Understanding Arterial Pressure from PIV data. *18th International Symposium on the Application of Laser and Imaging Techniques to Fluid Mechanics*, *2012*(Cvd).

Guerciotti, B., Vergara, C., Azzimonti, L., Forzenigo, L., Buora, A., Biondetti, P., & Domanin, M. (2016). Computational study of the fl uid-dynamics in carotids before and after endarterectomy. *Journal of Biomechanics*, *49*(1), 26–38. https://doi.org/10.1016/j.jbiomech.2015.11.009

Hernández-López, P., Cilla, M., Martínez, M., & Peña, E. (2021). Effects of the Haemodynamic Stimulus on the Location of Carotid Plaques Based on a Patient-Specific Mechanobiological Plaque Atheroma Formation Model. *Frontiers in Bioengineering and Biotechnology*, *9*(June), 1–19. https://doi.org/10.3389/fbioe.2021.690685

Ho, W. H., Tshimanga, I. J., Ngoepe, M. N., Jermy, M. C., & Geoghegan, P. H. (2020). Evaluation of a Desktop 3D Printed Rigid Refractive-Indexed-Matched Flow Phantom for PIV Measurements on Cerebral Aneurysms. *Cardiovascular Engineering and Technology*, *11*(1), 14–23. https://doi.org/10.1007/s13239-019-00444-z

Hong, H., Ji, H. S., Kim, H. D., & Kim, K. C. (2017). Temporal and spatial flow structures in a simulated vessel with stenotic lesion using time-resolved PIV technique. *Journal of Visualization*, *20*(4), 833–845. https://doi.org/10.1007/s12650-017-0432-8

Hoving, A. M., de Vries, E. E., Mikhal, J., de Borst, G. J., & Slump, C. H. (2020). A Systematic Review for the Design of In Vitro Flow Studies of the Carotid Artery Bifurcation. *Cardiovascular Engineering and Technology*, *11*(2), 111–127. https://doi.org/10.1007/s13239-019-00448-9

Huang, R. F., Yang, T. F., & Lan, Y. K. (2010). Pulsatile flows and wall-shear stresses in models simulating normal and stenosed aortic arches. *Experiments in Fluids*, *48*(3), 497–508. https://doi.org/10.1007/s00348-009-0754-y

Johari, & et al. (2020). A Computational Study of the Effect of Stent Design on Local Hemodynamic Factors at the Carotid Artery Bifurcation. *Artery Research*, *26*, 161–169. https://doi.org/10.2991/artres.k.200603.001

Johari, N. H., Wood, N. B., Cheng, Z., Torii, R., Oishi, M., Oshima, M., & Xu, X. Y. (2019). Disturbed Flow in a Stenosed Carotid Artery Bifurcation: Comparison of RANS-Based Transitional Model and les with Experimental Measurements. *International Journal of Applied Mechanics*, *11*(4), 1–21.

https://doi.org/10.1142/S1758825119500327

Johari, Nasrul Hadi. (2019). *Haemodynamics Analysis of Carotid Artery Stenosis and Carotid Artery Stenting*. *May*.

Kamada, H., Nakamura, M., & Ota, H. (2022). *Blood fl ow analysis with computational fl uid dynamics and 4D- fl ow MRI for vascular diseases*. *xxxx*. https://doi.org/10.1016/j.jjcc.2022.05.007

Kefayati, S. (2013). *PIV-based investigation of hemodynamic factors in diseased carotid artery bifurcations with varying plaque geometries*. *September*, xx + 180. http://ir.lib.uwo.ca/cgi/viewcontent.cgi?article=2896&context=etd

Kumar, N., Abdul, R. P. S. M., & Khan, K. S. H. (2022). Influence of blood pressure and rheology on oscillatory shear index and wall shear stress in the carotid artery. *Journal of the Brazilian Society of Mechanical Sciences and Engineering*, *5*. https://doi.org/10.1007/s40430-022-03792-5

Kumar, N., Khader, A., Pai, R., Kyriacou, P., Khan, S., & Koteshwara, P. (2019). Computational fluid dynamic study on effect of Carreau-Yasuda and Newtonian blood viscosity models on hemodynamic parameters. *Journal of Computational Methods in Sciences and Engineering*, *19*(2), 465–477. https://doi.org/10.3233/JCM-181004

Kumar, N., Khader, S. M. A., Pai, R., Khan, S. H., & Kyriacou, P. A. (2020). Fluid structure interaction study of stenosed carotid artery considering the effects of blood pressure. *International Journal of Engineering Science*, *154*, 103341. https://doi.org/10.1016/j.ijengsci.2020.103341

Lancellotti, R. M., Vergara, C., Valdettaro, L., Bose, S., & Quarteroni, A. (2017). Large eddy simulations for blood dynamics in realistic stenotic carotids. *International Journal for Numerical Methods in Biomedical Engineering*, *33*(11). https://doi.org/10.1002/cnm.2868

Lee, S. H., Han, K. S., Hur, N., Cho, Y. I., & Jeong, S. K. (2019). THE EFFECT of PATIENT-SPECIFIC NON-Newtonian BLOOD VISCOSITY on ARTERIAL HEMODYNAMICS PREDICTIONS. *Journal of Mechanics in Medicine and Biology*, *19*(8), 1–15. https://doi.org/10.1142/S0219519419400542

Lee, W. (2014). *General principles of carotid Doppler ultrasonography*. *33*(January), 11–17.

Li, C., Gao, B., Wang, J., Liu, J., Li, H., & Yang, S. (2019). Hemodynamic Factors Affecting Carotid Sinus Atherosclerotic Stenosis. *World Neurosurgery*, *121*, e262–e276. https://doi.org/10.1016/j.wneu.2018.09.091

Li, S., Jin, J., Zhang, C., Yang, X., Liu, Y., Lei, P., & Hu, Y. (2023). 3D bioprinting vascular networks in suspension baths. *Applied Materials Today*, *30*(December 2022), 101729. https://doi.org/10.1016/j.apmt.2022.101729

Li, Y., Verrelli, D. I., Yang, W., Qian, Y., & Chong, W. (2020). A pilot validation of CFD model results against PIV observations of haemodynamics in intracranial aneurysms treated with flow-diverting stents. *Journal of Biomechanics*, *100*,

UMPSA
UNIVERSITI MALAYSIA PAHANG
AL-SULTAN ABDULLAH

109590. https://doi.org/10.1016/j.jbiomech.2019.109590

Li, Z. Y., Tan, F. P. P., Soloperto, G., Wood, N. B., Xu, X. Y., & Gillard, J. H. (2015). Flow pattern analysis in a highly stenotic patient-specific carotid bifurcation model using a turbulence model. *Computer Methods in Biomechanics and Biomedical Engineering*, *18*(10), 1099–1107. https://doi.org/10.1080/10255842.2013.873033

Libby, P., & Plutzky, J. (2000). Atherosclerosis: An inflammatory disease. *International Congress and Symposium Series - Royal Society of Medicine*, *243*, 27–31.

Liu, J., Ma, X., Ren, X., Xiao, H., Yan, L., & Li, Z. (2021). *The Role of Blood Pressure in Carotid Plaque Incidence : Interactions With Body Mass Index , Age , and Sex-Based on a 7-Years Cohort Study*. *12*(August), 1–10. https://doi.org/10.3389/fphys.2021.690094

Lopes, D., Puga, H., Teixeira, J., & Lima, R. (2020). Blood flow simulations in patient-specific geometries of the carotid artery: A systematic review. *Journal of Biomechanics*, *111*, 110019. https://doi.org/10.1016/j.jbiomech.2020.110019

Lu, M., Cui, Y., Peng, P., Qiao, H., Cai, J., & Zhao, X. (2019). Shape and location of carotid atherosclerotic plaque and intraplaque hemorrhage: A high-resolution magnetic resonance imaging study. *Journal of Atherosclerosis and Thrombosis*, *26*(8), 720–727. https://doi.org/10.5551/jat.47449

Malek, A. M., & Alper, S. L. (1999). and Its Role in Atherosclerosis. *Stress: The International Journal on the Biology of Stress*, *282*(21), 2035–2042.

Medero, R., Hoffman, C., & Roldán-Alzate, A. (2018). Comparison of 4D Flow MRI and Particle Image Velocimetry Using an In Vitro Carotid Bifurcation Model. *Annals of Biomedical Engineering*, *46*(12), 2112–2122. https://doi.org/10.1007/s10439-018-02109-9

Mendieta, J. B., Fontanarosa, D., Wang, J., Paritala, P. K., McGahan, T., Lloyd, T., & Li, Z. (2020). The importance of blood rheology in patient-specific computational fluid dynamics simulation of stenotic carotid arteries. *Biomechanics and Modeling in Mechanobiology*, *19*(5), 1477–1490. https://doi.org/10.1007/s10237-019-01282-7

Menter, F. R., Langtry, R. B., Likki, S. R., Suzen, Y. B., Huang, P. G., & Völker, S. (2006). A correlation-based transition model using local variables - Part I: Model formulation. *Journal of Turbomachinery*, *128*(3), 413–422. https://doi.org/10.1115/1.2184352

Moradicheghamahi, J., Jahangiri, M., Mousaviraad, M., & Sadeghi, M. R. (2020). Computational studies of comparative and cumulative effects of turbulence, fluid–structure interactions, and uniform magnetic fields on pulsatile non-Newtonian flow in a patient-specific carotid artery. *Journal of the Brazilian Society of Mechanical Sciences and Engineering*, *42*(10), 1–22. https://doi.org/10.1007/s40430-020-02608-8

Muda, S., Hwei, S., Ng, Y., Shuib, A. S., & Phang, S. W. (2019). *Development of blood*

UMPSA
اونيۏرسيتي مليسيا ڤهڠ السلطان عبدالله
UNIVERSITI MALAYSIA PAHANG
AL-SULTAN ABDULLAH

mimicking fluid suspension using polymer particles Development of Blood Mimicking Fluid Suspension using Polymer Particles. *020012*(August).

Nagargoje, M., & Gupta, R. (2020). Effect of sinus size and position on hemodynamics during pulsatile flow in a carotid artery bifurcation. *Computer Methods and Programs in Biomedicine*, *192*, 105440. https://doi.org/10.1016/j.cmpb.2020.105440

Ningappa, A. H., Patil, S., Belur, G. S., Valerian, A. B., Kumar, N., Ballambat, R. P., Basri, A. A., Abdul, S. M., & Tamagawa, M. (2022). *Influence of Altered Pressures on Flow Dynamics in Carotid Bifurcation System Using Numerical Methods*. *1*(1), 47–61.

Noor, A. F. H. M., & Johari, N. H. (2022). *Brief review on recent technology in particle image velocimetry studies on hemodynamics in carotid artery*.

Noor, A. F. H. M., & Johari, N. H. (2023). Modeling the Effect of Different Locations of Carotid Atherosclerosis on Hemodynamics Parameters. *Lecture Notes in Electrical Engineering*, *882*(Cvd), 615–627. https://doi.org/10.1007/978-981-19-1577-2_45

Novakova, L., Kolinsky, J., Adamec, J., Kudlicka, J., & Malik, J. (2016). Vascular stenosis asymmetry influences considerably pressure gradient and flow volume. *Physiological Research*, *65*(1), 63–69. https://doi.org/10.33549/physiolres.932944

Onaizah, O., Poepping, T. L., & Zamir, M. (2017). A model of blood supply to the brain via the carotid arteries: Effects of obstructive vs. sclerotic changes. *Medical Engineering and Physics*, *49*, 121–130. https://doi.org/10.1016/j.medengphy.2017.08.009

Paisal, M. S. A., Taib, I., Ismail, A. E., Arifin, A. M. T., & Mahmod, M. F. (2019). Evaluation system on haemodynamic parameters for stented carotid artery: Stent pictorial selection method. *International Journal of Integrated Engineering*, *11*(1), 225–246. https://doi.org/10.30880/ijie. 2019.11.01.024

Roloff, C., Stucht, D., Beuing, O., & Berg, P. (2018). *Comparison of intracranial aneurysm flow quantification techniques : standard PIV vs stereoscopic PIV vs tomographic PIV vs phase- contrast MRI vs CFD*. 1–8. https://doi.org/10.1136/neurintsurg-2018-013921

Sardar, P., Chatterjee, S., Aronow, H. D., Kundu, A., Ramchand, P., Mukherjee, D., Nairooz, R., Gray, W. A., White, C. J., Jaff, M. R., Rosenfield, K., & Giri, J. (2017). Carotid Artery Stenting Versus Endarterectomy for Stroke Prevention: A Meta-Analysis of Clinical Trials. *Journal of the American College of Cardiology*, *69*(18), 2266–2275. https://doi.org/10.1016/j.jacc.2017.02.053

Schirmer, C. M., & Malek, A. M. (2007). Wall shear stress gradient analysis within an idealized stenosis using non-newtonian flow. *Neurosurgery*, *61*(4), 853–863. https://doi.org/10.1227/01.NEU.0000298915.32248.95

Sharma, N., Sastry, S., Sankovic, J. M., Kadambi, J. R., & Banerjee, R. K. (2020). Influence of near-wall PIV data on recirculation hemodynamics in a patient-

UMPSA
UNIVERSITI MALAYSIA PAHANG
AL-SULTAN ABDULLAH

specific moderate stenosis: Experimental-numerical comparison. *Biorheology*, *57*(2–4), 53–76. https://doi.org/10.3233/BIR-201001

Shuib, A., Hoskins, P., & Easson, W. (2011). Experimental investigation of particle distribution in a flow through a stenosed artery. *Journal of Mechanical Science and Technology*, *25*(2), 357–364. https://doi.org/10.1007/s12206-010-1232-4

Sia, S. F., Zhao, X., Yu, Y., & Zhang, Y. (2019). Multiphase particle-in-cell simulation in severe internal carotid artery stenosis. *Powder Technology*, *358*, 62–67. https://doi.org/10.1016/j.powtec.2018.07.091

Slagger, C. J., Wentzell, J. J., Gijsen, F. J. H., Thury, A., van der Waal, A. C., Schaar, J. A., & Serruys, P. W. (2005). The role of shear stress in the destabilization of vulnerable plaques and related therapeutic implications. *Nature Clinical Practice Cardiovascular Medicine*, *2*(9), 456–464. https://doi.org/10.1038/ncpcardio0298

Sousa, L. C., Castro, C. F., António, C. C., Sousa, F., Santos, R., Castro, P., & Azevedo, E. (2016). Computational simulation of carotid stenosis and flow dynamics based on patient ultrasound data - A new tool for risk assessment and surgical planning. *Advances in Medical Sciences*, *61*(1), 32–39. https://doi.org/10.1016/j.advms.2015.07.009

Stroud, J. S., Berger, S. A., & Saloner, D. (2000). Influence of stenosis morphology on flow through severely stenotic vessels: Implications for plaque rupture. *Journal of Biomechanics*, *33*(4), 443–455. https://doi.org/10.1016/S0021-9290(99)00207-9

Sun, N., Torii, R., Wood, N. B., Hughes, A. D., Thom, S. A. M., & Xu, X. Y. (2009). Computational modeling of LDL and albumin transport in an in vivo CT image-based human right coronary artery. *Journal of Biomechanical Engineering*, *131*(2), 1–9. https://doi.org/10.1115/1.3005161

Syed, F., Khan, S., & Toma, M. (2023). Modeling Dynamics of the Cardiovascular System Using Fluid-Structure Interaction Methods. *Biology*, *12*(7). https://doi.org/10.3390/biology12071026

Tada, S., & Tarbell, J. M. (2005). A computational study of flow in a compliant carotid bifurcation-stress phase angle correlation with shear stress. *Annals of Biomedical Engineering*, *33*(9), 1202–1212. https://doi.org/10.1007/s10439-005-5630-1

Tan, F. P. P., Wood, N. B., Tabor, G., & Xu, X. Y. (2011). Comparison of les of steady transitional flow in an idealized stenosed axisymmetric artery model with a RANS transitional model. *Journal of Biomechanical Engineering*, *133*(5), 1–12. https://doi.org/10.1115/1.4003782

Tarbell, J. M. (2003). Mass transport in arteries and the localization of atherosclerosis. *Annual Review of Biomedical Engineering*, *5*, 79–118. https://doi.org/10.1146/annurev.bioeng.5.040202.121529

Tayefi, H., Aghdam, Z. of A., Model, P. of A. in an A. B., Mode, P. of A. erosclerosis in an A. B. catio, Model, P. of A. in an A. B., Catio, P. of P. of A. in an A. B. M. P. of A. erosclerosis in n A. terial B., Mode, P. of A. erosclerosis in an A. B., Model, P. of A. in an A. B., Poss, P. of A., Model, P. of A. in an A. B., B, P. o A.

UNIVERSITI MALAYSIA PAHANG AL-SULTAN ABDULLAH

erosclerosis P. of A. in an A. B. M. P. of A. erosclerosis in n A. B. catioatio M. P. of A. in an A. B. M. P. P. ssiibility P., B, ossibility f A. in an A. terial, In, ossibility of A. erosclerosis insis, Of, O., Ssibility, Model, ibility of A. rosclerosis in an A. B., B, ibility o, Ather, ty of, L, ty o A. of A. f A. th rosclerosis in an A. t h erosclero rosclerosis in an A. ial B. B. cation M. rosclerosis in a rosclerosis in an A. B. cation M. rosclerosis rosclerosis in n A. terial B. ia B. osc osc lero sissis sis, … Shanehbandi, D. (2011). *Possibility of atherosclerosis in an bifurcation model*. *1*(4), 219–224. https://doi.org/10.5681/bi.2011.0

Trigui, A., Chiekh, M. Ben, Béra, J. C., & Gilles, B. (2021). Experimental and numerical investigation of pulsed flows in asevere aortic stenosed model. *Medical Engineering and Physics*, *90*, 33–42. https://doi.org/10.1016/j.medengphy.2021.02.006

Usmani, A. Y., & Muralidhar, K. (2016). Pulsatile flow in a compliant stenosed asymmetric model. *Experiments in Fluids*, *57*(12), 1–24. https://doi.org/10.1007/s00348-016-2274-x

Velasquez-Valencia, A., מזלי, ר., Dezzeo, Nelda, Flores, S., Zambrano-martínez, S., Rodgers, Louise & Ochoa, E., Flora, D., Río, F. G., Dueñas, A., Betancur, J., & Galindo, R. (2018). World health statistics in 2018. In *Interciencia* (Vol. 489, Issue 20).

Wang, Y., Joannic, D., Patrick, J., Keromnes, A., Aur, M., Lalande, A., Fontaine, J., Wang, Y., Joannic, D., Patrick, J., Keromnes, A., & Aur, M. (2016). Comparison of Flow Measurement by 4D Flow Magnetic Resonance Imaging and by Particles Image Velocimetry on Phantom of Abdominal Aortic Aneurysm To cite this version : *SM Vasc Med*, *1*(2), 1008. https://hal.archives-ouvertes.fr/hal-01463873/document

Webb, L. (2020). Mimicking Blood Rheology for More Accurate Modeling in Benchtop Research. *The Pegasus Review: UCF Undergraduate Research Journal (URJ)*, *12*(1), 28–34.

Woo, H. G., Heo, S. H., Kim, E. J., Chang, D. Il, Song, T. J., & Kim, B. J. (2020). Atherosclerotic plaque locations may be related to different ischemic lesion patterns. *BMC Neurology*, *20*(1), 1–7. https://doi.org/10.1186/s12883-020-01868-0

Wood, N. B. (1999). Aspects of fluid dynamics applied to the larger arteries. *Journal of Theoretical Biology*, *199*(2), 137–161. https://doi.org/10.1006/jtbi.1999.0953

Yang, K., Hoskins, P. R., Corner, G. A., Xia, C., & Huang, Z. (2023). Wall Shear Stress Measurement in Carotid Artery Phantoms with Variation in Degree of Stenosis Using Plane Wave Vector Doppler. *Applied Sciences (Switzerland)*, *13*(1). https://doi.org/10.3390/app13010617

Yao, X., Dai, Z., Zhang, X., Gao, J., Xu, G., Cai, Y., & Li, Z. (2019). Carotid geometry as a predictor of in-stent neointimal hyperplasia: A computational fluid dynamics study. *Circulation Journal*, *83*(7), 1472–1479. https://doi.org/10.1253/circj.CJ-18-1152

Yazdi, S. G., Geoghegan, P. H., Docherty, P. D., Jermy, M., & Khanafer, A. (2018). A

UMPSA
UNIVERSITI MALAYSIA PAHANG
AL-SULTAN ABDULLAH

Review of Arterial Phantom Fabrication Methods for Flow Measurement Using PIV Techniques. *Annals of Biomedical Engineering*, *46*(11), 1697–1721. https://doi.org/10.1007/s10439-018-2085-8

Yazdi, S. G., Huetter, L., Docherty, P. D., Williamson, P. N., Clucas, D., Jermy, M., & Geoghegan, P. H. (2019). A novel fabrication method for compliant silicone phantoms of arterial geometry for use in particle image velocimetry of haemodynamics. *Applied Sciences (Switzerland)*, *9*(18). https://doi.org/10.3390/app9183811

Yoon, J. H., & Lee, S. J. (2002). Direct comparison of 2D PIV and stereoscopic PIV measurements. *Measurement Science and Technology*, *13*(10), 1631–1642. https://doi.org/10.1088/0957-0233/13/10/317

Yousif, M. Y., Holdsworth, D. W., & Poepping, T. L. (2011). A blood-mimicking fluid for particle image velocimetry with silicone vascular models. *Experiments in Fluids*, *50*(3), 769–774. https://doi.org/10.1007/s00348-010-0958-1

Zarins, C. K., Giddens, D. P., Bharadvaj, B. K., Sottiurai, V. S., Mabon, R. F., & Glagov, S. (1983). Carotid bifurcation atherosclerosis. Quantitative correlation of plaque localization with flow velocity profiles and wall shear stress. *Circulation Research*, *53*(4), 502–514. https://doi.org/10.1161/01.RES.53.4.502

Zhao, S. Z., Xu, X. Y., Hughes, A. D., Thom, S. A., Stanton, A. V., Ariff, B., & Long, Q. (2000). Blood flow and vessel mechanics in a physiologically realistic model of a human carotid arterial bifurcation. *Journal of Biomechanics*, *33*(8), 975–984. https://doi.org/10.1016/S0021-9290(00)00043-9

Zhou, H., Meng, L., Zhou, W., Xin, L., Xia, X., Li, S., Zheng, H., & Niu, L. (2017). Computational and experimental assessment of influences of hemodynamic shear stress on carotid plaque. *BioMedical Engineering Online*, *16*(1), 1–11. https://doi.org/10.1186/s12938-017-0386-z

UMPSA
اونيۏرسيتي مليسيا ڤهڠ السلطان عبدالله
UNIVERSITI MALAYSIA PAHANG
AL-SULTAN ABDULLAH

APPENDICES

UMPSA
اونيۏرسيتي مليسيا ڤهڠ السلطان عبدالله
UNIVERSITI MALAYSIA PAHANG
AL-SULTAN ABDULLAH

Appendix A: Publication of paper

Publication of paper:

1. Humens Engineering (HUMENS) Symposium 2021. Title paper: Brief review on recent technology in particle image velocimetry studies on hemodynamics in carotid artery

   -

2. International Conference on Mechanical Engineering Research (6th ICMER 2021). Title paper: Modeling the Effect of Different Locations of Carotid Atherosclerosis on Hemodynamics Parameters

UMPSA
اونيۏرسيتي مليسيا ڤهڠ السلطان عبدالله
UNIVERSITI MALAYSIA PAHANG
AL-SULTAN ABDULLAH

Appendix B: Mesh independence on patient specific and idealised geometry

1) Patient specific carotid artery

Table 1: Mesh quality analysis for healthy model between different size of elements for healthy carotid artery

Element size (mm)	Number of elements	Number of nodes	Mesh Quality: Orthogonal Quality (1.0> X >0.2)	Skewness (X < 0.85)	Aspect Ratio (X < 5.0)
0.6	1272651	250290	0.17222	0.82778	1.1614
0.5	1637297	321029	0.16894	0.83106	1.1595
0.45	1882313	367847	0.19436	0.80564	1.1598
0.4	2004357	392864	0.20046	0.79954	1.1601

2) Idealised carotid artery

Table 1: Mesh quality analysis for healthy model between different size of elements for healthy carotid artery

Element size (mm)	Number of elements	Number of nodes	Mesh Quality: Orthogonal Quality (1.0> X >0.2)	Skewness (X < 0.85)	Aspect Ratio (X < 5.0)
0.3	852211	190124	0.20903	0.79097	1.8523
0.25	1264832	279256	0.20731	0.79269	1.8529
0.2	1692437	367583	0.20638	0.79362	1.8545
0.15	2142593	501620	0.20644	0.79356	1.8362

اونيۏرسيتي مليسيا ڤهڠ السلطان عبدالله
UNIVERSITI MALAYSIA PAHANG
AL-SULTAN ABDULLAH

Table 2. Mesh quality analysis for stenosed model between different size of elements for stenosis on top of carotid artery.

Element size (mm)	Number of elements	Number of nodes	Mesh Quality		
			Orthogonal Quality (1.0> X >0.2)	Skewness (X < 0.85)	Aspect Ratio (X < 5.0)
0.3	838194	166794	0.20051	0.79949	1.1602
0.25	921172	183176	0.16035	0.83965	1.1589
0.2	1260796	249224	0.206954	0.79406	1.1576
0.15	1982582	389391	0.20279	0.79721	1.1576

Table 3: Mesh quality analysis for stenosed model between different size of elements for stenosis mid position of carotid artery.

Element size (mm)	Number of elements	Number of nodes	Mesh Quality		
			Orthogonal Quality (1.0> X >0.2)	Skewness (X < 0.85)	Aspect Ratio (X < 5.0)
0.30	993697	197056	0.20161	0.79839	1.1595
0.25	1055902	209263	0.20432	0.79568	1.1592
0.20	1670938	330913	0.20218	0.79782	1.1602
0.15	2372329	464401	0.20396	0.79604	1.1587

UMPSA
اونيۏرسيتي مليسيا ڤهڠ السلطان عبدالله
UNIVERSITI MALAYSIA PAHANG
AL-SULTAN ABDULLAH

Table 4: Mesh quality analysis for stenosed model between different size of elements for stenosis downstream position of carotid artery.

Element size (mm)	Number of elements	Number of nodes	Mesh Quality		
			Orthogonal Quality (1.0> X >0.2)	Skewness (X < 0.85)	Aspect Ratio (X < 5.0)
0.3	973612	193202	0.20306	0.79694	1.1646
0.25	1187230	234818	0.20309	0.79691	1.1605
0.20	1565482	308096	0.20233	0.79767	1.1607
0.15	2306114	454564	0.20212	0.79788	1.1599

UMPSA
اونيۏرسيتي مليسيا ڤهڠ السلطان عبدالله
UNIVERSITI MALAYSIA PAHANG
AL-SULTAN ABDULLAH